

An *Ab Initio* Investigation of Nickel(II) Complexes with
Water, Chloride, Hydroxide and Ammonia

by

Liwei Cheng

A Thesis Submitted to Saint Mary's University, Halifax, Nova Scotia,
in Partial Fulfillment of the Requirements for the
Degree of Master of Science in Applied Science

February 28, 2013, Halifax, Nova Scotia

Copyright Liwei Cheng, 2013

Approved: Dr. Cory Pye
Supervisor
Department of Chemistry

Approved: Dr. Galina Orlova
External Examiner
Department of Chemistry
St. Francis Xavier University

Approved: Dr. Christa Brosseau
Supervisory Committee Member
Department of Chemistry

Approved: Dr. Rituparna Kanungo
Supervisory Committee Member
Department of Astronomy and Physics

Approved: Dr. Hai Wang
Graduate Studies Representative

Date: February 28, 2013

An *Ab Initio* Investigation of Nickel(II) Complexes with Water, Chloride, Hydroxide and Ammonia

By Liwei Cheng

Abstract

One of the main undesirable processes in Supercritical Water-Cooled Reactors (SCWR) is the possible formation of metal ligand complexes from ions present in coolant which is very poorly understood both experimentally and theoretically. As pressurized and heated solutions are difficult to work with, computational methods have now become an important research tool in this respect. A series of *ab initio* calculations of nickel(II) with hydroxide, ammonia, water and chloride have been performed at HF, MP2 and B3LYP levels with 6-31+G* basis sets. A thorough examination of geometries, energies and vibrational frequencies has been carried out for all species up to and including hexacoordinate species. The computational results are compared with experimental data where available.

Date: February 28, 2013

ACKNOWLEDGEMENTS

It would not have been possible to write this master's thesis without the help and support of the kind people around me, to only some of whom it is possible to give particular mention here.

Above all, I wish to thank, first and foremost, my supervisor Dr. Cory Pye who supervised this project and read my numerous revisions with help, patience and support. Also thanks to my committee members, Dr. Christa Brosseau and Dr. Rituparna Kanungo who offered guidance and support.

I would like to thank the Natural Sciences and Engineering Research Council (NSERC), Atomic Energy of Canada Limited (AECL) and Natural Resources Canada (NRCan) for funding the research project that I am so appreciative to have been a part of. I am also grateful to the Saint Mary's University Faculty of Graduate Studies and Research for partially funding my graduate experience at SMU. Also, thanks to the Atlantic Computational Excellence network (ACEnet) for computer time.

I would like to thank my lab group members, Daniel Whynot, Yaoting Zhang, Jane Ferguson, Barbara Goodall, Rajesh Satyamurti, Marwa Yasmin, Fernanda Rodrigues and Shifat Sharmin for their kindness, support and friendship. I am particular grateful to Jane for providing me with the calculation results of most complexes with chloride and water.

Finally, thanks to my parents and numerous friends who endured the long process with me, always offering support and love.

TABLE OF CONTENTS

Chapter 1: Introduction	1
1.1 Supercritical Water-Cooled Reactor	1
1.2 Nickel.....	2
1.3 Computational Chemistry	4
1.3.1 Quantum Mechanics	4
1.3.2 Hartree-Fock Theory.....	8
1.3.3 Basis Sets	10
1.3.4 Møller–Plesset perturbation theory	13
1.3.5 Density Functional Theory.....	15
1.3.6 Conductor-like Screening Model (COSMO)	17
1.4 Objectives	18
Chapter II: Methods	19
Chapter III: Hydrated Nickel(II) and Nickel(II) Complexes Combines with Water, Chloride, Hydroxide and Ammonia.....	21
3.1 Water, Hydroxide, Chloride and Ammonia Ligands	22
3.2 Aquanickel(II) Complexes, $[\text{Ni}(\text{H}_2\text{O})_n]^{2+}$, where $n=1-6$	23
3.2.1 Results.....	23
3.2.2 Discussion/Literature Comparison.....	25
3.3 Aquachloronickel(II) Complexes, $[\text{NiCl}_n(\text{H}_2\text{O})_m]^{2-n}$, where $n=1-4$, $m=0-(6-n)$	33
3.3.1 Results.....	33
3.3.2 Discussion/Literature Comparison.....	38
3.4 Aquahydroxynickel(II) Complexes, $[\text{Ni}(\text{OH})_n(\text{H}_2\text{O})_m]^{2-n}$, where $n=1-4$, $m=0-(6-n)$.	43

3.4.1	Results.....	44
3.4.2	Discussion/Literature Comparison.....	48
3.5	Amminenickel(II) Complexes, $[\text{Ni}(\text{NH}_3)_m(\text{H}_2\text{O})_n]^{2+}$, where $m=1-6$, $n=0-(6-n)$	55
3.5.1	Results.....	56
3.5.2	Discussion/Literature Comparison.....	60
3.6	Chlorohydroxonickel(II) Complexes, $[\text{NiCl}_m(\text{OH})_n(\text{H}_2\text{O})_l]^{2-m-n}$, where $m=1-3$, $n=1-(4-m)$, $l=0-(6-m-n)$	67
3.6.1	Results.....	67
3.6.2	Discussion/Literature Comparison.....	73
3.7	Chloroamminenickel(II) Complexes, $[\text{NiCl}_m(\text{NH}_3)_n(\text{H}_2\text{O})_l]^{2-n}$, where $m=1-4$, $n=1-(6-m)$, $l=0-(6-m-n)$	77
3.7.1	Results.....	77
3.7.2	Discussion/Literature Comparison.....	87
3.8	Hydroxoamminenickel(II) Complexes, $[\text{Ni}(\text{OH})_m(\text{NH}_3)_n(\text{H}_2\text{O})_l]^{2-m}$, where $m=1-4$, $n=1-(6-m)$, $l=0-(6-m-n)$	92
3.8.1	Results.....	92
3.8.1	Discussion/Literature Comparison.....	100
3.9	Chlorohydroxoamminenickel(II) Complexes, $[\text{NiCl}_m(\text{OH})_n(\text{NH}_3)_l(\text{H}_2\text{O})_k]^{2-m-n}$, where $m=1-3$, $n=1-(4-m)$, $l=0-(6-m-n)$, $k=0-(6-m-n-l)$	105
3.9.1	Results.....	105
3.9.2	Discussion/Literature Comparison.....	113
Chapter 4:	Conclusion and Future Work	117
4.1	Conclusions.....	117
4.1.1	Aquanickel(II).....	117
4.1.2	Chloronickel(II)	118
4.1.3	Hydroxonickel(II)	118
4.1.4	Amminenickel(II).....	119

4.1.5	Chlorohydroxonickel(II)	119
4.1.6	Chloroamminenickel(II).....	119
4.1.7	Hydroxoamminenickel(II)	120
4.1.8	Chlorohydroxoamminenickel(II)	120
4.2	Future Work	121
Reference:	122

Appendix A – Supplementary Materials

LIST OF ABBREVIATIONS

ACEnet	Atlantic Computational Excellence Network
AECL	Atomic Energy of Canada Limited
B3LYP	Becke 3-Parameter Lee-Yang-Parr Hybrid Functional
CANDU	Canada Deuterium Uranium
COSMO	Conductor-like Screening Model
C-PCM	Conductor-like Polarizable Continuum Model
DFT	Density Functional Theory
GTO	Gaussian-Type Orbital
HF	Hartree-Fock
HPC	High-Performance Computing
LCAO	Linear Combination of Atomic Orbitals
LWR	Light Water Reactor
MO	Molecular Orbital
MP2	Second-order Møller-Plesset Perturbation Theory
NMR	Nuclear Magnetic Resonance
PCM	Polarizable Continuum Model
SCF	Self-Consistent Field
SCWR	Supercritical Water-cooled Reactor
STO	Slater-Type Orbital
UV/Vis	Ultraviolet/Visible

LIST OF FIGURES

- Figure 3-1: The nickel(II) and chloride ions as well as optimized MP2 and B3LYP geometries for the remaining ligands used in the calculations of nickel(II) complexes. 21
- Figure 3-2: Optimized MP2 and B3LYP geometries for $[\text{Ni}(\text{H}_2\text{O})_n]^{2+}$, where $n=1 - 6$. All structures are similar with the exception of the dihydrate which is D_{2d} at MP2 and D_{2h} at B3LYP. 23
- Figure 3-3: Ni-O bond lengths (left) and vibrational stretching frequencies (right) for $[\text{Ni}(\text{H}_2\text{O})_n]^{2+}$, where $n=1 - 6$, calculated at the HF/6-31+G* level. 29
- Figure 3-4: Ni-O bond lengths (left) and vibrational stretching frequencies (right) for $[\text{Ni}(\text{H}_2\text{O})_n]^{2+}$, where $n=1 - 6$, calculated at the MP2/6-31+G* level. 30
- Figure 3-5: Ni-O bond lengths (left) and vibrational stretching frequencies (right) for $[\text{Ni}(\text{H}_2\text{O})_n]^{2+}$, where $n=1 - 6$, calculated at the B3LYP/6-31+G* level. 31
- Figure 3-6: Optimized MP2 and B3LYP geometries for $[\text{NiCl}_n(\text{H}_2\text{O})_m]^{2-n}$, where $n=1 - 2$ and $m=0 - (6-n)$. 33
- Figure 3-7: Optimized MP2 and B3LYP geometries for $[\text{NiCl}_n(\text{H}_2\text{O})_m]^{2-n}$, where $n=3 - 4$ and $m=0 - (6-n)$. There was no distinction between structures for MP2 and B3LYP. 35

Figure 3-8: Ni-O (+) and Ni-Cl (l) bond lengths (left) and vibrational stretching frequencies (right) for $[\text{NiCl}_n(\text{H}_2\text{O})_m]^{2-n}$, where $n=1 - 4$ and $m=0 - (6-n)$, calculated at the HF/6-31+G* level.	39
Figure 3-9: Ni-O (+) and Ni-Cl (l) bond lengths (left) and vibrational stretching frequencies (right) for $[\text{NiCl}_n(\text{H}_2\text{O})_m]^{2-n}$, where $n=1 - 4$ and $m=0 - (6-n)$, calculated at the MP2/6-31+G* level.	40
Figure 3-10: Ni-O (+) and Ni-Cl (l) bond lengths (left) and vibrational stretching frequencies (right) for $[\text{NiCl}_n(\text{H}_2\text{O})_m]^{2-n}$, where $n=1 - 4$ and $m=0 - (6-n)$, calculated at the B3LYP/6-31+G* level.	41
Figure 3-11: Optimized MP2 and B3LYP geometries for $[\text{Ni}(\text{OH})(\text{H}_2\text{O})_m]^+$ and $[\text{Ni}(\text{OH})_2(\text{H}_2\text{O})_m]$.	44
Figure 3-12: Optimized MP2 and B3LYP geometries for $[\text{Ni}(\text{OH})_3(\text{H}_2\text{O})_m]^-$ and $[\text{Ni}(\text{OH})_4(\text{H}_2\text{O})_m]^{2-}$.	46
Figure 3-13: Ni-O bond lengths (left) and vibrational stretching frequencies (right) for $[\text{Ni}(\text{OH})_n(\text{H}_2\text{O})_m]^{2-n}$, where $n=1 - 4$ and $m=0 - (6-n)$, calculated at the HF/6-31+G* level.	51
Figure 3-14: Ni-O bond lengths (left) and vibrational stretching frequencies (right) for $[\text{Ni}(\text{OH})_n(\text{H}_2\text{O})_m]^{2-n}$, where $n=1 - 4$ and $m=0 - (6-n)$, calculated at the MP2/6-31+G* level.	52
Figure 3-15: Ni-O bond lengths (left) and vibrational stretching frequencies (right) for $[\text{Ni}(\text{OH})_n(\text{H}_2\text{O})_m]^{2-n}$, where $n=1 - 4$ and $m=0 - (6-n)$, calculated at the B3LYP/6-31+G* level.	53
Figure 3-16: Optimized MP2 and B3LYP geometries for $[\text{Ni}(\text{NH}_3)_n(\text{H}_2\text{O})_m]^{2+}$, where $n=1 - 2$, $m=0 - (6-n)$. “*” indicates MP2 and B3LYP structures with different symmetry are similar.	56

- Figure 3-17: Optimized MP2 and B3LYP geometries for $[\text{Ni}(\text{NH}_3)_n(\text{H}_2\text{O})_m]^{2+}$, where $n=3 - 6$, $m=0 - (6-n)$. “*” indicates MP2 and B3LYP structures with different symmetry are similar. 58
- Figure 3-18: Ni-N (+) and Ni-O (|) bond lengths (left) and vibrational stretching frequencies (right) for $[\text{Ni}(\text{NH}_3)_n(\text{H}_2\text{O})_m]^{2+}$, where $n=1 - 6$ and $m=0 - (6-n)$, calculated at the HF/6-31+G* level. 64
- Figure 3-19: Ni-N (+) and Ni-O (|) bond lengths (left) and vibrational stretching frequencies (right) for $[\text{Ni}(\text{NH}_3)_n(\text{H}_2\text{O})_m]^{2+}$, where $n=1 - 6$ and $m=0 - (6-n)$, calculated at the MP2/6-31+G* level. 65
- Figure 3-20: Ni-N (+) and Ni-O (|) bond lengths (left) and vibrational stretching frequencies (right) for $[\text{Ni}(\text{NH}_3)_n(\text{H}_2\text{O})_m]^{2+}$, where $n=1 - 6$ and $m=0 - (6-n)$, calculated at the B3LYP/6-31+G* level. 66
- Figure 3-21: Optimized MP2 and B3LYP geometries for $[\text{NiCl}(\text{OH})_m(\text{H}_2\text{O})_l]^{1-m}$, where $m=1 - 2$, $l=0 - (5-m)$. 68
- Figure 3-22: Optimized MP2 and B3LYP geometries for $[\text{NiCl}_n(\text{OH})_m(\text{H}_2\text{O})_l]^{1-n-m}$, where $n=1 - 3$, $m=0 - (4-n)$, $l=0 - (6-n-m)$. 71
- Figure 3-23: Ni-Cl (|) and Ni-O (+) bond lengths (left) and vibrational stretching frequencies (right) for $[\text{NiCl}_n(\text{OH})_m(\text{H}_2\text{O})_l]^{2-n-m}$, where $n=1 - 3$, $m=1 - (4-n)$ and $l=0 - (6-n-m)$, calculated at the HF/6-31+G* level. 75
- Figure 3-24: Ni-Cl (|) and Ni-O (+) bond lengths (left) and vibrational stretching frequencies (right) for $[\text{NiCl}_n(\text{OH})_m(\text{H}_2\text{O})_l]^{2-n-m}$, where $n=1 - 3$, $m=1 - (4-n)$ and $l=0 - (6-n-m)$, calculated at the MP2/6-31+G* level. 76
- Figure 3-25: Ni-Cl (|) and Ni-O (+) bond lengths (left) and vibrational stretching frequencies (right) for $[\text{NiCl}_n(\text{OH})_m(\text{H}_2\text{O})_l]^{2-n-m}$, where $n=1 - 3$, $m=1 - (4-n)$ and $l=0 - (6-n-m)$, calculated at the B3LYP/6-31+G* level. 77

- Figure 3-26: Optimized MP2 and B3LYP geometries for $[\text{NiCl}_m(\text{NH}_3)_n(\text{H}_2\text{O})_l]^{2-n}$, where $m=1-2$, $n=1-(6-m)$, $l=0-(6-m-n)$. All symmetries marked with “*” indicate B3LYP otherwise all MP2 and B3LYP structure are similar. 82
- Figure 3-27: Optimized MP2 and B3LYP geometries for $[\text{NiCl}_m(\text{NH}_3)_n(\text{H}_2\text{O})_l]^{2-n}$, where $m=3-4$, $n=1-(6-m)$, $l=0-(6-m-n)$. 87
- Figure 3-28: Ni-Cl (|), Ni-N (x) and Ni-O (+) bond lengths (left) and vibrational stretching frequencies (right) for $[\text{NiCl}_n(\text{NH}_3)_m(\text{H}_2\text{O})_l]^{2-n-m}$, where $n=1-4$, $m=1-(6-n)$ and $l=0-(6-n-m)$, calculated at the HF/6-31+G* level. 90
- Figure 3-29: Ni-Cl (|), Ni-N (x) and Ni-O (+) bond lengths (left) and vibrational stretching frequencies (right) for $[\text{NiCl}_n(\text{NH}_3)_m(\text{H}_2\text{O})_l]^{2-n-m}$, where $n=1-4$, $m=1-(6-n)$ and $l=0-(6-n-m)$, calculated at the MP2/6-31+G* level. 91
- Figure 3-30: Ni-Cl (|), Ni-N (x) and Ni-O (+) bond lengths (left) and vibrational stretching frequencies (right) for $[\text{NiCl}_n(\text{NH}_3)_m(\text{H}_2\text{O})_l]^{2-n-m}$, where $n=1-4$, $m=1-(6-n)$ and $l=0-(6-n-m)$, calculated at the B3LYP/6-31+G* level. 92
- Figure 3-31: Optimized MP2 and B3LYP geometries for $[\text{Ni}(\text{OH})_m(\text{NH}_3)_n(\text{H}_2\text{O})_l]^{2-m}$, where $m=1-2$, $n=1-(6-n)$, $l=0-(6-m-n)$. 96
- Figure 3-32: Optimized MP2 and B3LYP geometries for $[\text{Ni}(\text{OH})_m(\text{NH}_3)_n(\text{H}_2\text{O})_l]^{2-m}$, where $m=3-4$, $n=1-(6-n)$, $l=0-(6-m-n)$. 100
- Figure 3-33: Ni-N (+) and Ni-O (|) bond lengths (left) and vibrational stretching frequencies (right) for $[\text{Ni}(\text{NH}_3)_n(\text{OH})_m(\text{H}_2\text{O})_l]^{2-m}$, where $n=1-5$, $m=1-(5-n)$ and $l=0-(6-n-m)$, calculated at the HF/6-31+G* level. 102

- Figure 3-34: Ni-N (+) and Ni-O (|) bond lengths (left) and vibrational stretching frequencies (right) for $[\text{Ni}(\text{NH}_3)_n(\text{OH})_m(\text{H}_2\text{O})_l]^{2-m}$, where $n=1-5$, $m=1-(5-n)$ and $l=0-(6-n-m)$, calculated at the MP2/6-31+G* level. 103
- Figure 3-35: Ni-N (+) and Ni-O (|) bond lengths (left) and vibrational stretching frequencies (right) for $[\text{Ni}(\text{NH}_3)_n(\text{OH})_m(\text{H}_2\text{O})_l]^{2-m}$, where $n=1-5$, $m=1-(5-n)$ and $l=0-(6-n-m)$, calculated at the B3LYP/6-31+G* level. 104
- Figure 3-36: Optimized MP2 and B3LYP geometries for $[\text{NiCl}(\text{OH})_n(\text{NH}_3)_l(\text{H}_2\text{O})_k]^{1-n}$, where $n=1-3$, $l=1-3$, $k=0-(6-n-l)$. 108
- Figure 3-37: Optimized MP2 and B3LYP geometries for $[\text{NiCl}_m(\text{OH})_n(\text{NH}_3)_l(\text{H}_2\text{O})_k]^{1-n}$, where $m=2-3$, $n=1-2$, $l=1-3$, $k=0-(6-m-n-l)$. 111
- Figure 3-38: Ni-O (+), Ni-Cl (|) and Ni-N (x) bond lengths (left) and vibrational stretching frequencies (right) for $[\text{NiCl}_m(\text{NH}_3)_n(\text{OH})_m(\text{H}_2\text{O})_l]^{2-m-n}$, where $m=1-3$, $n=1-(4-m)$, $l=0-(6-m-n)$, $k=0-(6-m-n-l)$, calculated at the HF/6-31+G* level. 114
- Figure 3-39: Ni-O (+), Ni-Cl (|) and Ni-N (x) bond lengths (left) and vibrational stretching frequencies (right) for $[\text{NiCl}_m(\text{NH}_3)_n(\text{OH})_m(\text{H}_2\text{O})_l]^{2-m-n}$, where $m=1-3$, $n=1-(4-m)$, $l=0-(6-m-n)$, $k=0-(6-m-n-l)$, calculated at the MP2/6-31+G* level. 115
- Figure 3-40: Ni-O (+), Ni-Cl (|) and Ni-N (x) bond lengths (left) and vibrational stretching frequencies (right) for $[\text{NiCl}_m(\text{NH}_3)_n(\text{OH})_m(\text{H}_2\text{O})_l]^{2-m-n}$, where $m=1-3$, $n=1-(4-m)$, $l=0-(6-m-n)$, $k=0-(6-m-n-l)$, calculated at the B3LYP/6-31+G* level. 116

Chapter 1: Introduction

1.1 Supercritical Water-Cooled Reactor

CANDU Supercritical Water-Cooled Reactors (SCWR) are one of the six innovative concepts selected for Gen IV nuclear reactors based on safety and environmental issues which are being developed by Atomic Energy of Canada Limited (AECL) [1]. The SCWR can be considered a hybrid between a LWR (Light Water Reactor) and a fossil-fuel SCW power plant. The power cycle proposed for SCWR would be a direct power cycle using a single phase coolant [2]. The SCWR concept is being built for several applications, such as hydrogen production, steam applications such as extraction of oil from oil sands, desalination, etc. [3] The SCWR offers many advantages such as the elimination of components like steam generators, steam separators, dryers, and a low coolant mass inventory resulting in smaller components with much higher thermal efficiency (about 45% versus about 33% efficiency for LWRs) [4]. One of the primary objectives is to lower unit energy costs via advancements in thermodynamic efficiency which is attained by increasing the coolant core mean temperature in excess of 500 °C, leading to plant thermodynamic efficiencies as high as 50%. Thus, the SCWR power cycle would be a direct cycle operating at a pressure of 25 MPa, with core inlet and outlet temperatures of about 550 K and as high as 900 K respectively [5].

Unfortunately, accompanying the increased efficiency, supercritical water at high operating temperatures and pressures is very reactive especially in an oxidizing environment. Under extreme conditions, the properties of water affected include the density, hydrogen bonding, ionization product, dielectric constant, heat capacity, and

transport properties. These properties have a large impact on the corrosion properties of metal alloys in the construction materials, resulting in anodic dissolution of the alloys. [6] In addition, certain aggressive ions (e.g. Cl^- , Br^-) can induce passivity breakdown, resulting in various forms of localized corrosion, such as pitting attack and stress corrosion cracking. [7] The transition metal in the metal alloys could be leached into the environment and form aqua ions, which combine with the surrounding anions such as Cl^- and OH^- . However, there will be no phase separation in the SCWR coolant, and the corrosion product formed in the reactor core will be carried out of core with the supercritical coolant. Those corrosion products may lead to deposition in the fuel or turbines. [8]

1.2 Nickel

Nickel is a hard, silvery white metallic element, (relative atomic mass 58.69) found in the first transition series group VIIIb of the periodic table. Nickel was first isolated in 1751 in impure form by Axel F. Cronstedt, a Swedish chemist. [9] The density of nickel is 8.908 g/cm^3 , its melting point is $1453 \text{ }^\circ\text{C}$, and its boiling point is $2732 \text{ }^\circ\text{C}$. [10] Five natural isotopes are known, of which ^{58}Ni (68.27%) and ^{60}Ni (26.10%) are the most abundant. The common oxidation states of nickel are 0 and +2, but other states (+1, +3, +4, and +6) are found in a few compounds. However, the +2 oxidization state is the most prevalent form in aqueous solution. Nickel(VI) is known in NiO_4^{2-} , which is a very powerful oxidizing agent and will oxidize water. Nickel (IV) is found in NiO_2 , which is also a very strong oxidizing agent. Some nickel(III) species, such as $\text{NiO}(\text{OH})$, are also

known and are strong oxidizing agents. Besides these species, various oxidization states of nickel are found in complex ions. [11]

Nickel-based alloys are vitally important to modern industry due to their ability to withstand a wide variety of severe operating conditions involving corrosive environments, high temperatures, high stress, and combinations of these factors. [12] In the nuclear industry, nickel-based alloys are chosen and used in gas turbine engines and a spectrum of other applications of relevant use. [13] In particular, nickel-based alloys are chosen because of their generally higher creep strength compared to austenitic and ferritic-martensitic steels for the supercritical water reactor, [14] nickel-base alloys have been proposed for Gen IV reactor in-core components. [15]

The excellent corrosion resistance of nickel-based alloys is largely due to the surface protection in aqueous electrolytes or moist air by ultrathin dense oxide/hydroxide films. [16] However, the passive film does not afford complete protection of the substrate alloys. For instance, tribological contact or aggressive ions can often damage or even remove the passive film, and expose the active substrate alloy surface to the corrosion environment. [17] In this case, nickel(II) ion could be leached into the environment and form aqua complexes with surrounding anions and/or ammonia, which could be introduced by pH adjustment. The anions could be introduced through the cooling system (i.e. Cl^- from river water) or from the addition of water itself (OH^- ions). These nickel complexes can be transported out of core, and may deposit in the fuel or turbines and corroding these areas. Therefore, it is necessary to carry out the investigation of the possible complexes nickel will form in SCWR for both scientific research and

engineering practices. As pressurized and heated solutions are difficult to work with, computational methods have now become an important research tool.

1.3 Computational Chemistry

1.3.1 Quantum Mechanics

Computational chemistry is based on quantum mechanics, which provides a very detailed picture of molecules. The postulates and theorems of quantum mechanics form the rigorous foundation for the prediction of observable chemical properties from first principles. The fundamental postulates of quantum mechanics assert that microscopic systems are described by wave functions that completely characterize all of the physical properties of the system. [26]

In the late seventeenth century, Isaac Newton summarized classical mechanics, the laws of motion of macroscopic objects. In the early twentieth century, physicists found that classical mechanics does not correctly describe the behavior of very small particles such as the electrons and nuclei of atoms and molecules. [18] Quantum mechanics determines the properties of nanomaterials (objects with at least one dimension in the range 1 to 100 nm), and calculation methods to deal with nanomaterials are being developed. [18]

The development of quantum mechanics began in 1900 with Planck's study of blackbody radiation, which is the light emitted by a heated solid that absorbs all light falling on it.[18] When physicists used classical mechanics to predict the intensity-

versus-frequency curve for emitted blackbody radiation, they found a result in complete disagreement with the high-frequency portion of the experimental curves. [18] Planck assumed the radiation emitters and absorbers in the blackbody to be harmonically oscillating electric charges (resonators), and the total energy of those resonators whose frequency is ν , consisted of N indivisible “energy elements” which led to curves that agreed with the experimental blackbody curves. [18] Thus the energy of each resonator was quantized, meaning that only certain discrete values were allowed for resonator energy. [18]

The second application of energy quantization was to the photoelectric effect, in which light shining on a metal causes emission of electrons. [18] Physicists found it difficult to reconcile their observations with the classical electromagnetic wave theory of light. An explanation was suggested in 1905 by Einstein who proposed that the incident light be viewed as being comprised of discrete units of energy. [19] The photoelectric effect shows that light can exhibit particlelike behavior in addition to the wavelike behavior it shows in diffraction experiments. [18] De Broglie proposed that all material particles are associated with waves, but that the existence of these waves is likely to be observable only in the behavior of extremely light particles. [19] Quantum mechanics is required for those microscopic particles as classical mechanics only applies to macroscopic particles.

Microscopic particles have a wave nature. When such a particle is located by using radiation of photons of large momentum, the interaction of photon and the electron changes the momentum of the electron. [20] Thus both position and velocity of the

particle cannot be measured simultaneously. Heisenberg [21] stated the uncertainty principle, which can be derived from quantum theory,

$$\Delta p \Delta x \geq \frac{\hbar}{2} \quad (1)$$

That means to locate an electron to within a region Δx , there will be an uncertainty in the momentum Δp of the electron. [22]

Therefore, a wave equation is needed for quantum systems. Schrödinger [23] obtained such an equation which is written as:

$$\hat{H}\Psi = E\Psi \quad (2)$$

In the Schrödinger equation, Ψ is used for an unspecified quantum mechanical wave function, E is the energy eigenvalue. \hat{H} is called the Hamiltonian operator. The wave function Ψ is an eigenfunction of the Hamiltonian operator, and the energy E is an eigenvalue of the Hamiltonian operator as the result of operating \hat{H} on Ψ is simply to give Ψ back again, only multiplied by a constant factor, the energy E . The Hamiltonian operator is written as:

$$\hat{H} = -\frac{\hbar^2}{2m} \frac{d^2}{dx^2} + V(x) \quad (3)$$

In this equation, the $-\frac{\hbar^2}{2m} \frac{d^2}{dx^2}$ is the kinetic energy part, and $V(x)$ is the potential energy part. m is the mass of the particle at position x .

Equation 2 does not contain time and is called the time-independent Schrödinger equation. The wave function obtained from equation 2 is called the stationary-state wave

function, and many problems of chemical interest can be described in terms of stationary-state wave functions. [21] The wave function contains all possible information of a system. Also, the one-dimensional, one-particle systems can be extended to three-dimensional, many-particle systems. For a three-dimensional, one-particle system, the Schrödinger equation is:

$$-\frac{\hbar^2}{2m} \left(\frac{\partial^2 \Psi}{\partial x^2} + \frac{\partial^2 \Psi}{\partial y^2} + \frac{\partial^2 \Psi}{\partial z^2} \right) + V(x, y, z) = E\Psi(x, y, z) \quad (4)$$

The first term of the Hamiltonian operator in equation 4 is called Laplacian operator, denoted as ∇^2 :

$$\nabla^2 = \frac{\partial^2}{\partial x^2} + \frac{\partial^2}{\partial y^2} + \frac{\partial^2}{\partial z^2} \quad (5)$$

The Schrödinger equation for many-particle, three-dimensional systems are to sum up all the kinetic energy and potential energy components:

$$\left[-\sum_{i=1}^n \frac{\hbar^2}{2m_i} \nabla_i^2 + V(x_1, y_1, z_1, \dots, x_i, y_i, z_i) \right] = E\Psi \quad (6)$$

The quantum mechanical description of a hydrogen atom is the starting point for computational chemistry, and it can be solved analytically. [24] However, atoms with more than one electron cannot be solved exactly as there is a interelectron repulsion term in the Schrödinger equation. In order to simplify the problem, the Born-Oppenheimer approximation is invoked. [25] As the nuclei of molecular systems are moving much more slowly than the electrons, it is convenient to decouple the motions of nuclei, and compute electronic energies for fixed nuclear position. [26] Therefore, to calculate the

energy of a molecule is to solve the electronic Schrödinger equation and then add the electronic energy to the internuclear repulsion to get the total internal energy.[27] A deeper consequence of the Born-Oppenheimer approximation is that a molecule has a shape. [27]

1.3.2 Hartree-Fock Theory

The Hartree-Fock (HF) calculation is the simplest kind of ab initio calculation which was first performed on atoms by Hartree in 1928. [28] The fundamental assumption of HF theory, that each electron sees all of the others as an average field, allows for tremendous progress to be made in carrying out practical molecular orbital calculations. [26] The HF method is used to solve Schrödinger equations of atoms and molecules and predict their properties such as geometries and vibrational frequencies. According to the Pauli Exclusion Principle, the wave function for a HF calculation is one or more antisymmetrized products of one-electron spin-orbitals. A convenient way to produce an antisymmetrized product is to use Slater determinants:

$$\Psi(1,2,\dots,2N) = \frac{1}{\sqrt{(2N)!}} \begin{vmatrix} \psi_1\alpha(1) & \psi_1\beta(1) & \cdots & \psi_N\alpha(1) & \psi_N\beta(1) \\ \psi_1\alpha(2) & \psi_1\beta(2) & \cdots & \psi_N\alpha(2) & \psi_N\beta(2) \\ \vdots & \vdots & \ddots & \vdots & \vdots \\ \psi_1\alpha(2N) & \psi_1\beta(2N) & \cdots & \psi_N\alpha(2N) & \psi_N\beta(2N) \end{vmatrix} \quad (7)$$

$2N$ is the number of electrons in the closed shell system as the wave functions are represented by N doubly occupied spatial orbitals. α and β are spin orbitals, and $\frac{1}{\sqrt{(2N)!}}$

is the normalization constant. The wavefunctions in the Slater determinants are functions that are properly antisymmetric with respect to exchange of coordinates of any pair of

electrons. Such an exchange would correspond to interchanging two rows of the Slater determinant according to property of determinants that their value changes sign if two rows are exchanged. [24] If there are two identical spin-orbitals, then there will be two identical columns in the Slater determinant according to the property of determinants that their value is zero if two columns are identical. [24] It follows from the Schrödinger equation that the energy of a system is given by:

$$E = \frac{\int \Psi^* \hat{H} \Psi d\tau}{\int \Psi^* \Psi d\tau}. \quad (8)$$

Using Dirac notation it can be written:

$$E = \langle \Psi(1,2, \dots, 2N) | \hat{H} | \Psi(1,2, \dots, 2N) \rangle, \quad (9)$$

while the Hamiltonian operator for a molecule with $2N$ electrons and M atomic nuclei (the M^{th} nucleus has the charge Z_M can be written as:

$$\hat{H} = \sum_{i=1}^{2N} -\frac{1}{2} \nabla_i^2 - \sum_{\text{all } i,j} \frac{Z_M}{r_{Mi}} + \sum_{\text{all } i,j} \frac{1}{r_{ij}}. \quad (10)$$

The Hamiltonian is composed of electron kinetic energy terms, nucleus-electron attraction potential energy terms, and electron-electron repulsion potential energy terms. From the Born-Oppenheimer approximation, the nucleus-nucleus repulsion potential energy terms have been omitted, and these can simply be added to the electronic energy as they are constants. The energy can be written as:

$$E = 2 \sum_{i=1}^N H_{ii} + \sum_{i=1}^N \sum_{j=1}^N (2J_{ij} - K_{ij}). \quad (11)$$

The terms in Eq. 11 have these meanings

$$H_{ii} = \int \Psi_i^*(1) \left(-\frac{1}{2} \nabla_1^2 - \sum_{all M} \frac{Z_M}{r_{M1}} \right) \Psi_i(1) dr \quad (12)$$

$$J_{ij} = \int \Psi_i^*(1) \Psi_i(1) \left(\frac{1}{r_{12}} \right) \Psi_j(2) \Psi_j^*(2) dr_1 dr_2 \quad (13)$$

$$K_{ij} = \int \Psi_i^*(1) \Psi_j^*(2) \left(\frac{1}{r_{12}} \right) \Psi_i(2) \Psi_j(1) dr_1 dr_2 \quad (14)$$

H_{ii} is the electronic energy of a single electron moving simply under the attraction of a nuclear core, with all the other electrons stripped away. J_{ij} is called a Coulomb integral, and it represents the electrostatic repulsion between an electron in Ψ_i and one in Ψ_j . K_{ij} is called an exchange integral, and it differs only in exchange of electrons.

The energy calculated from Eq. 9 will be the exact, true energy of the molecule only if the wavefunction and the Hamiltonian are exact. The variation principle states that the energy calculated from Eq. 9 must be greater than or equal to the true ground-state energy of the molecule. [27] The energy associated with the wave function is determined from all the coefficients. The Hartree-Fock method follows a SCF (self-consistent field) procedure, where the orbital coefficients are first estimated and then iterated to convergence.

1.3.3 Basis Sets

The basis set is the set of mathematical functions (basis functions), linear combinations of which yield molecular orbitals. [27] The functions are usually centred on

nuclei. Approximating molecular orbitals as linear combinations of basis functions is called the LCAO-MO approach. [27] However, the functions are not necessarily conventional atomic orbitals, they can be any set of mathematical functions that are convenient to manipulate and which in linear combination give useful representations of molecular orbitals. Physically, several basis functions describe the electron distribution around an atom and combining atomic basis functions yields the electron distribution in the molecule as a whole. [27] The electron distribution around an atom can be represented in two ways, Slater functions and Gaussian functions. [29] Slater functions are used in semiempirical methods, and modern molecular ab initio programs employ Gaussian functions.

The essence of STO (Slater-type-orbital) is to place on each nucleus one or more STOs. [27] Generally, the larger the number of STOs and/or the greater the care taken in selecting orbital exponents, the more accurate the final wavefunction and the energy will be. The mathematical form of a normalized STO is:

$$S(r, \theta, \zeta, \phi, n, l, m) = N_{nl} r^{n-1} e^{-\zeta r} Y_l^m(\theta, \phi), \quad (15)$$

where ζ is an exponent that can be chosen according to a simple set of rules developed by Slater that depend on the atomic number. [30] N_{nl} is the normalization constant. r is the distance between the nucleus and the electron. n is the principal quantum number for the valence orbital, and the spherical harmonic functions $Y_l^m(\theta, \phi)$ depend on the angular momentum quantum numbers l and m .

In ab initio HF theory, STOs suffer from a fairly significant limitation. There is no analytical solution available for the general two-electron integral. [26] The requirement

that such integrals be solved by numerical methods severely limits their utility in molecular systems of any significant size. To speed up molecular integral evaluation, Boys [31] proposed in 1950 the use of Gaussian-type functions instead of STOs for the atomic orbitals in an LCAO wave function. The Gaussian-type functions can be written as:

$$G(r, \theta, \alpha, \phi, n, l, m) = N_l r^l e^{-\alpha r^2} Y_l^m(\theta, \phi), \quad (16)$$

where α is the shielding constant which is an exponent controlling the width of the Gaussian type orbital (GTO). In GTO, the radial decay of the STOs are changed from e^{-r} to e^{-r^2} . Gaussian integral evaluation takes much less computer time than Slater integral evaluation because the product of two Gaussians on two centres is a Gaussian on a third centre. [27] Thus all three- and four- centre two electron repulsion integrals are reduced to two-centre integrals. However, there are two obvious problems connected with using Gaussian functions as basis functions: one is that they do not have cusps at $r=0$ as s-type hydrogen-like atomic orbitals (AOs) do, the other is that they decay faster at larger r than do hydrogen-like AOs. [19] This led to a practice of replacing each STO in a basis set by a number of Gaussian functions. When a basis function is defined as a linear combination of Gaussians, it is referred to as a contracted basis function, and the individual Gaussians from which it is formed are called primitive Gaussians.

There are many terms used to describe a STO basis set. A minimal basis set consists of one STO for each inner-shell and valence-shell AO of each atom. [18] During most molecular bonding, it is the valence electrons which principally take part in the bonding. In recognition of this fact, a split-valence basis set uses two or more STOs for

each valence AO but only one STO for each inner-shell (core) AO. Upon molecule formation, AOs are distorted in shape and have their centres of charge shifted, in asymmetric molecule environments orbitals become distorted from their atomic shapes (polarization). A polarized basis set is adding basis function STOs whose angular quantum numbers are greater than the maximum angular quantum number of the valence shell of the ground-state atom, which is denoted by “*”. [18] Anions tend to have their orbitals expanded compared to neutral molecules, so diffuse functions need to be included. A basis set with diffuse Gaussian functions with fairly small orbital exponents is designated by “+”. [22]

1.3.4 Møller–Plesset perturbation theory

The Hartree-Fock wave function takes into account the interactions between electrons only in an average way which does not consider the instantaneous interactions between electrons. Møller–Plesset perturbation theory is a post-Hartree-Fock method which treats correlated motion of electron pairs better than the Hartree-Fock method. The Møller–Plesset treatment of electron correlation is based on perturbation theory, and this particular approach was described by Møller and Plesset in 1934 [32] and developed into a practical molecular computational method by Binkley and Pople in 1975. [33] There is a hierarchy of Møller–Plesset energy levels: MP0, MP1, MP2, etc... which successively account more thoroughly for interelectronic repulsion. [27] MP0 would use the electronic energy obtained by simply summing the Hartree-Fock one-electron energies, and MP1 is just the Hartree-Fock energy. [27] MP2 is the first MP level to go beyond the Hartree-

Fock treatment, and the MP2 energy is the Hartree-Fock energy plus a correction term that represents a lowering of energy brought about by allowing the electrons to avoid one another better than in Hartree-Fock treatment:

$$E_{MP2} = E_{HF} + E^{(2)} \quad (17)$$

The $E^{(2)}$ is a purely electronic term which represents the perturbation correction, and it can be written as:

$$E^{(2)} = \sum_{s \neq 0} \frac{|\langle \psi_s^{(0)} | \hat{H}' | \phi_0 \rangle|^2}{E_0 - E_s^{(0)}}, \quad (18)$$

where ϕ_0 is the ground-state Hartree-Fock wave function, E_0 is the zeroth order MP energy, $\psi_s^{(0)}$ is the unperturbed wave function, and $E_s^{(0)}$ is the correlated energy. The perturbation \hat{H}' is the difference between the true interelectronic repulsions and the Hartree-Fock interelectronic potential.

Calculated properties like geometries and relative energies tend to be better when done with Møller–Plesset perturbation theory. [27] The essence of the Møller–Plesset method is that the correction term handles electron correlation by promoting electrons from occupied to unoccupied MOs, giving electrons more room to move and thus making it easier for them to avoid one another, and the decreased interelectronic repulsion results in a lower electronic energy. [27]

MP3 calculations take a lot longer than MP2 calculations, but provide little improvement over MP2 molecular properties and so are rarely done. By far, the most common MP level used is MP2. [18]

1.3.5 Density Functional Theory

Density functional theory is based on the two Hohenberg-Kohn [34] theorems, which state that the ground-state properties of an atom or molecule are determined by its electron density function, and that a trial electron density must give energy greater than or equal to the true energy. [27] Density functional theory is based on the electron probability density or the charge density, and designated by $\rho(x, y, z)$. [27] This electron density ρ is measurable by X-ray diffraction or electron diffraction. [35] The electron density is a function of position only, that is, no matter how big the molecule may be, the electron density remains a function of three variables (while the wavefunction of an n -electron molecule will have $4n$ variables). Thus, the density trumps the wavefunction in three ways: it is measurable; it is intuitively comprehensible, and it is mathematically more tractable. [27] The main advantage of density functional theory is that in about the same time needed for a Hartree-Fock calculation one can often obtain results of about the same quality as from MP2 calculations. [27]

The ground state electronic energy E_o is a functional of ρ_o and is written as:

$$E_o = E_o[\rho_o], \quad (19)$$

where the square brackets denote a functional relation. The ground state electronic energy of the real molecule is the sum of the electron kinetic energies, the nucleus-electron attraction potential energies, and the electron-electron repulsion potential energies:

$$E_o = \langle T[\rho_o] \rangle + \langle V_{Ne}[\rho_o] \rangle + \langle V_{ee}[\rho_o] \rangle \quad (20)$$

The angle brackets indicate that these energy terms are quantum-mechanical average values, and each is a functional of the ground-state electron density. For an accurate treatment of the electronic kinetic energy term, Kohn and Sham [36] proposed the density in terms of one-electron orbitals ϕ . Then the electron density can be written as:

$$\rho_s = \sum_i^n |\phi_i|^2 \quad (21)$$

The electron-electron repulsion term can be decomposed into Coulomb and exchange terms, $J[\rho]$ and $K[\rho]$. The final DFT energy expression then can be written as:

$$E_{DFT} = T_s[\rho] + V_{Ne}[\rho] + J[\rho] + E_{xc}[\rho], \quad (22)$$

where the exchange correlation functional $E_{xc}[\rho]$ contains the difference between the exact kinetic energy and T_s , the exchange part of electron-electron repulsions, $K[\rho]$, and correlations to both $K[\rho]$ and $J[\rho]$.

In the Kohn-Sham case, the HF exchange operators are replaced by the functional derivative of the exchange correlation energy.[19] The exact form of $E_{xc}[\rho]$ is not currently known, but a rapidly growing list of approximate exchange correlation functionals have appeared in the literature. [19] Generally, most existing exchange correlation functionals are split into a pure exchange and correlation contribution, $E_x[\rho]$ and $E_c[\rho]$. The functional used in this research is B3LYP method which is a hybrid functional. B3LYP stands for Becke, three-parameter, Lee-Yang-Parr, and it includes 20% exact exchange and involves three semiempirical parameters that were obtained by fits to experimental thermochemical data of small molecules.[37]

1.3.6 Conductor-like Screening Model (COSMO)

All the previous methods of calculations have been done in the gas phase. However, the properties of molecules and transition states can differ considerably between the gas phase and solution. [38] COSMO is a calculation method for determining the electrostatic interaction of a molecule with a solvent which was developed by Klamt and Schüürmann.[39]

The COSMO model is a dielectric model in which the solute molecule is embedded in a molecule-shaped cavity surrounded by a dielectric medium with given dielectric constant ϵ . [27] The key algorithms for calculating the properties of a molecule in solution is to formulate a solution Hamiltonian operator in which these energy terms appear in addition to the in vacuo terms of the electron kinetic energy, electron-nucleus attraction, and electron-electron repulsion. [27] The COSMO model uses a conducting medium (ϵ infinite) and introduces the solvent dielectric constant as a correction factor. [39] The COSMO method is very fast when used, as is usually the case, with gas phase geometries followed by single-point calculations in solvent. The method used in this research is a particular implementation of COSMO that allows efficient geometry optimization in solution is called C-PCM (conductor polarizable continuum model).

1.4 Objectives

The primary objective of this research is to perform a comprehensive ab initio computational study of nickel(II) complexes with water, chloride, hydroxide and ammonia. These series of complexes will be studied up to and including the hexacoordinate species. The studies will include geometry optimization and bond length and frequency analysis. Single point C-PCM calculations will be performed based on the optimized B3LYP/6-31+G* structures. Calculated Raman spectra will be plotted for the optimized HF/6-31+G* complexes. Although this research will not include data at high temperature and pressure, it will provide a good starting point for the experimental work that will be performed at the University of Guelph by the Peter Tremaine group. Even with the Raman data being calculated at zero Kelvin and in the gas phase it will still be applicable to the high temperature, high pressure experiments because the frequencies will not actually deviate that much due to anharmonicity and weaker molecular bonds at high temperature.

Chapter II: Methods

All the calculations were performed using the Gaussian 03 software package on Atlantic Computational Excellence Network (ACEnet). [40]

Gaussian is a computational chemistry software program initially released in 1970 by John Pople and his research group as Gaussian 70 [41], and it has been continuously updated since then. The Gaussian package can do a variety of calculations, like molecular mechanics, semi-empirical calculations, ab initio calculations, etc. In this research, the Unix/Linux version of Gaussian 03 was used. ACEnet is a consortium of Atlantic Canada Universities providing researchers with high performance computing resources. [42] ACEnet has six primary clusters in Atlantic Canada, and the specific cluster used in this research is located at Memorial University of Newfoundland and is named “Placentia”.

The levels of theory used in this research are Hartree-Fock (HF), second order Møller–Plesset perturbation theory (MP2) and B3LYP hybrid density functional theory, and the basis set is 6-31+G* which is widely used for studies of transition metal containing systems. [120] Geometries were optimized using a stepping stone approach, in which the geometries at HF, MP2 and B3LYP levels were optimized sequentially. When this approach failed (as one or more ligands dissociated), the problematic level was skipped. Default optimization specifications were normally used. After each level, a frequency calculation was performed at the same level and the resulting Hessian was used in the following optimization (geom=allcheck). The frequencies depend on the second derivative of the energy with respect to the nuclear positions. A minimum on the

potential energy surface has all the force constants positive. [27] Since a frequency calculation involves taking square root of a force constant, and the square root of a negative number is an imaginary number, and it is called imaginary frequency. [38] Z-matrix coordinates constrained to the appropriate symmetry were used as required to speed up the optimizations. The calculated potential energy surface stationary points were characterized by the vibrational frequencies from the Hessian. All frequencies were real for a true minimum. Optimizations were carried out to completion for all levels in the sequence even if one or more of the levels proved not to be local minima. The structures were visualized with the MOLDEN software package. [43]

The polarized Raman spectra are plotted using a code created by my supervisor, Dr. Cory C. Pye. These spectra were created from the frequency data obtained in the output file of the HF/6-31+G* calculation primarily because Raman intensity calculations are standard in Hartree-Fock frequency calculations. Conductor-like polarizable continuum model (C-PCM) calculations were performed only on the stable, optimized B3LYP/6-31+G* structures. These calculations were single-point calculations and are completed by inserting SCRF=CPCM in the input line of the calculation along with the level of theory and basis set. Water is used as the default solvent.

Chapter III: Hydrated Nickel(II) and Nickel(II) Complexes Combines with Water, Chloride, Hydroxide and Ammonia

The ab initio investigation of nickel(II) complexes throughout this thesis involve four ligands and the complexes that they make with the nickel(II) ion. These ligands are hydroxide (OH^-), water (H_2O), chloride (Cl^-) and ammonia (NH_3). These ligands, and the complexes of them, are all important with respect to the development of the Supercritical Water-Cooled Reactor (SCWR). The formation of these complexes and their transportation throughout the reactor environment may lead to enhanced corrosion and deposition of the pipes and valves and, ultimately, a nuclear leakage.

This chapter includes the computational results and discussion/literature comparison of the nickel(II) complexes with water, chloride, hydroxide and ammonia. These aqua complexes were studied up to and including the hexa-coordinate species. The chloro, hydroxo, and ammine complexes were studied up to hexa-coordinate species with and without water molecules. The water molecules were added to investigate how hydration affects the stability of the given species. All of the results regarding total energies, bond lengths and vibrational frequencies are from the HF, MP2 and B3LYP calculations utilizing the 6-31+G* basis set. These calculations are all zero Kelvin, gas-phase calculations. Molecular geometries are presented for the MP2/6-31+G* and B3LYP/6-31+G* calculations. The aqueous C-PCM results are all from single-point calculations using the fully optimized B3LYP/6-31+G* calculations. All simulated Raman spectra are from the vibrational frequency data calculated from HF/6-31+G* because Raman intensities are standard for HF calculations. All structures shown will

only be those of the absolute energy minima, unless other local minima were found that had noticeably different geometries.

3.1 Water, Hydroxide, Chloride and Ammonia Ligands

Ab initio calculations were performed on the ligands involved with the nickel(II) (with the triplet spin state) complexes for reasons of stability comparison. Table 3A.1, found in the supplementary material section, gives the total energies of the ligands with the given levels of theory (the basis set will be excluded in all energy tables because only results utilizing the 6-31+G* basis set will be reported). Also included in Table 3A.1 is the total free energy in solution, calculated using C-PCM and the optimized B3LYP geometry.

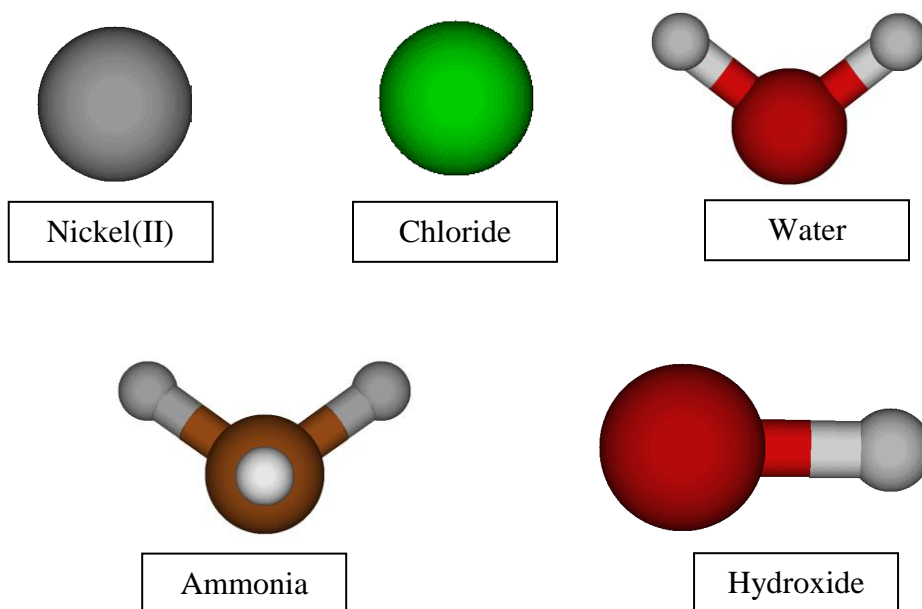


Figure 3-1: Optimized MP2 and B3LYP geometries for the Ni(II) ion and all ligands used in the calculations of nickel(II) complexes.

3.2 Aquanickel(II) Complexes, $[\text{Ni}(\text{H}_2\text{O})_n]^{2+}$, where $n=1-6$

The hydration structure of the Ni(II) ion has been well investigated using various experimental and computational methods. Hydrated nickel(II) complexes are known to form octahedral geometry species with 6-coordinated water molecules at room temperature, as well as tetrahedral complexes with 4-coordinated water molecules at high temperature. [79] Hoffmann et al. [59] showed that the structure about Ni^{2+} changes from 6- to 4- coordinate upon increasing the temperature from 25 °C to 425 °C by XAFS measurement. The majority of the studies on hydrated nickel(II) complexes show that Ni(II) ion is coordinated by six H_2O molecules in the first coordination sphere. The $[\text{Ni}(\text{H}_2\text{O})_6]^{2+}$ ion has been studied by infrared photodissociation spectroscopy [80], X-ray absorption fine structure [81], X-ray absorption near-edge structure [50], molecular dynamics method (MD) [45,50,81,82], Monte Carlo method (MC) [51], ab initio [44,51,53,55,56,61,83], water exchange [47,57], NMR [46], Raman Spectroscopy [68,69], neutron diffraction [58], and X-ray crystallography [48]. The results for the monohydrate [44,45,51,60,67,84] and pentahydrate [44,53,80] have also been reported. Fewer studies have been completed on the dihydrate, trihydrate and tetrahydrate ions. [44]

3.2.1 Results

Stable structures were found for all aquanickel(II) complexes up to and including the hexaaquanickel(II) ion. The total energies, including the aqueous C-PCM energy, for all aqua complexes studied are given in Table 3A.2 in the supplementary materials. The

lowest energy optimized MP2 and B3LYP structures of these complexes are given in Figure 3-2 along with their respective symmetries.

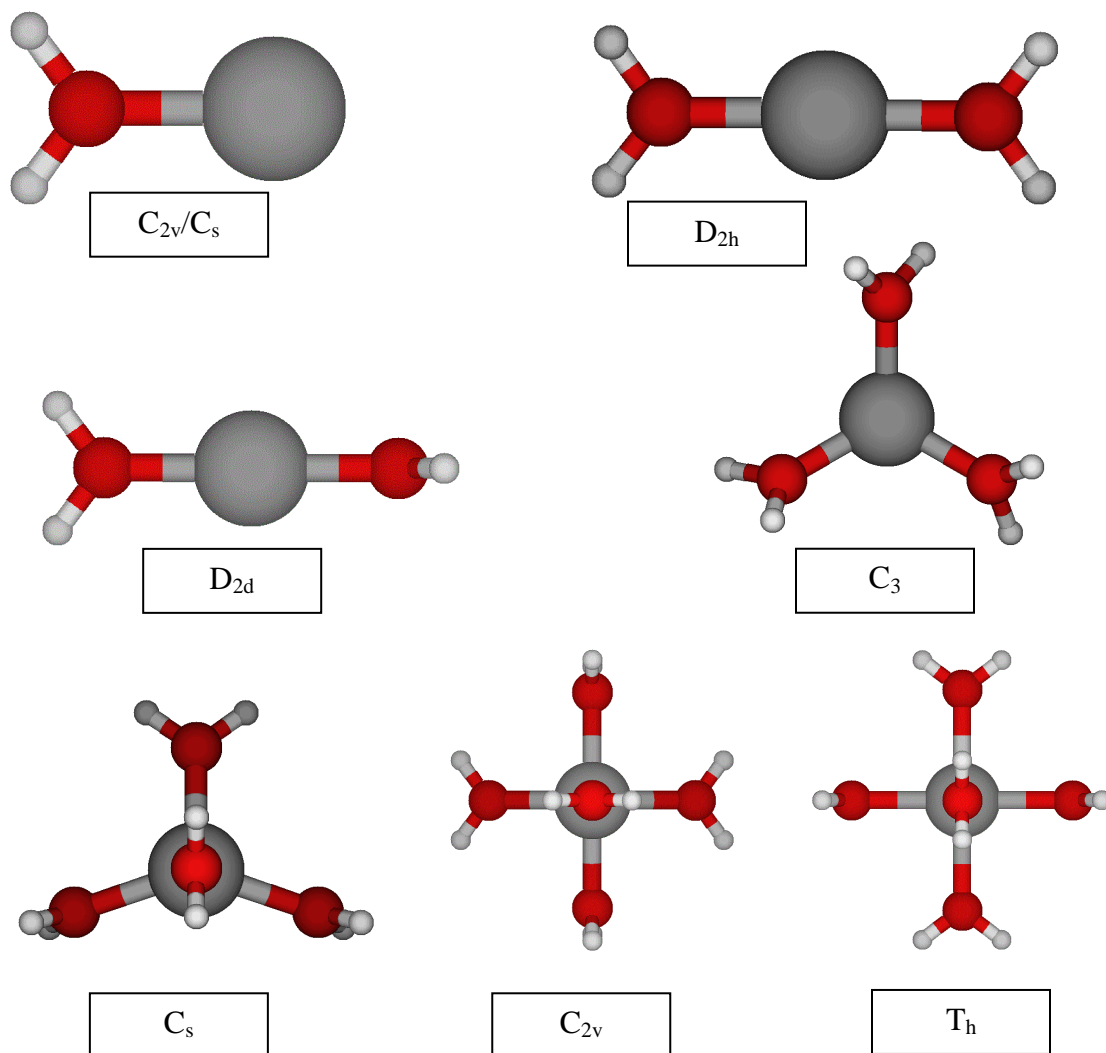


Figure 3-2: Optimized MP2 and B3LYP geometries for $[\text{Ni}(\text{H}_2\text{O})_n]^{2+}$, where $n=1-6$. All structures are similar with the exception of the dihydrate which is D_{2d} at MP2 and D_{2h} at B3LYP. (grey=nickel, red=oxygen, white=hydrogen)

The monohydrate has a preferred symmetry dependent on the level of theory. For MP2 the most stable geometry is C_{2v} , but the C_{2v} structure has an imaginary frequency at B3LYP level. The B3LYP structure was most stable with C_s symmetry. For the dihydrate, D_{2h} and D_{2d} structures were tried first, and D_{2h} structure has lowest energy at B3LYP level, whereas the D_{2d} structure has lowest structure at MP2 level. The preferred structure for triaquanickel was C_3 at both levels. The tetrahydrate has C_s symmetry and the pentahydrate has C_{2v} symmetry. Finally, the hexahydrate has a preferred T_h geometry at both levels.

Plots were constructed of the Ni-O bond lengths and vibrational stretching frequencies and are shown in Figure 3-3, Figure 3-4 and Figure 3-5 for HF, MP2 and B3LYP respectively. The simulated polarized Raman spectrum for the hexaaquanickel(II) species can be found in Figure 3-6.

3.2.2 Discussion/Literature Comparison

The structure found for the monohydrate complex is consistent with the computational study by Bustamante et al. [44]. The Ni-O bond length they found is 1.892 Å, which is slightly longer than the MP2 and B3LYP results presented here of 1.882 Å and 1.861 Å respectively. This difference can be attributed to the fact that Bustamante et al. used BPW91 theory with a larger basis set, 6-311+G(d,p). Iuchi et al. [45] found a value of about 1.900 Å from MD simulation for the Ni-O distance which is also slightly longer than the result from this research. Magnusson and Moriarty [60] found the Ni-O

distance to be 1.906 Å using MP2/6-311+G**. No experimental data was found regarding the monohydrate complex.

The bond lengths for the dihydrate are 1.902 Å and 1.876 Å for MP2 (D_{2d}) and B3LYP (D_{2h}) respectively. Bustamante et al. [44] reported the 1.867 Å for D_{2h} structure which is in agreement with the B3LYP result presented here. Overall the Ni-O bond has increased slightly when compared to the monohydrate. No experimental data was found to compare these results to.

The most stable structure for the trihydrate complex proved to be C_3 for both levels of theory. The Ni-O bond lengths for these structures were found to be 1.942 Å and 1.928 Å for MP2 and B3LYP respectively. Bustamante [44] found Ni-O bond length of about 1.931 Å which is in agreement with the MP2 and B3LYP results. The bond lengths are longer when compared to the mono- and dihydrate values. The result can be attributed to there being an increased number of ligands which would have the effect of repulsion forcing the bonds to be longer. Again, no experimental data was available for comparison.

The tetrahydrate species has C_s symmetry which is most stable. The average Ni-O bond lengths are 1.989 Å and 1.986 Å for MP2 and B3LYP respectively. Bustamante et al. [44] reported a bond length of 1.990 Å for the C_4 geometry. The C_4 structure has also been tested, and it is stable at both levels, but the energies are slightly higher than the C_s structure. Since the symmetry is different, the results from this research cannot be compared to those of Ref. [44]. Other than this study, no others were found regarding molecular structure of tetrahydrate species.

The pentahydrate species that proved to be most stable has C_{2v} symmetry. The average Ni-O bond lengths are 2.032 Å and 2.036 Å for MP2 and B3LYP respectively. Bustamante et al. [44] reported a bond length of 2.047 Å for the same symmetry which is also slightly longer than our results. Mare et al. [53] found the Ni-O distance to be 2.017 Å – 2.052 Å from different basis sets. These values are in agreement with our results.

The hexahydrate species is the most reported of the nickel(II) aqua ion in the literature. The most stable geometry for this ion has been found to be T_h . The Ni-O distances that have been found are 2.071 Å and 2.079 Å for MP2 and B3LYP respectively. There have been many studies on the hexaaquanickel(II) ion. Bustamante et al. [44] reported a bond length of 2.093 Å for the same symmetry. Natália et al. [49] performed classical MD and classical MC simulations and reported Ni-O bond lengths of 2.250 Å and 2.210 Å respectively. Aguilar et al.[51] reported the bond lengths of 2.05 Å and 2.092 Å from MC simulation and B3LYP/LANL2DZ calculation respectively. Mare et al. [53] performed calculations with various programs and basis sets, and obtained values of Ni-O as 2.073 Å (def2-SVP), 2.086 Å (def2-TZVP, def2-aug-TZVP, def2-QZVP), 2.089 Å (TZVP), 2.092 Å (QZV3P), 2.093 Å (TZV2P) and 2.100 Å (DZVP). Varadwaj et al. [55] reported a value of 2.093 Å by RX3LYP/6-311++G(d,p) calculation. Rulíšek et al. [56] used B3LYP/6-311++G(d,p) to give a bond length of 2.087 Å. Akesson et al. [57] reported an average value of 2.108 Å at the HF-SCF level of theory. Fujii et al. [61] found a value of 2.086 Å from B3LYP/6-311+G(d,p) calculation. There are some experimental values of 2.002 Å [46], 2.060 Å [47], 2.10 Å [58] and 2.056 Å [48] determined in the liquid for the coordination of the Ni^{2+} ion with six water molecules. D'Angelo et al.[50] performed a XANES (X-ray absorption near-edge

structure) study on aquanickel(II) and reported a value of 2.03 Å. Inada et al. [52] reported a value of 2.05 Å from extended X-ray absorption experiment. Neilson et al. [54] found the Ni-O distance to be 2.06 Å by ND experiment. Waizumi et al. [62] reported the bond length to be 2.002 Å by XRD method. Magini et al. [63,64] and Caminiti et al. [65] also performed XRD experiments and found the value of 2.069 Å, 2.056 Å - 2.072 Å and 2.05 Å - 2.06 Å respectively in NiCl₂ solution. Sandstrom et al. [66] performed extended X-ray absorption fine structure study on NiCl₂ solutions and give a value of 2.07 Å for Ni-O distance. These computational and experimental data are all in good agreement with our results.

Vibrational stretching frequencies were also calculated for this set of hydrated nickel(II) complexes as seen in Figure 3-3 to 3-5. One of the reasons for calculating these complexes is so that they can be compared to experimental Raman studies that have been or will be completed. They can be used to confirm or refute any experimental Raman findings that cannot be unambiguously assigned to a specific complex. Solution Raman data that could be found regarding these complexes were for hexaaquanickel(II) ion. Fujii et al. [61] performed B3LYP/6-311+G(d,p) calculations and reported the totally symmetric vibrational frequencies to be 347 cm⁻¹, which is in consistent with our results of 335 cm⁻¹ (HF), 355 cm⁻¹ (MP2) and 350 cm⁻¹ (B3LYP). Edwards and Knowles [68] and Bickley et al. [69] performed Raman spectroscopy in formate solution and malonate solution respectively, and their results were 390 cm⁻¹ and 395 cm⁻¹. The calculated results underestimate the values obtained experimentally by 40 cm⁻¹ - 60 cm⁻¹ due to the fact that our calculation did not include solvation effects. These underestimations are consistent

with similar studies completed previously on scandium chloro complexes [70] and zinc chloro complexes [71].

Some general trends can be drawn from the plots of bond lengths and stretching frequencies shown in Figures 3-3 to 3-5. Concerning the bond lengths, as more water ligands are added to the nickel, the Ni-O bond lengths show a general increasing trend. This is caused by overcrowding of the nickel resulting in the electronic repulsion between the water ligands. The opposite trend is seen in the Ni-O vibrational stretching frequencies. As the Ni-O bond lengths increase the vibrational stretching frequencies decrease. This trend is logical because if a bond is longer it will take less energy to cause it to vibrate and therefore have a corresponding frequency that is lower.

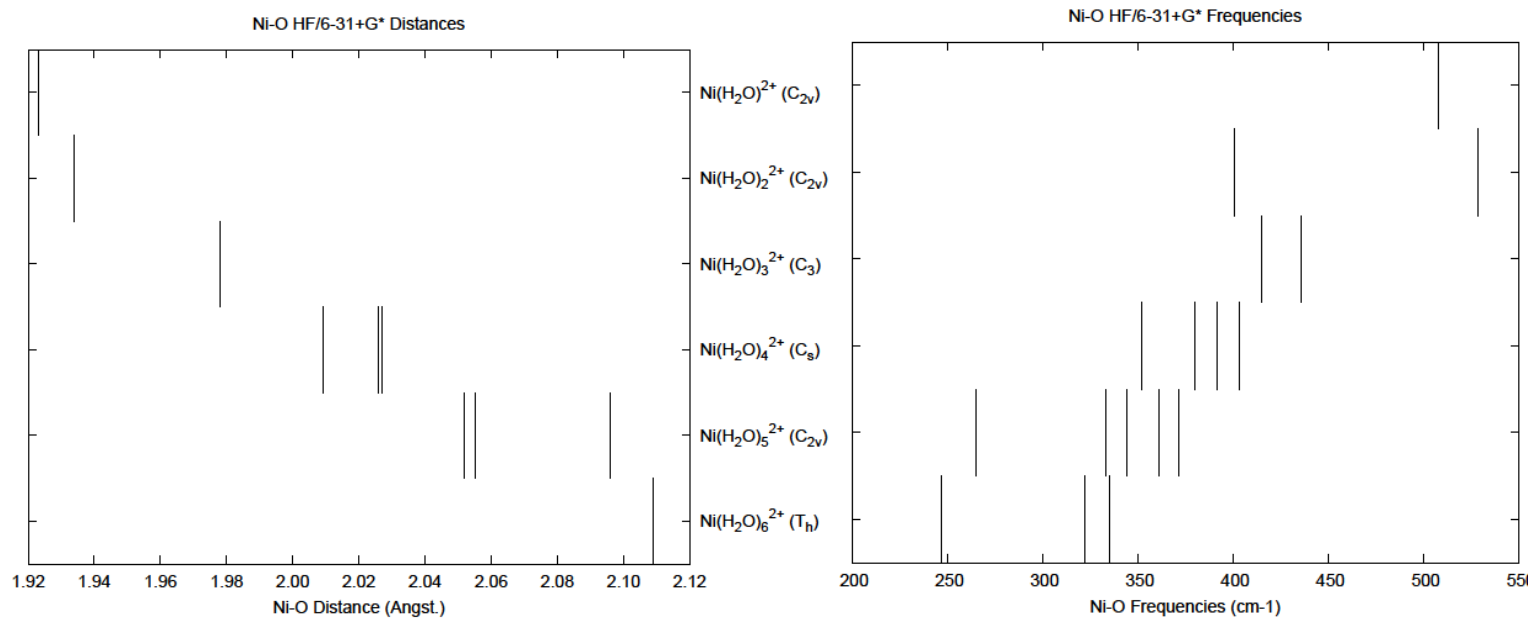


Figure 3-3: Ni-O bond lengths and vibrational stretching frequencies for $[\text{Ni}(\text{H}_2\text{O})_n]^{2+}$, where $n=1-6$, calculated at the HF/6-31+G* level.

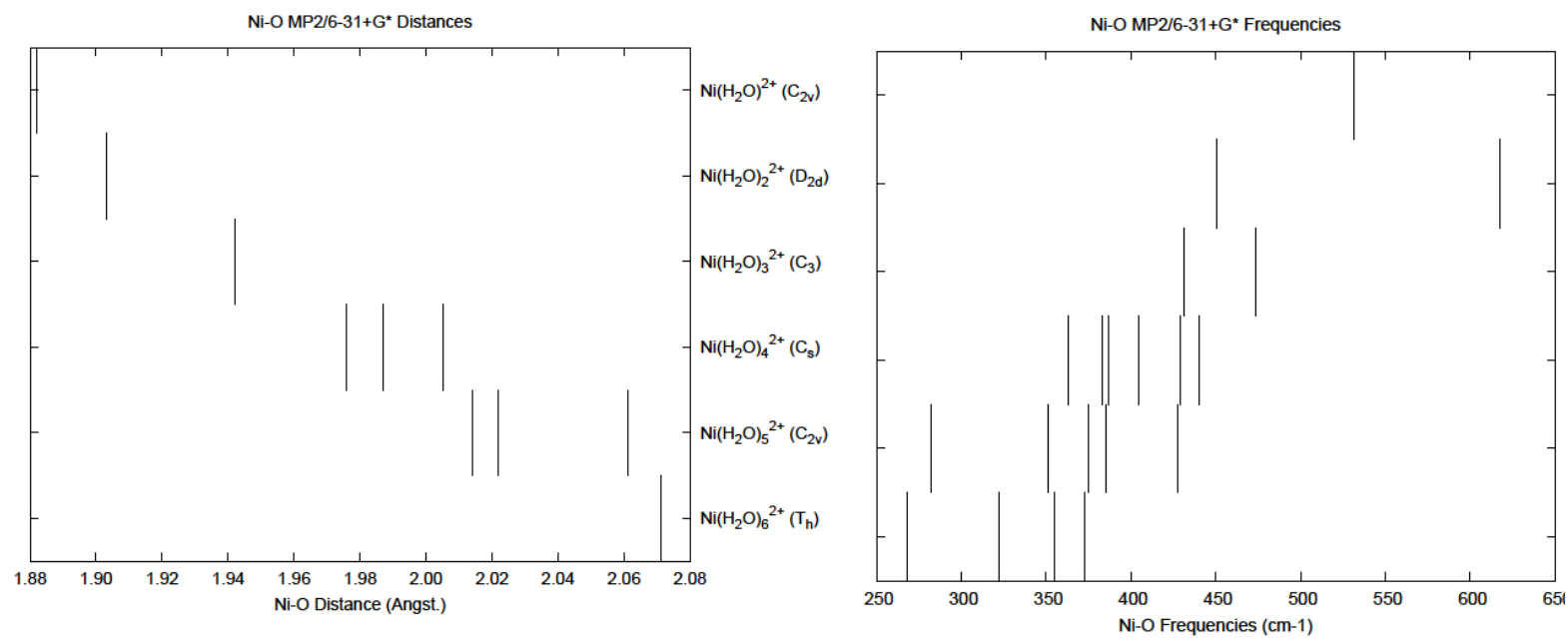


Figure 3-4: Ni-O bond lengths and vibrational stretching frequencies for $[\text{Ni}(\text{H}_2\text{O})_n]^{2+}$, where $n=1-6$, calculated at the MP2/6-31+G* level.

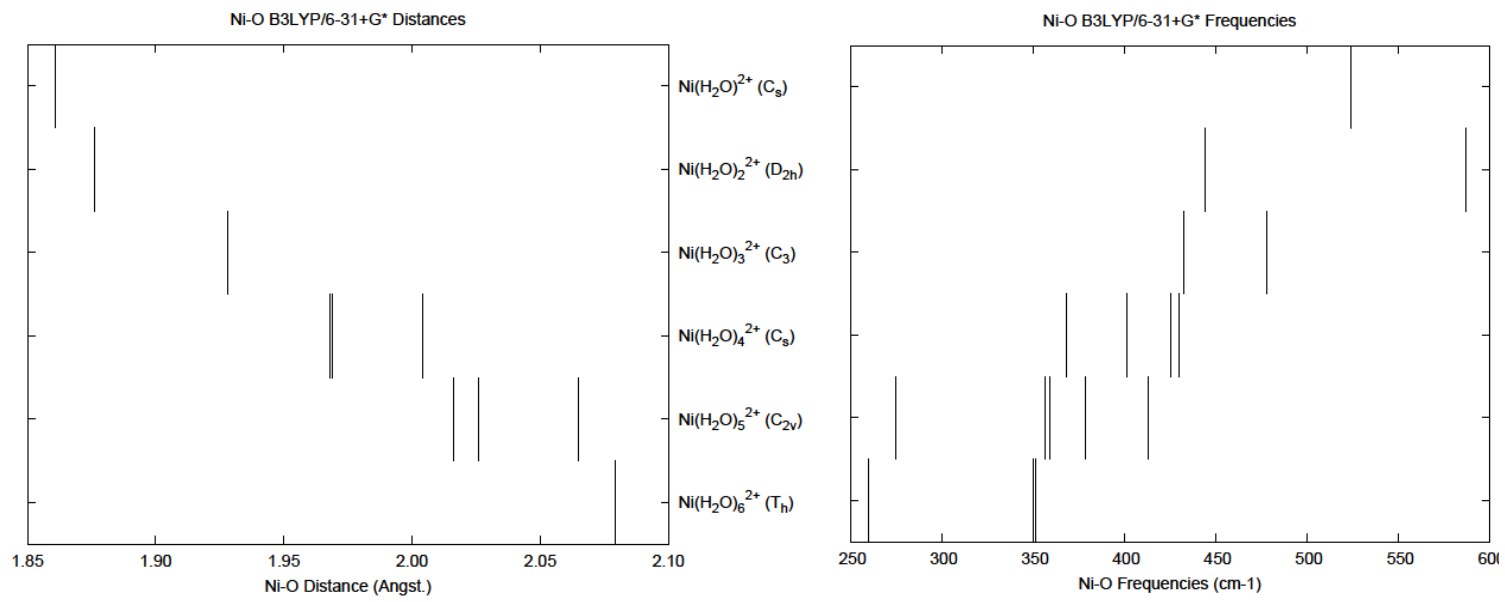


Figure 3-5: Ni-O bond lengths and vibrational stretching frequencies for $[\text{Ni}(\text{H}_2\text{O})_n]^{2+}$, where $n=1-6$, calculated at the B3LYP/6-31+G* level.

3.3 Aquachloronickel(II) Complexes, $[\text{NiCl}_n(\text{H}_2\text{O})_m]^{2-n}$, where $n=1-4$, $m=0-(6-n)$

3.3.1 Results

Nickel chloride complexes are most frequently reported as neutral dichloronickel complex, which has been studied comprehensively by electron diffraction [73], ab initio methods [72,87], X-ray diffraction [74], crystal field study [88], Raman[90], Infrared[89], and UV-vis-NIR[78]. All these studies showed that the NiCl_2 molecule is linear. [85] Lemaire et al. [72] investigated NiCl_n^{2-n} complexes by DFT calculations, and suggested that the NiCl_3^- is the most stable complex. The hydrated nickel chloride is known to form diaquadichloro- [74,91], tetraaquadichloro- [61,62,74,77,86], and pentaquamono-chloro- [61] species. Light green translucent crystals of $\text{NiCl}_2(\text{H}_2\text{O})_4$ (s) can be grown from an aqueous solution of NiCl_2 . [77] In the neutral $\text{NiCl}_2(\text{H}_2\text{O})_4$ complex, the nickel(II) ion is surrounded by four water molecules and two chloride ions, and two of the water molecules are coordinated to nickel approximately in one of the tetrahedral directions; the other two are trigonally coordinated.[77] $\text{NiCl}_2(\text{H}_2\text{O})_4$ can be either the trans- or cis-isomer, where cis- $\text{NiCl}_2(\text{H}_2\text{O})_4$ is more stable than trans- $\text{NiCl}_2(\text{H}_2\text{O})_4$ without solvation, while trans- $\text{NiCl}_2(\text{H}_2\text{O})_4$ is more stable than cis- $\text{NiCl}_2(\text{H}_2\text{O})_4$ when solvation is included. [61] Thermodynamic studies of dehydration have been completed on dichloronickel(II) complexes. [91]

Stable structures were found for all anhydrous chloronickel(II) complexes up to and including tetra-coordinate species. These aquanickel complexes were hydrated and studied further up to and including hexa-coordinate species. The penta- and hexachloronickel were also studied but these structures underwent dissociation of one or

more chloride ligands. Therefore, stable structures for those complexes were not found. The total energies for the stable geometries, as well as the others that were attempted can be found in Table 3A.7 of the supplementary materials section. The geometries of the lowest energy structures can be found in Figure 3-6 for the mono- and dichloronickel complexes and Figure 3-7 for the tri- and tetrachloronickel complexes.

The anhydrous monochloronickel complex has $C_{\infty v}$ symmetry. The monohydrate has C_s symmetry. The dihydrate has stable C_{2v} structure at both levels, but the most stable structure is C_1 . The most stable structure for the trihydrate is C_3 at MP2, but the same symmetry has an imaginary at B3LYP, and the preferred geometry is C_1 at B3LYP. The tetrahydrate has a preferred symmetry dependent on the level of theory. The most stable structure is C_2 for MP2, whereas the most stable structure at B3LYP is C_1 . The most stable pentahydrate has no symmetry at both levels.

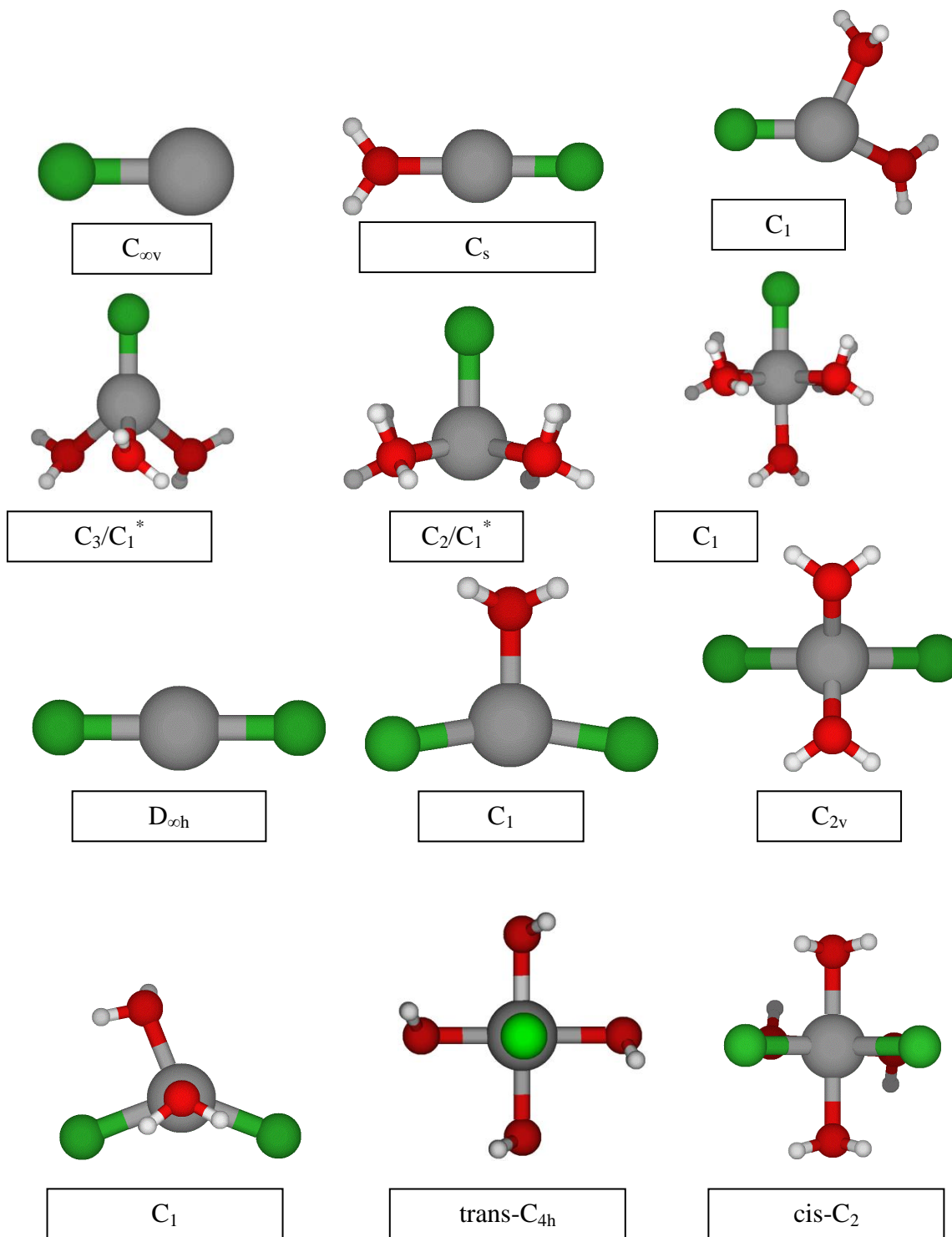


Figure 3-6: Optimized MP2 and B3LYP geometries for $[\text{NiCl}_n(\text{H}_2\text{O})_m]^{2-n}$, where $n=1-2$ and $m=0-(6-n)$. All symmetries marked with “*” indicate B3LYP otherwise all MP2 and B3LYP structure are similar. (grey=nickel, red=oxygen, white=hydrogen, green=chloride)

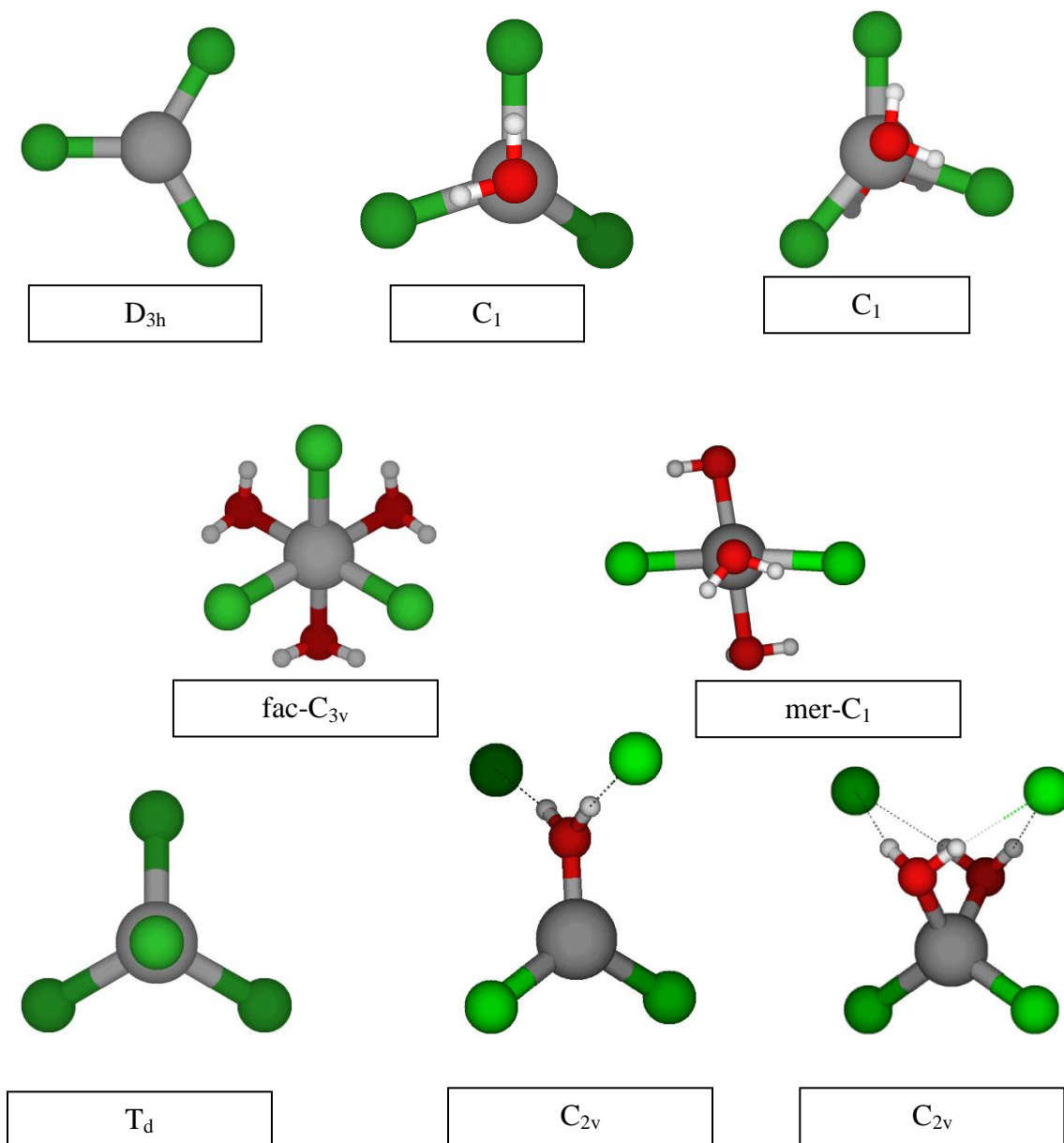


Figure 3-7: Optimized MP2 and B3LYP geometries for $[NiCl_n(H_2O)_m]^{2-n}$, where $n=3-4$ and $m=0-(6-n)$.

The anhydrous dichloronickel complex has D_{3h} symmetry. The stable structure of the monohydrate is C_1 at both levels. The dihydrate is stable with C_{2v} symmetry. The stable structure of the trihydrate is without symmetry at C_1 . The tetrahydrate has stable $cis-C_2$ and $trans-C_{4h}$ (with lowest energy) structures at both levels.

The anhydrous trichloronickel complex did not cause any symmetry problems, and at both levels showed a preferred D_{3h} symmetry. The monohydrate has a stable C_s structure at HF level, but it showed an imaginary frequency at MP2 and B3LYP levels. The C_1 symmetry was preferred at both levels. The stable structure of the dihydrate is without symmetry at C_1 at both levels. The trihydrate complex has lowest structure C_{3v} at both levels. The meridional (mer) C_1 structure is also stable and competitive in energy.

The anhydrous tetrachloronickel complex did not cause any symmetry problems and at both levels showed a preferred T_d symmetry. The stable structure of the monohydrate has C_{2v} geometry with two chlorides hydrogen bonded to the hydrogen atoms respectively. The stable structure of the dihydrate has C_{2v} symmetry with two chlorides hydrogen bonded with two hydrogen atoms from two different water molecules.

No stable structures were found for the penta- and hexachloronickel(II) complexes. All the geometries attempted showed dissociation of chloride ligands. Since stable structures were not found for these complexes, they will not be discussed further.

Plots of the Ni-O and Ni-Cl bond lengths and vibrational stretching frequencies were constructed and can be seen in Figure 3-8, Figure 3-9, and Figure 3-10 for HF, MP2 and B3LYP respectively. Within the plots, the lines highlighted in red indicate which bond lengths and stretching vibrations involve chloride ligands. Simulated polarized Raman spectra were also created for the stable HF structures and can be found in Figure 3A-2 of the supplementary materials section.

3.3.2 Discussion/Literature Comparison

Structural comparisons made between our results and the literature found on these complexes will be done primarily through bond length data. Lemaire et al. [72] reported from BLYP/6-31G* calculations of NiCl_n^{2-n} ($n=1-4$) with the same symmetry as our results. The bond lengths reported by Lemaire et al. [72] are 2.11 Å, 2.11 Å, 2.23 Å, and 2.38 Å respectively (NiCl_n^{2-n} , $n=1-4$). Our results for NiCl_3^- and NiCl_4^{2-} are 2.24 Å and 2.40 Å at B3LYP level which are in good agreement with their results, and our results for NiCl^+ and NiCl_2 are 2.02 Å and 2.07 Å which are lower than their results about 0.09 Å – 0.04 Å at B3LYP level. Their study also showed that nickel complexes with more than four chlorine atoms are not stable. Hargittai et al. [73] reported the NiCl_2 bond distance of 2.076 Å by a combined gas-phase electron diffraction and vibrational spectroscopic experiment which is in consistent with our result. Ashworth et al. [75] reported the experimental value of NiCl_2 bond length to be 2.056 Å. Marcus [76] reported the Ni-Cl distance of NiCl_2 to be 2.07 Å. Waizumi et al. [74] reported the Ni-Cl bond length of NiCl_2 to be 2.06 Å. All these data are in good agreement with our results.

A few data have been found for hydrated nickel chloride. Fujii et al. [61] reported the Ni-O and Ni-Cl bond lengths for $\text{NiCl}(\text{H}_2\text{O})_5^+$ to be 2.11-2.13 Å and 2.29 Å respectively by B3LYP/6-311+G(d,p) calculations. Fujii et al. [61] also calculated the Ni-O and Ni-Cl bond lengths for *cis*- $\text{NiCl}_2(\text{H}_2\text{O})_4$ to be 2.108-2.109 Å and 2.347 Å respectively. They also reported the geometries for *trans*- $\text{NiCl}_2(\text{H}_2\text{O})_4$, which has higher energy than the *cis*-isomer. Waizumi et al. [62] and Ptasiwicz-Bak et al. [77] performed X-ray diffraction experiments on $\text{NiCl}_2(\text{H}_2\text{O})_4$ crystals, and obtained the Ni-O bond

lengths to be 2.063 Å and 2.089 Å, and the Ni-Cl bond lengths to be 2.375 Å and 2.400 Å respectively. Waizumi et al. [74] reported the Ni-O and Ni-Cl bond lengths of $\text{NiCl}(\text{H}_2\text{O})_5^+$ to be 2.05 Å and 2.36 Å respectively by X-ray diffraction experiments. For the $\text{NiCl}(\text{H}_2\text{O})_5^+$, our results are 2.0887-2.1088 Å (Ni-O) and 2.2507 Å (Ni-Cl) at MP2, and 2.1007-2.1366 Å (Ni-O) and 2.2904 Å (Ni-Cl) at B3LYP. For the $\text{cis-NiCl}_2(\text{H}_2\text{O})_4$, our results are 2.082-2.135 Å (Ni-O) and 2.309 Å at MP2, and 2.104-2.152 Å (Ni-O) and 2.353 Å at B3LYP. Our results are in good agreement with the computational results, and underestimate the Ni-Cl bond lengths by 0.022-0.091 Å when compared with the XRD experimental results.

The plots of Ni-O and Ni-Cl bond lengths and vibrational stretching frequencies can be found in Figures 3-8 to 3-10, and some general trends can be seen from the plots. As more water molecules are added to the system, the Ni-O and Ni-Cl bond lengths increased and the vibrational stretching frequencies decreased respectively. The Ni-O bond lengths are uniformly shorter than the Ni-Cl bond length by 0.1-0.3 Å. As the Ni-O and Ni-Cl bond lengths increase, the bond becomes weaker and it requires less energy to stretch, so that the vibrational frequency becomes lower. The Raman active frequencies are important for comparison with experiment. Simulated polarized Raman plots are located in Figure 3A-2 in the supplementary materials section. These plots are based on Raman intensities calculated at the HF level of theory. Unfortunately no experimental Raman data was found to compare these results with.

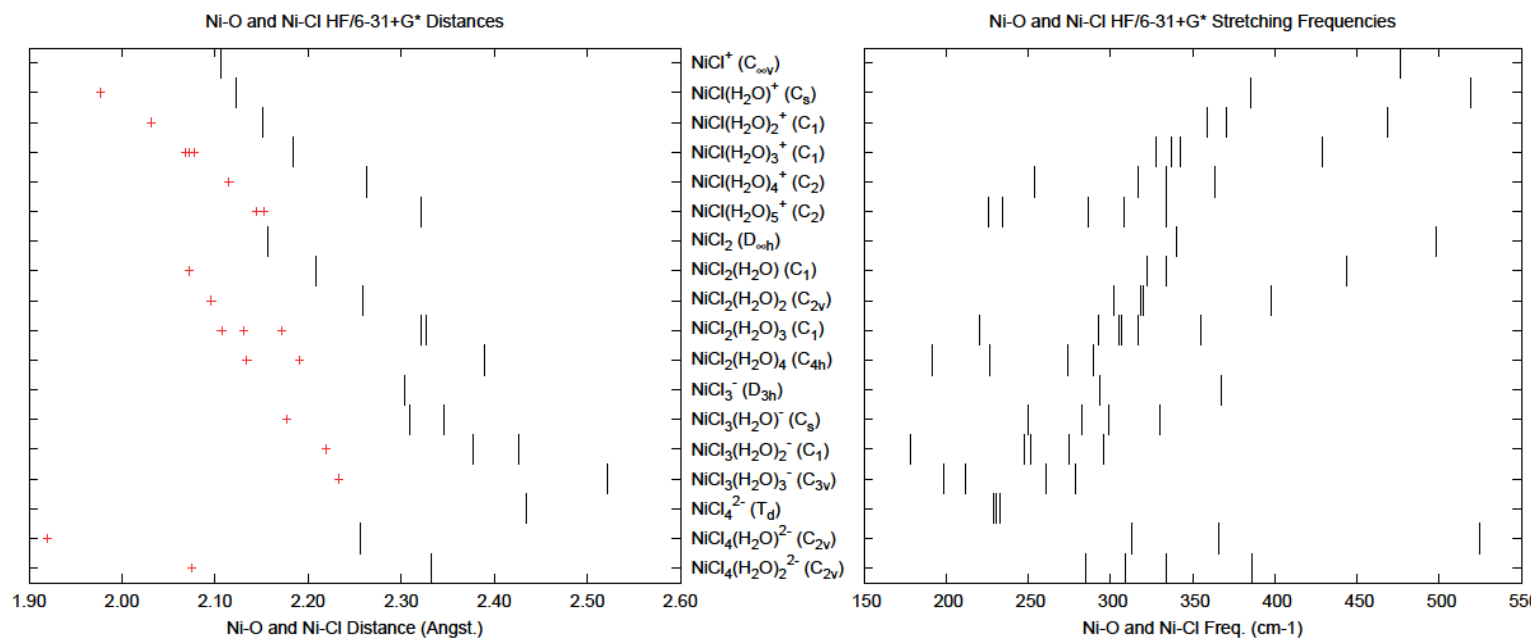


Figure 3-8: Ni-O (red “+”) and Ni-Cl bond lengths and vibrational stretching frequencies for $[\text{NiCl}_n(\text{H}_2\text{O})_m]^{2-n}$, where $n=1-4$, $m=0-(6-n)$, calculated at the HF/6-31+G* level.

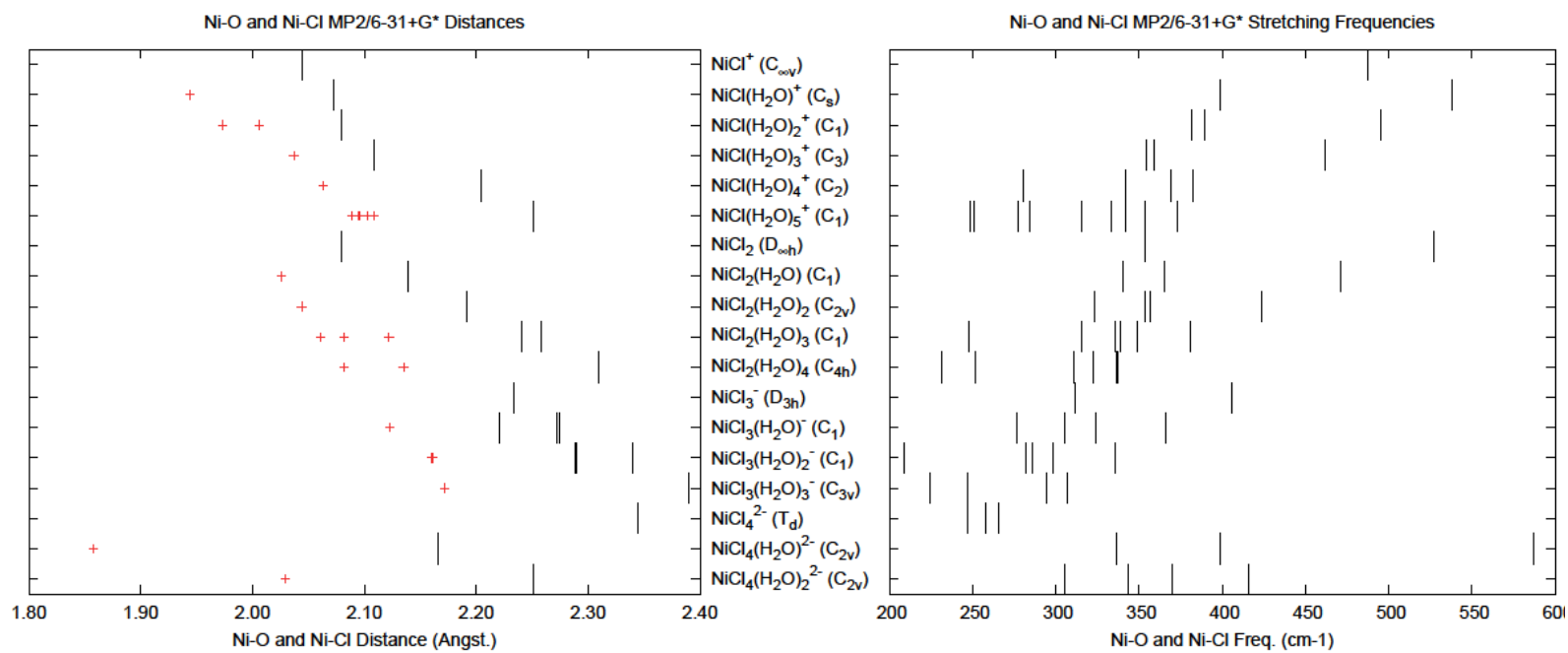


Figure 3-9: Ni-O (red “+”) and Ni-Cl bond lengths and vibrational stretching frequencies for $[\text{NiCl}_n(\text{H}_2\text{O})_m]^{2-n}$, where $n=1-4$, $m=0-(6-n)$, calculated at the MP2/6-31+G* level.

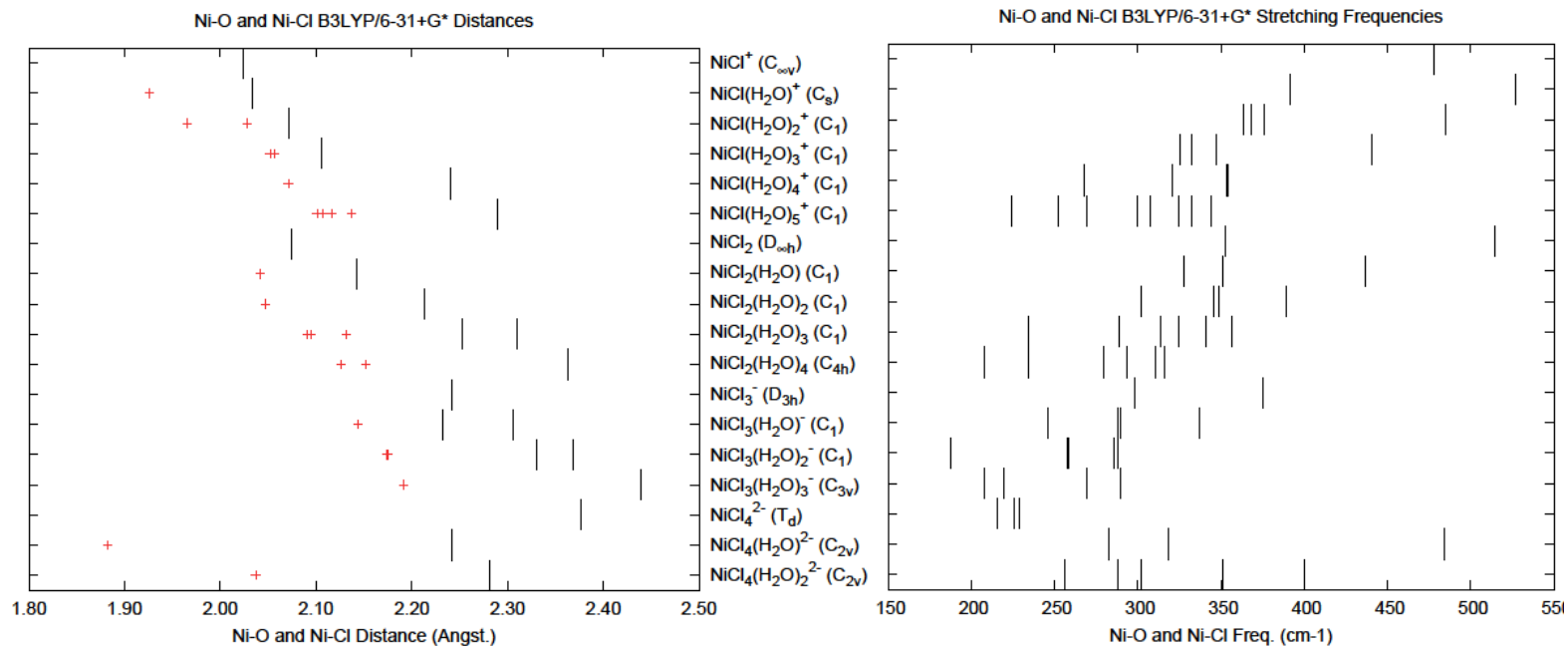


Figure 3-10: Ni-O (red “+”) and Ni-Cl bond lengths and vibrational stretching frequencies for $[\text{NiCl}_n(\text{H}_2\text{O})_m]^{2-n}$, where $n=1-4$, $m=0-(6-n)$, calculated at the B3LYP/6-31+G* level.

3.4 Aquahydroxynickel(II) Complexes, $[\text{Ni}(\text{OH})_n(\text{H}_2\text{O})_m]^{2-n}$, where $n=1-4$, $m=0-(6-n)$

Nickel radioisotopes are known to form poorly crystalline $\text{Ni}(\text{OH})_2$ under highly alkaline conditions ($\text{pH} > 12.5$). [97] Nickel hydroxide is widely used as the active material for positive electrode in alkaline secondary batteries. [99] Nickel hydroxide has a hexagonal layered structure with two polymorphs, α and β . [100] The β - $\text{Ni}(\text{OH})_2$ is well crystallized, and it possesses a brucite-like structure, whereas the α - $\text{Ni}(\text{OH})_2$ is unstable, poorly crystallized and consists of a stacking of positively charged $\text{Ni}(\text{OH})_{2-x}$ layers, with intercalated anions and water molecules in the interlayer space to restore charge neutrality. [101] The α -nickel hydroxide is a metastable phase and it changes rapidly to the β -form in strong alkali. [100] The nickel hydroxide has been studied comprehensively by experiments. Spectroscopic studies on nickel hydroxide have been completed by Infrared [94], UV/Vis spectroscopy [95], Extended X-ray absorption fine structure [96], diffuse reflectance spectroscopy (DRS) [97], X-ray diffraction [98], inductively coupled plasma atomic emission spectroscopy (ICP-AES) [99] and Raman spectroscopy [102,103]. There are additional reports on nickel hydroxide, like synthesis of the α - [99,100] and β - [99,100,101] forms and solubility under various temperature and pH conditions [104,105]. The monohydroxide nickel(I) is used as an additive to increase the discharge capacity of Cd electrodes. [94] The NiOH^+ has been studied by computational methods [60,92-94], and the bond lengths, binding energies and infrared spectra have been calculated. For $\text{Ni}(\text{II}) \sim 10^{-8}$ M and $\text{pH} \sim 8$, higher order hydrolysis complexes like $\text{Ni}(\text{OH})_3^-$, $\text{Ni}(\text{OH})_4^{2-}$ have been reported by Baes and Mesmer [106]. Solubility measurements of NiO have also shown the existence of tri- and tetrahydroxo nickel complexes, as well as the

existence of $\text{Ni}_4(\text{OH})_4^+$ in a high pH environment.[104] A computational study of the structures for $[\text{Ni}(\text{OH})(\text{H}_2\text{O})_5]^+$ and $[\text{Ni}(\text{OH})_2(\text{H}_2\text{O})_4]$ has been completed. [61] The structural, energetic and electronic properties of $[\text{Ni}(\text{OH})(\text{H}_2\text{O})_5]^+$, $[\text{Ni}(\text{OH})_2(\text{H}_2\text{O})_2]$, $[\text{Ni}(\text{OH})_2(\text{H}_2\text{O})_3]$, $[\text{Ni}(\text{OH})_2(\text{H}_2\text{O})_4]$ have also been studied by computational methods. [95]

3.4.1 Results

Stable structures were found for all hydroxide complexes up to and including the hexacoordinate tetrahydroxo species. Calculations were also completed on the penta- and hexahydroxo complexes, but these species showed dissociation of one or more hydroxide ligand and preferred to exist as ion pairs. Stable structures of these ion pair complexes were not found. Total energies, as well as C-PCM energies for all hydroxide complexes studied can be found in Table 3A-12 of the supplementary materials section. Optimized geometries of the stable complexes are located in Figure 3-11 for the mono- and dihydroxo complexes and in Figure 3-12 for the tri- and tetrahydroxo complexes.

The anhydrous monohydroxo complex did not cause any symmetry problems as all levels showed a preferred C_s symmetry with the bent Ni-O-H angle. For the monohydrate, C_s structure was tried first, and it is stable but higher in energy than the C_1 species at both levels. The C_1 structure looks similar to the C_s structure, but the hydroxide ligand is slightly twisted. Two C_s structures were tried for the dihydrate, but they both showed imaginary frequencies at both levels. The C_1 symmetry is preferred at both levels. Various C_s structures were also tried for the trihydrate, and ultimately the only stable structure is C_1 . The preferred tetrahydrate structure is C_1 , and no stable structures with

higher symmetry were found. The most stable pentahydrate has no symmetry at both levels.

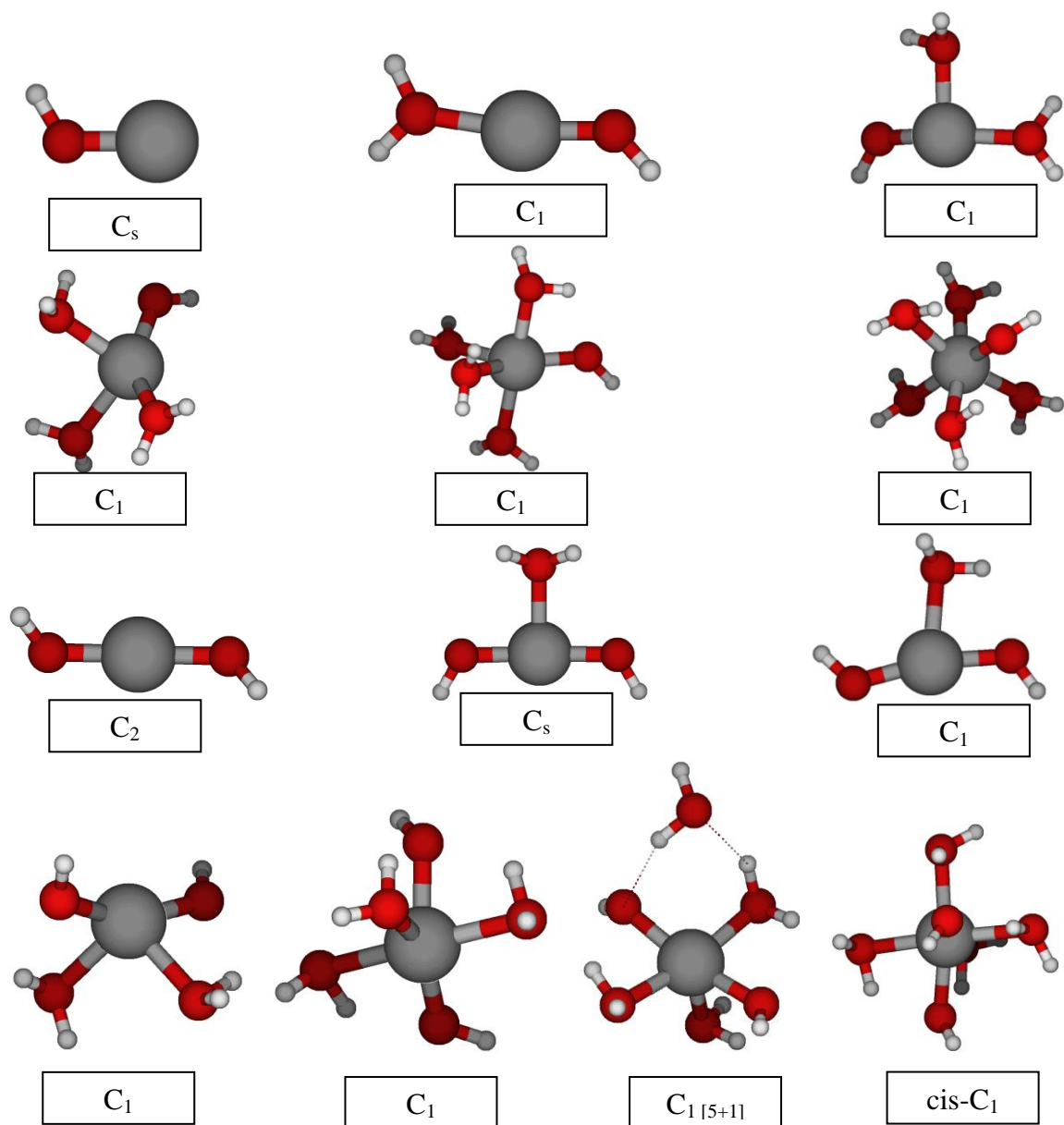


Figure 3-11: Optimized MP2 and B3LYP geometries for $[\text{Ni}(\text{OH})(\text{H}_2\text{O})_n]^+$ and $[\text{Ni}(\text{OH})_2(\text{H}_2\text{O})_n]$. (grey=nickel, white=hydrogen, red=oxygen)

For the anhydrous dihydroxonickel, two C_{2v} structures were tried first, but only the “W” shaped structure was stable at both levels, and a C_2 structure was proved to be an energy minimum. For the monohydrate, the C_s structure was only a minimum at MP2 level, and the C_1 structure was preferred otherwise. The only stable geometry found for the dihydrate and trihydrate has C_1 symmetry at both levels. The tetrahydrate was stable with C_1 symmetry with a water molecule in the second hydration sphere. A cis- C_1 structure with all the ligands directly bonded to nickel is also stable but competitive in energy.

The anhydrous trihydroxonickel has stable C_3 and C_1 structures at both levels, and they are competitive in energy. The C_3 structure proved to be a minimum. When a single water adds to $Ni(OH)_3^-$, a C_s structure is formed although it is not stable at both levels. The only stable structure found for the monohydrate has C_1 symmetry with a water molecule migrated to the second solvation shell. For the dihydrate, also the only stable structure found was C_1 with a water molecule in the second hydration sphere and hydrogen bonded to the other water molecule which is directly bonded to the central nickel and one of the hydroxide. For the trihydrate, a facial (fac) C_{3v} structure with all the ligands directly bonded to the central nickel was located, but it is only stable at MP2 level. The three water molecules migrated to the second hydration sphere to form new C_{3v} and C_3 (with lower energy) structure at B3LYP level.

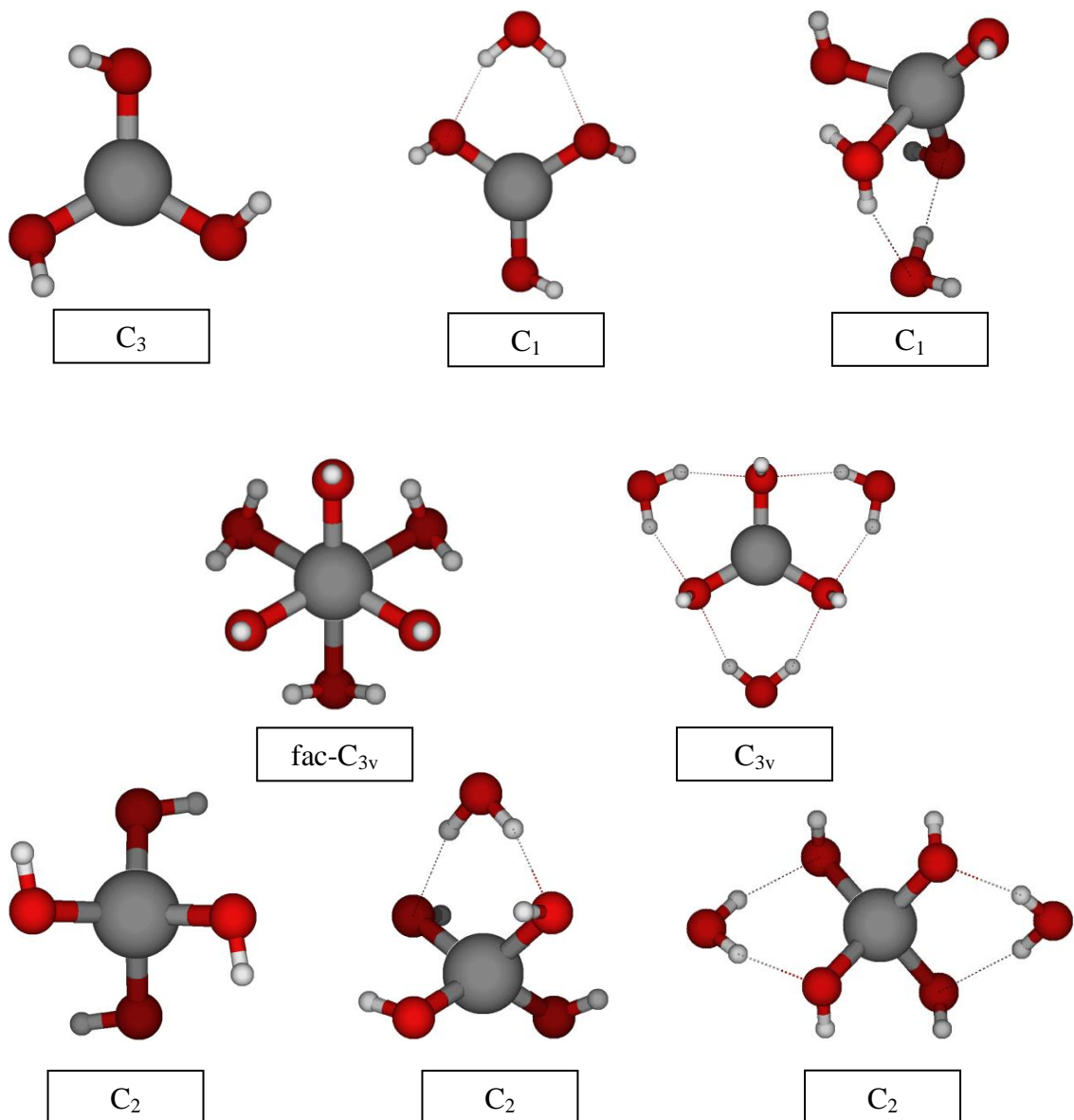


Figure 3-12: Optimized MP2 and B3LYP geometries for $[\text{Ni}(\text{OH})_3(\text{H}_2\text{O})_n]^-$ and $[\text{Ni}(\text{OH})_4(\text{H}_2\text{O})_n]^{2-}$.

For the anhydrous tetrahydroxonickel, stable structures found were S_4 and C_2 , with C_2 being energetically preferred at both levels. The only stable structure found for monohydrate was also with C_2 symmetry in which the water molecule in the second hydration sphere and hydrogen bonded to the hydroxide ligands. The dihydrate was also

only stable at C_2 geometry with two water molecules in the second hydrogen sphere and hydrogen bonded to the hydroxide ligands.

Bond length and vibrational stretching frequency data was also tabulated for all the stable aquahydroxo complexes and can be found in the supplementary materials section. Plots of the bond lengths and vibrational stretching frequencies can be found in Figure 3-13, Figure 3-14 and Figure 3-15 for HF, MP2 and B3LYP respectively. Simulated polarized Raman spectra can be found in Figure 3A-3 of the supplementary materials section.

3.4.2 Discussion/Literature Comparison

The geometries that have been found can primarily be confirmed by comparison with available data from crystal structures found in literatures, or other computational studies that have been completed on similar complexes. The Ni-O-H bond angles are always bent in all the aquahydroxo complexes at all levels.

Previous ab initio calculations can be compared to this work. Our results for the Ni-O bond length of $Ni(OH)^+$ are 1.734 Å and 1.768 Å for the MP2 and B3LYP levels respectively. Magnusson and Moriarty [60] found 1.76 Å for the Ni-O distance which is in good agreement with our B3LYP calculations. Trachtman et al. [92] found that the $Ni(OH)^+$ ion had a Ni-O distance of 1.779 Å which is slightly longer than our results. It could be explained by their relatively larger basis set (6-311++G**). Ricca and Bauschlicher [93] obtained the Ni-O bond length to be 1.712 Å which is about 0.022-0.056 Å as they used a different basis set ([8s4p3d] contraction of the (14s9p5d) primitive set). Wang et al. [94] reported the Ni-O distance to be 1.764 Å by B3LYP/6-

311++G(3df,3pd) calculations. Although Wang et al. used a larger basis set, their result is consistent with our B3LYP result. No one has examined the partially hydrated structures, so only the pentahydrate structures can be compared. Fujii et al. [61] obtained 1.944 Å (Ni-OH) and 2.11-2.14 Å (Ni-OH₂) for the pentahydrate Ni(OH)⁺ by B3LYP/6-311+G calculations. Their results are in agreement with what been found for the Ni-O distances to be 1.926 Å (Ni-OH) and 2.090-2.119 Å (Ni-OH₂) at MP2 level, and 1.936 Å (Ni-OH) and 2.110-2.138 Å (Ni-OH₂) at B3LYP level respectively.

The calculated Ni-O bond distance for Ni(OH)₂ is 1.761 Å and 1.730 Å for MP2 and B3LYP respectively. Wang et al. [94] obtained a C_{2h} structure with the Ni-O distance of 1.737 Å using B3LYP/6-311++G(3df,3pd). Our C₁ structure is very similar to the C_{2h} structure, and the C_{2h} structure was also been tested, but there are imaginary frequencies at both levels. These results could also been compared to previous experimental data. Pandya et al. [96] examined the EXAFS data of β-Ni(OH)₂ and reported the Ni-O bond length to be 2.07 Å. Vespa et al. [97] found the Ni-O distance to be 2.06 Å by EXAFS. McEwen [98] found 2.14 Å for the Ni-O bond length from crystallographic analysis. All their results are much higher than our calculated data as our calculations are performed on single Ni(OH)₂ molecule in gas phase, and their experiments used nickel hydroxide crystals with the nickel surrounded by six equidistant oxygen atoms. Godelitsas et al. [95] reported a computational study containing results for the di-, tri, and tetrahydrate species using B3LYP/LANL2DZ calculations. The dihydrate dihydroxo complex that they found contained Ni-O bond lengths of 1.874 Å and 1.878 Å (Ni-OH) and 2.076 Å and 2.107 Å (Ni-OH₂). They also reported the Ni-O distances of the trihydrate to be 1.899-2.033 Å (Ni-OH) and 2.077-2.153 Å (Ni-OH₂). These results are in agreement with what been

found for MP2 as 1.860-1.863 Å (Ni-OH) and 2.104-2.134 Å (Ni-OH₂), B3LYP as 1.837-1.841 Å (Ni-OH) and 1.955-2.213 Å (Ni-OH₂) for the dihydrate; MP2 as 1.871-1.950 Å (Ni-OH) and 2.157-2.191 Å (Ni-OH₂), B3LYP as 1.842-1.953 Å (Ni-OH) and 2.176-2.238 Å for the trihydrate. The structure they reported for the tetrahydrate has two water molecules in the second hydration sphere, whereas our structure has only one water molecule in the second hydration shell. Fujii et al. [61] found 1.998 Å (Ni-OH) and 2.17-2.19 Å (Ni-OH₂) for the tetrahydrated nickel hydroxide which is slightly longer than our results of 1.924-1.957 Å (Ni-OH) and 2.102-2.155 Å (Ni-OH₂) at MP2; 1.933-1.968 Å (Ni-OH) and 2.104-2.179 Å (Ni-OH₂) at B3LYP due to the larger basis set (6-311+G(d,p)). There were no other literature reports found regarding the remaining nickel complexes which have been investigated in this study and therefore nothing could be compared with the optimized geometries.

Plots were constructed of the Ni-O bond lengths and vibrational stretching frequencies and can be found in Figures 3-13 to 3-15. Within each of these plots a trend can be seen of increasing Ni-O bond length and decreasing Ni-O vibrational stretching frequencies with addition of water ligands. The Ni-OH₂ and Ni-OH bond lengths separated clearly, and the Ni-OH bond lengths are always significantly shorter than that of Ni-OH₂ due to its stronger attraction to Ni²⁺, and the Ni-OH stretching frequencies are always about 200-400 cm⁻¹ larger than Ni-OH₂ stretching frequencies.

Raman spectroscopy will be the primary experimental technique used to identify these compounds at high temperatures and pressures, based on the Raman active bands that have been calculated. This experimental work has not been completed yet and no

Raman data was found in the literature related to this set of nickel(II) hydroxide complexes. However, predicted polarized Raman spectra have been constructed based on intensities calculated at the HF level of theory and can be found in Figure 3A-3 of the supplementary materials section.

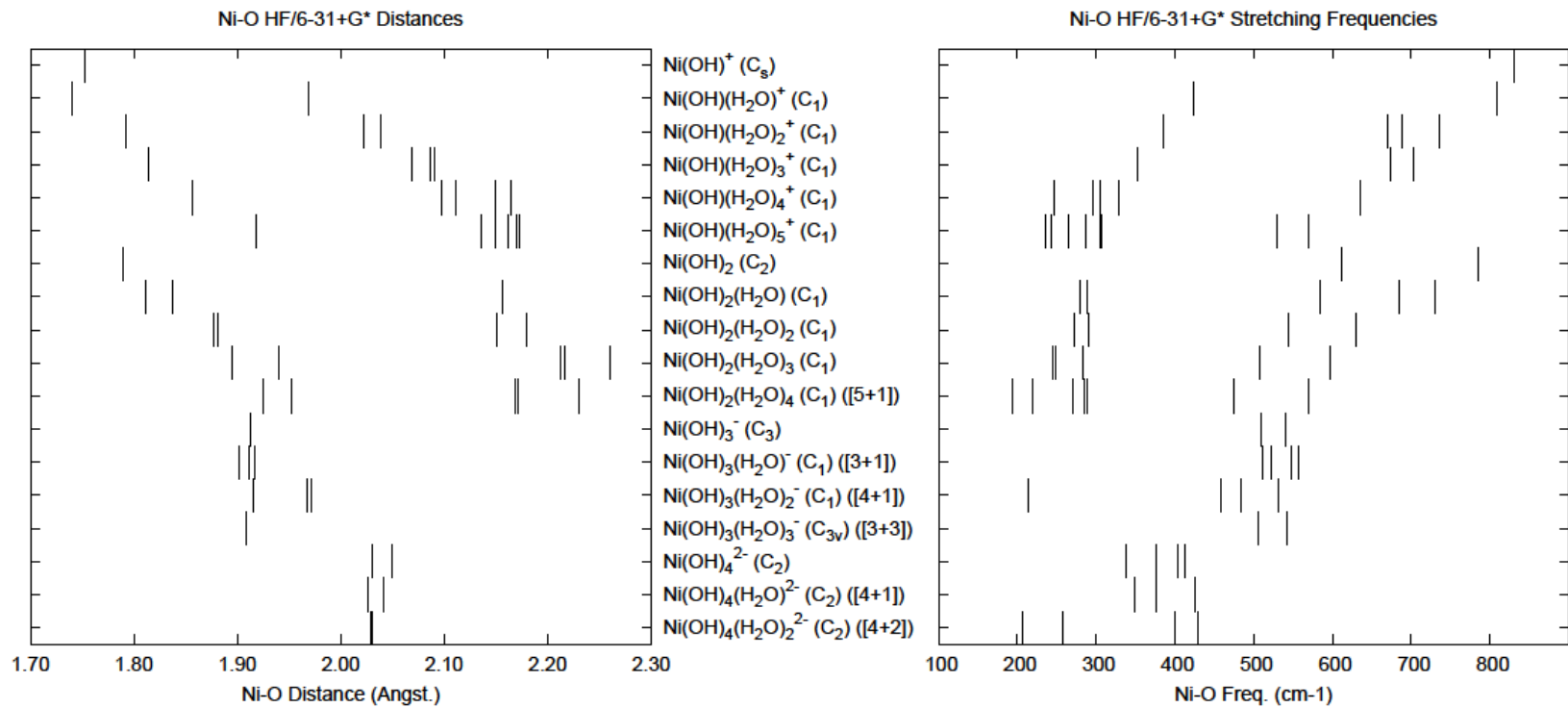


Figure 3-13: Ni-O bond lengths and vibrational stretching frequencies for $[\text{Ni}(\text{OH})_m(\text{H}_2\text{O})_n]^{2-m}$, where $m=1-4$, $n=0-(6-n)$, calculated at the HF/6-31+G* level.

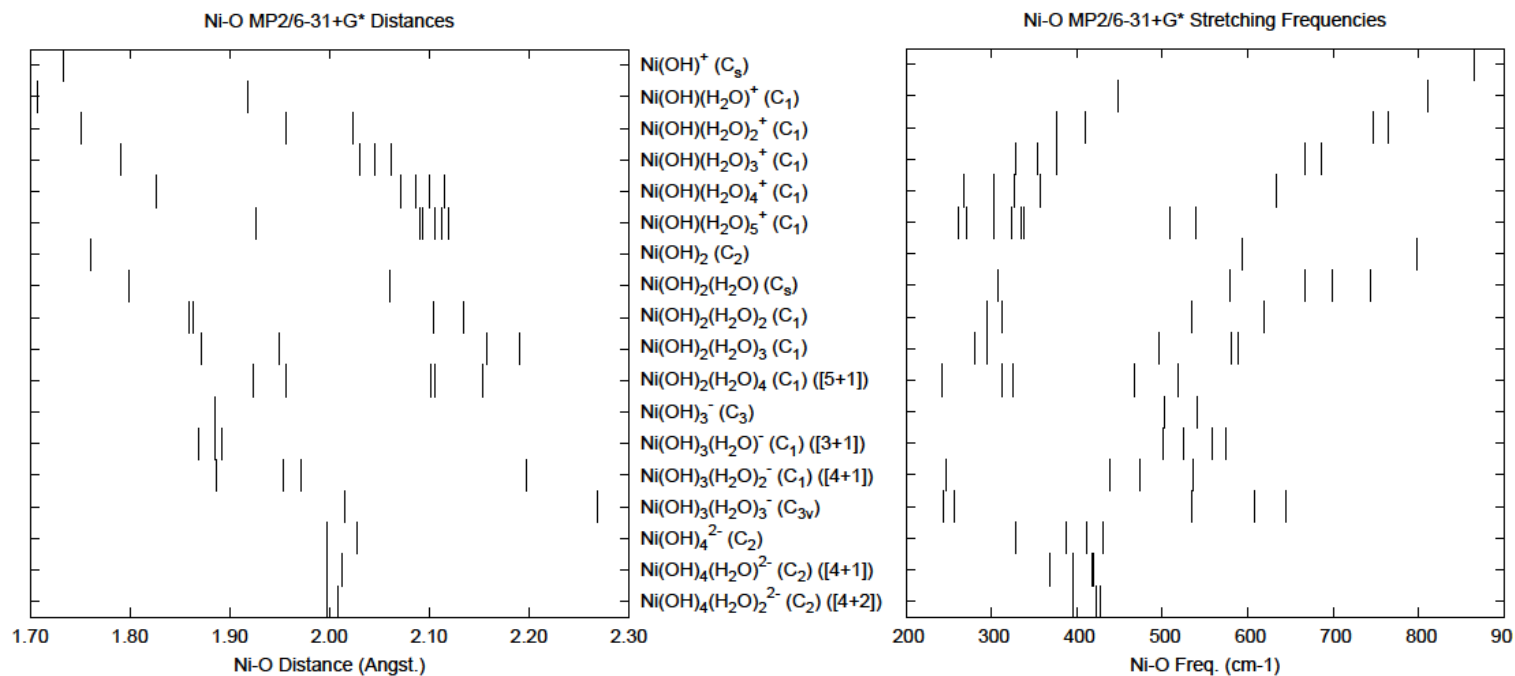


Figure 3-14: Ni-O bond lengths and vibrational stretching frequencies for $[\text{Ni}(\text{OH})_m(\text{H}_2\text{O})_n]^{2-m}$, where $m=1-4$, $n=0-(6-n)$, calculated at the MP2/6-31+G* level.

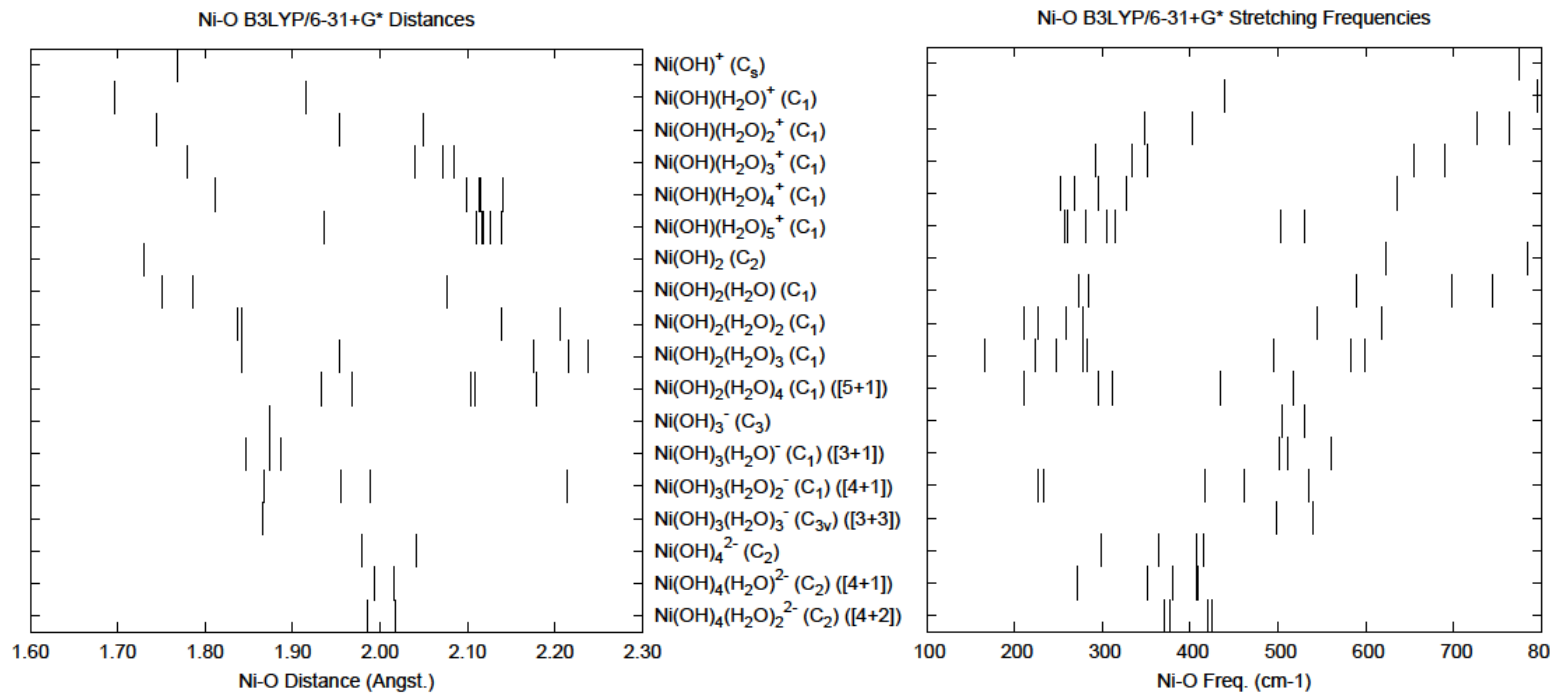


Figure 3-15: Ni-O bond lengths and vibrational stretching frequencies for $[\text{Ni}(\text{OH})_m(\text{H}_2\text{O})_n]^{2-m}$, where $m=1-4$, $n=0-(6-n)$, calculated at the B3LYP/6-31+G* level.

3.5 Amminenickel(II) Complexes, $[\text{Ni}(\text{NH}_3)_m(\text{H}_2\text{O})_n]^{2+}$, where $m=1-6$, $n=0-(6-n)$

A number of studies on amminenickel ions have been carried out by experimental or computational methods. Studies on crystal structures of Ni^{2+} complexes show that nickel(II) usually favors four-coordinate and six-coordinate complexes. [108] A solubility study of nickel(II) ammino complexation also showed that the mono- and diammine nickel(II) ions occur at free ammonia concentrations above 2 mmolkg^{-1} and 6.5 mmolkg^{-1} respectively. [105] The monoamine nickel(II) ion has been studied by computational methods [60, 67, 107], and the geometries, electronic structures, and binding energies have been reported. The hexaammine complex has been studied comprehensively by ab initio calculations and experiments. The experimental studies include ^{14}N NMR and proton magnetic resonance to determine the exchange rate [111, 113], infrared spectroscopy [112, 114, 115], extended X-ray fine absorption structure [46], Raman spectroscopy [115, 116], and solubility and stability studies [105]. In addition, ab initio investigations involving DFT-RX3LYP calculations on low spin hexaammine complexes [55], DFT studies on ammonia adsorption on Ni_n clusters [107], and HF calculations on the reactivity of Ni^{2+} in solutions have been completed [110]. For the hydrated amminenickel(II) complexes, only the hexa-coordinated species are reported by computational methods in the literature. [55, 108, 110]. Varadwaj et al. [108] performed computational studies on $[\text{Ni}(\text{NH}_3)_n(\text{H}_2\text{O})_{6-n}]^{2+}$ complexes, and reported that the $[\text{Ni}(\text{H}_2\text{O})_6]^{2+}$ is predicted to be the least stable, and the successive replacement of H_2O by NH_3 results in a monotonic increase in the stabilization of the complex. It is reported that the stability of nickel(II) ammonia complexes is generally greater than that of water complexes according to computational studies which can be explained by the diffuse

character of the NH_3 lone pair which enhance the dispersion and σ donation contributions.
[67]

3.5.1 Results

The nickel(II) ammine complexes were studied up to and including hexacoordinate species with and without water molecules. Stable geometries were found for all of the complexes studied. Total molecular energies as well as C-PCM energies of all the geometries studied can be found in Table 3A.16 of the supplementary materials section. The optimized geometries of the stable structures can be found in Figure 3-16 for the mono- and diammine complexes and in Figure 3-17 for the tri-, tetra-, penta- and hexaammine complexes.

The anhydrate monoamine posed no problems at the highest possible symmetry C_{3v} . For the monohydrate, two C_s structures were tried, but only the C_s species with the oxygen atoms symmetric to the plane was stable (at MP2/6-31+G*). A C_1 structure (looks like C_s , but the ammine is slightly twisted) is preferred at B3LYP level. Four C_s structures were tried for the dihydrate, and the one in which one water molecule in the O-Ni-N plane and the other bisected by the plane was stable (at MP2/6-31+G*), whereas it reduced to C_1 symmetry (although still looks similar to C_s) at B3LYP level. C_{3v} , C_3 , C_s , and C_1 structures were sequentially attempted for the trihydrate, and only the C_1 structure is stable at both levels. For the tetrahydrate, a stable C_s structure was located, and the pentahydrate also has C_s symmetry.

The D_{3d} and D_{3h} geometries were tried for the anhydrate diammine complex, and the D_{3h} species is only stable at B3LYP level, while the D_{3d} structure has the lowest

energy at both levels. For the monohydrate, C_{2v} structures were tried first, but they all have imaginary frequencies at both levels. After desymmetrization along the imaginary modes, the structure became stable at C_2 (B3LYP/6-31+G*) and the global minimum C_1 (both levels). For the dihydrate, the C_{2v} structure was tried first, but it has imaginary modes at both levels. The C_2 symmetry is only stable at MP2, whereas C_s structure is preferred at B3LYP level. The preferred trihydrate structure is C_2 . For the tetrahydrate, high symmetry structures trans C_{2h} and trans C_{2v} were tried first, but the trans C_{2h} structure is only stable at MP2 level, and trans C_{2v} shows imaginary frequencies at both levels. Two trans C_2 structures were also attempted, and the one in which the rotation axis along with the O-Ni-O is stable at both levels, whereas the other in which the rotation axis only pass the Ni atom is only stable at MP2 level. A cis C_s structure is energetically preferred at both levels. The C_1 structure is also stable and competitive in energy.

For the anhydrous triammine species, the C_{3h} structure is only stable at MP2 level, and C_3 structure is energetically preferred at both levels. C_s structure was tried for the monohydrate, but it showed imaginary frequencies at both levels. The C_1 structure (looks similar to C_s) is preferred at both levels. For the dihydrate, only the C_s structure in which two ammines are symmetric with plane is stable at both levels. The highest possible symmetry C_{3v} was tried for the trihydrate, but it has numerous imaginary frequencies at both levels. The fac C_3 structure proved to be a minimum. The mer C_1 structure is also stable at both levels and competitive in energy.

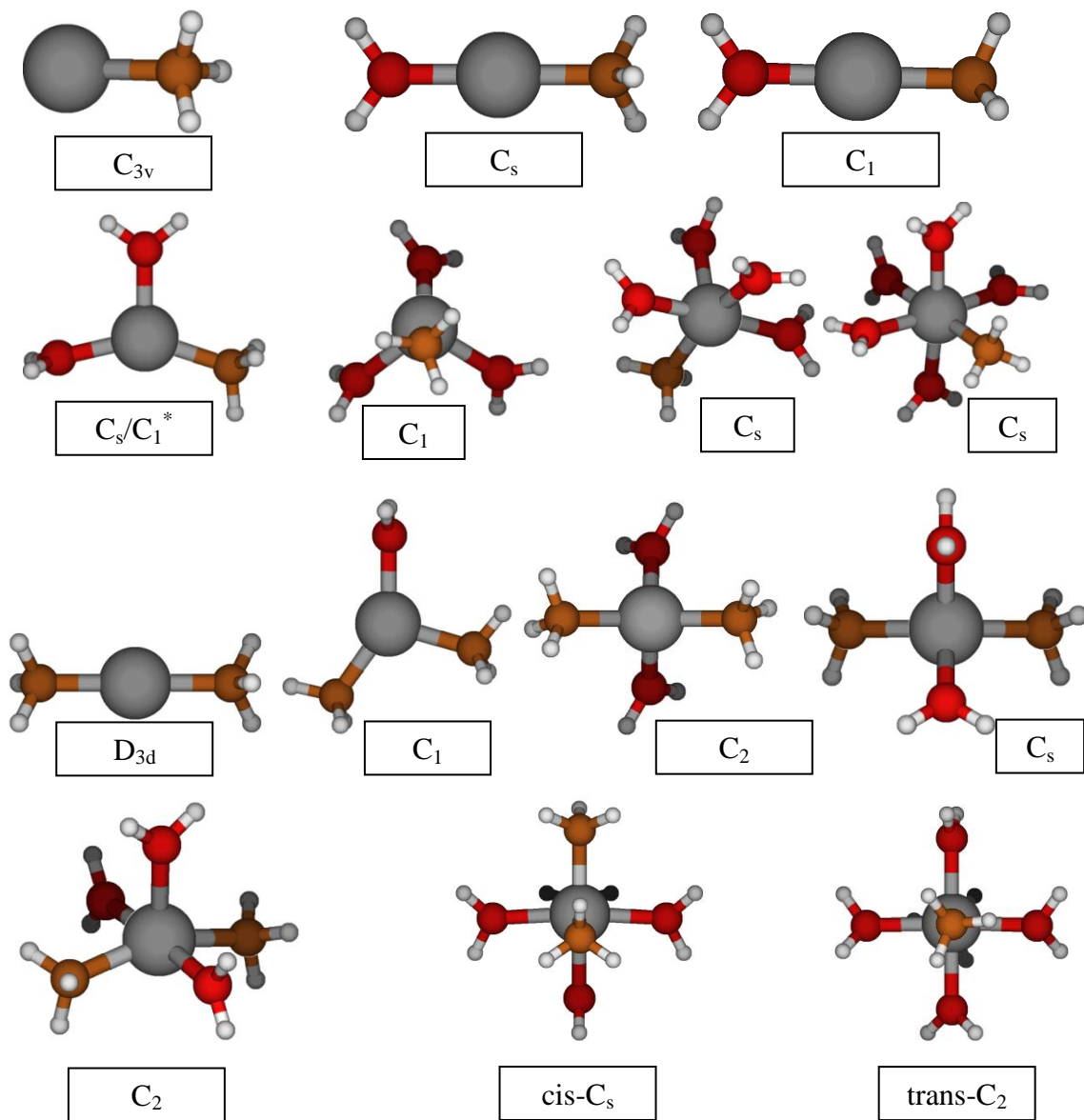


Figure 3-16: Optimized MP2 and B3LYP geometries for $[\text{Ni}(\text{NH}_3)_m(\text{H}_2\text{O})_n]^{2+}$, where $m=1-2$, $n=0-(6-m)$. “*” indicates MP2 and B3LYP structures with different symmetry are similar. (grey=nickel, red=oxygen, white=hydrogen, brown=nitrogen)

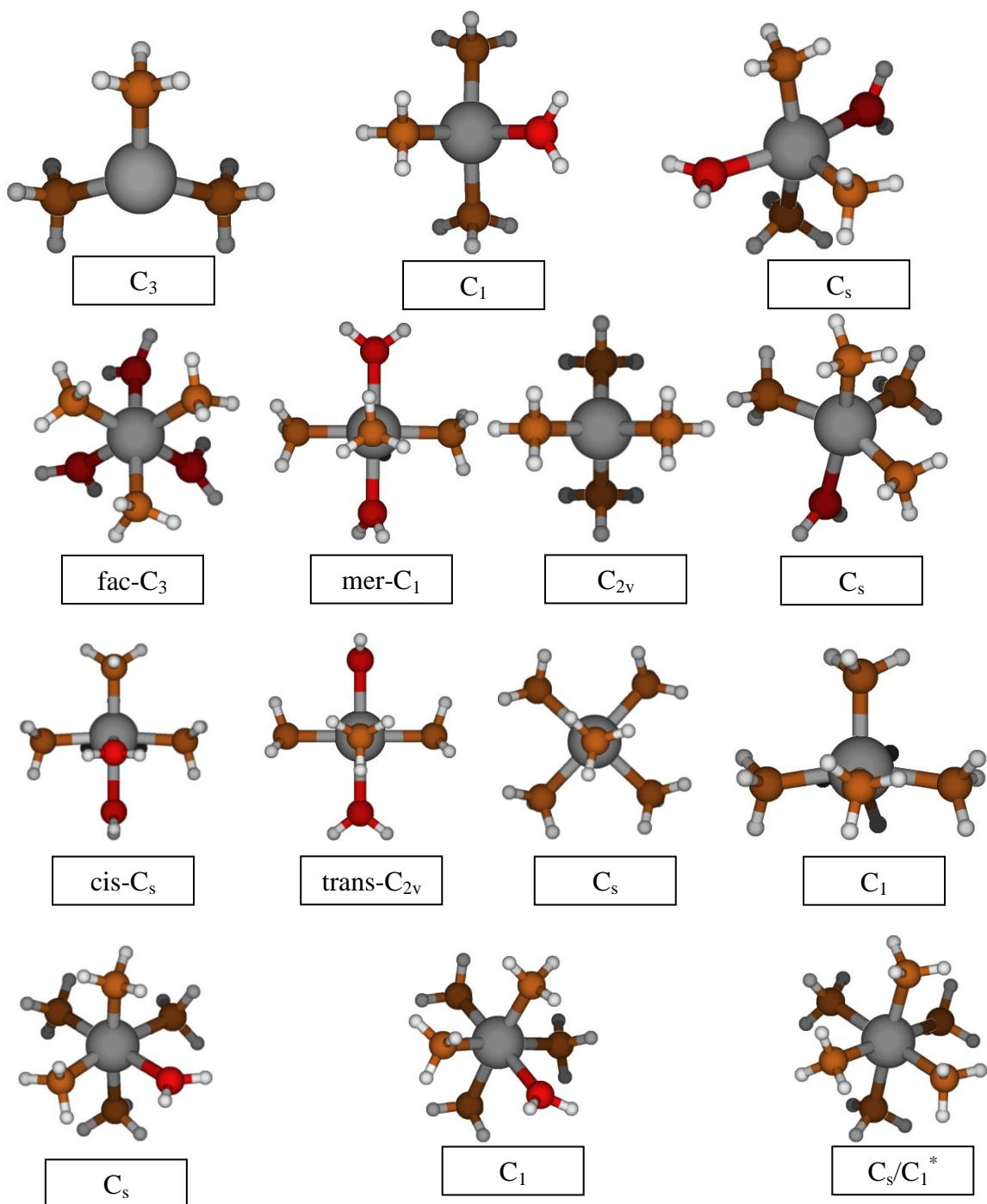


Figure 3-17: Optimized MP2 and B3LYP geometries for $[Ni(NH_3)_m(H_2O)_n]^{2+}$, where $m=3-6$, $n=0-(6-m)$. “*” indicates MP2 and B3LYP structures with different symmetry are similar.

The anhydrous tetraammine complex has C_{2v} symmetry. For the monohydrate, C_{2v} and C_2 were tried and they are both unstable at both levels, whereas a C_s structure is proved to be a minimum. The trans dihydrate is stable with C_{2v} and C_s symmetry at both levels, although C_{2h} (has imaginary frequencies at both levels) and C_2 (revert back to C_{2v} after optimization) were attempted, and a cis C_s structure is energetically preferred at both levels.

For the anhydrous pentaammine species, C_{3h} , C_{3v} , C_3 , C_s , and C_1 structures were sequentially tried, and only the C_1 and C_s structures are stable at B3LYP level, whereas only the C_1 structure is stable at both levels. The C_s structure is energetically preferred at B3LYP level. For the monohydrate, a C_s structure is only stable at MP2 level with the lowest energy, and it reduced to C_1 symmetry at B3LYP level. Finally, the anhydrous hexaammine species has stable C_1 symmetry at both levels, and a C_s structure only stable at B3LYP and is energetically preferred at this level.

Bond length and vibrational stretching frequency data were collected and plots were constructed which can be seen in Figure 3-18, Figure 3-19 and Figure 3-20 for HF, MP2 and B3LYP respectively. Raman intensities were calculated at the HF level and therefore simulated polarized Raman plots were able to be created and these can be found in the supplementary materials section in Figure 3A-4.

3.5.2 Discussion/Literature Comparison

The geometries that have been calculated for $Ni(NH_3)_n^{2+}$ (where $n=1-6$) can be compared to computational results reported in the literature. Pilme et al. [67] found 2.091 Å for the Ni-N distance in anhydrous monoamminenickel(II) species by ROB3LYP/6-

311+G(2d) calculations. Magnusson and Moriarty [60] reported the Ni-N bond length to be 2.081 Å based on MP2/6-311+G** calculations. Chen et al. [107] obtained 2.05 Å for the Ni-N distance in $\text{Ni}(\text{NH}_3)^{2+}$ using the NRLMOL set of codes developed by Pederson et al. Our results for Ni-N distance are 2.005 Å (MP2) and 2.016 Å (B3LYP) which are slightly shorter due to our relatively smaller basis set. Chen et al. [107] also reported the Ni-N bond lengths for anhydrous di-, tri-, and tetraammine species which are 2.03 Å, 2.02-2.04 Å, and 2.06-2.19 Å respectively which are also slightly longer than our results of 1.979 Å, 2.014 Å and 2.060 Å for MP2, and 1.997 Å, 2.013 Å and 2.068-2.069 Å for B3LYP respectively. It should be noted that the structures which Chen et al. obtained did not use symmetry whereas our structures are constrained to the appropriate symmetry, so that their geometries are slightly different from ours. Aguilar et al. [51] obtained the Ni-N distance of $\text{Ni}(\text{NH}_3)_6^{2+}$ to be 2.206 – 2.210 Å based on B3LYP/LANL2DZ calculations which are slightly longer than our results of 2.195 – 2.204 Å at B3LYP/6-31+G*, and our MP2 results (2.175-2.177 Å) are still lower. The basis set- LANL2DZ does not include diffuse or polarization functions. Varadwaj et al. [108] reported the Ni-N bond length to be 2.205 Å (mean value) by UX3LYP/6-311++G(d,p) calculations which is in good agreement with our result. [108] There were no literature reports found for anhydrous pentaammine complex.

For the aquaamminenickel(II) complexes, Varadwaj et al. [108] calculated the structures of $[\text{Ni}(\text{NH}_3)_n(\text{H}_2\text{O})_{6-n}]^{2+}$ (where n=0-6) at UX3LYP/6-311++G(d,p) level. Although they did not do the calculations with symmetry, they still obtained the similar geometries with ours, and their results are very comparable with our results. Results from

Varadwaj et al. [108] are tabulated in Table 3.1 along with the results from this research for comparison.

Table 3.1: Geometry comparison of hexacoordinate aquaammine complexes (B3LYP level) with results reported by Varadwaj et al. [108]. All bond lengths (Å) are averages where appropriate.

Complex	Varadwaj et al. [108]		Our Results	
	Ni-N	Ni-O	Ni-N	Ni-O
$\text{Ni}(\text{NH}_3)(\text{H}_2\text{O})_5^{2+}$	2.082	2.113	2.075	2.110
$\text{trans-Ni}(\text{NH}_3)_2(\text{H}_2\text{O})_4^{2+}$	2.095	2.157	2.090	2.160
$\text{cis-Ni}(\text{NH}_3)_2(\text{H}_2\text{O})_4^{2+}$	2.100	2.146	2.091	2.150
$\text{fac-Ni}(\text{NH}_3)_3(\text{H}_2\text{O})_3^{2+}$	2.116	2.190	2.106	2.198
$\text{mer-Ni}(\text{NH}_3)_3(\text{H}_2\text{O})_3^{2+}$	2.116	2.201	2.108	2.203
$\text{trans-Ni}(\text{NH}_3)_4(\text{H}_2\text{O})_2^{2+}$	2.151	2.211	2.145	2.221
$\text{cis-Ni}(\text{NH}_3)_4(\text{H}_2\text{O})_2^{2+}$	2.140	2.250	2.129	2.270
$\text{Ni}(\text{NH}_3)_5(\text{H}_2\text{O})^{2+}$	2.169	2.323	2.162	2.329

Plots were created for the Ni-O and Ni-N bond lengths and vibrational stretching frequencies which can be seen in Figures 3-18 to 3-20. These plots showcase the trends in the bond lengths and vibrational stretching frequencies as more ligands, either ammonia or water, are added to the system. The Ni-N bond lengths are uniformly shorter than the Ni-O bond lengths that could be due to the fact that N has a lower electronegativity than O and is more polarizable, and hence NH_3 forms the stronger bonds to nickel. As more water molecules are added to the system, both of the Ni-O and Ni-N distances become longer. This could be explained by the mutual repulsion between water and ammonia attached to the same metal center will lead to increases in bond distances. The stretching frequencies show the opposite trends, the stretching frequencies become lower as more ligands are added to the system.

Schmidt et al. [115] reported the experimental Raman data for the $\text{Ni}(\text{NH}_3)_6^{2+}$ to be 370 cm^{-1} for the Ni-N symmetric stretch. Our values are 312 cm^{-1} , 334 cm^{-1} , and 320 cm^{-1} at HF, MP2 and B3LYP respectively which underestimate this by $35 - 58\text{ cm}^{-1}$. It is known that there are systematic errors in calculated frequencies at HF, MP2 and B3LYP levels depending on the system and basis sets. [38] Pye et al. [70] also assumed that this underestimation is systematic for the mixed complexes. The polarized Raman data are also plotted which can be seen in Figure 3A-4.

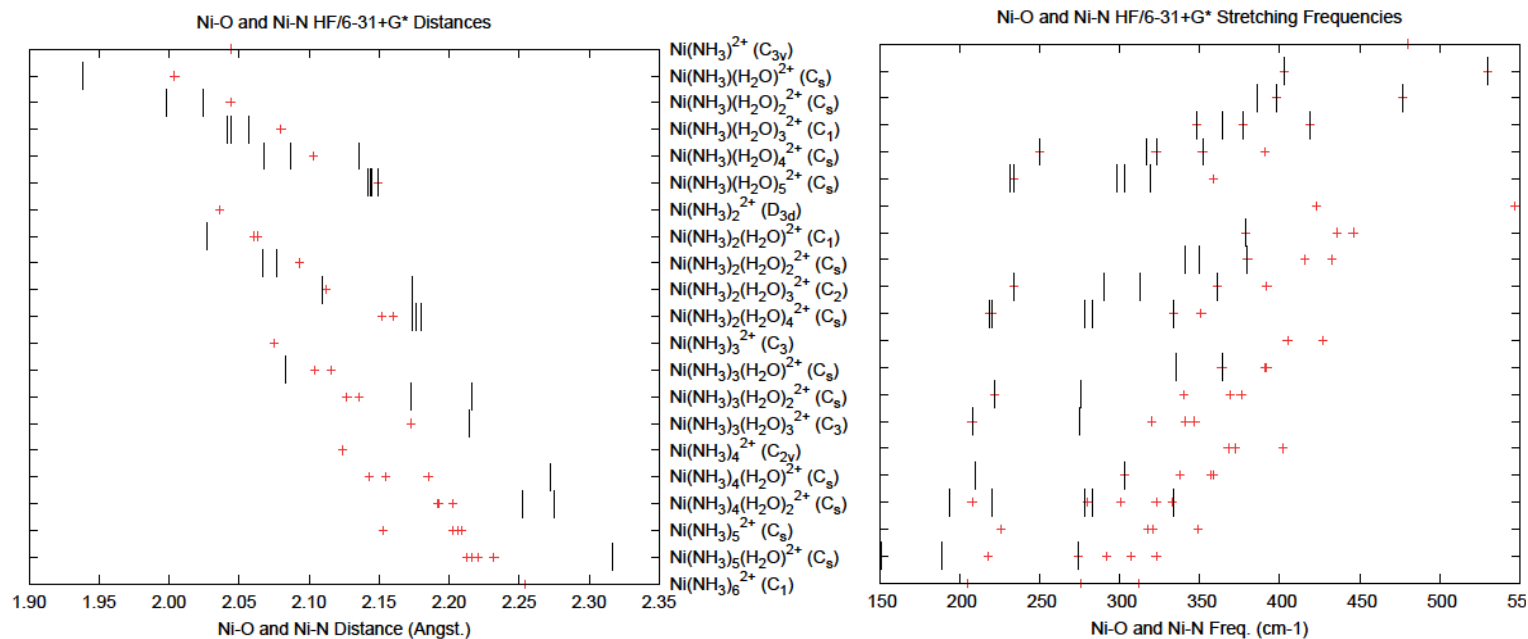


Figure 3-18: Ni-O and Ni-N (red “+”) bond lengths and vibrational stretching frequencies for [Ni(NH₃)_m(H₂O)_n]²⁺, where m=1-6, n=0-(6-n), calculated at the HF/6-31+G* level.

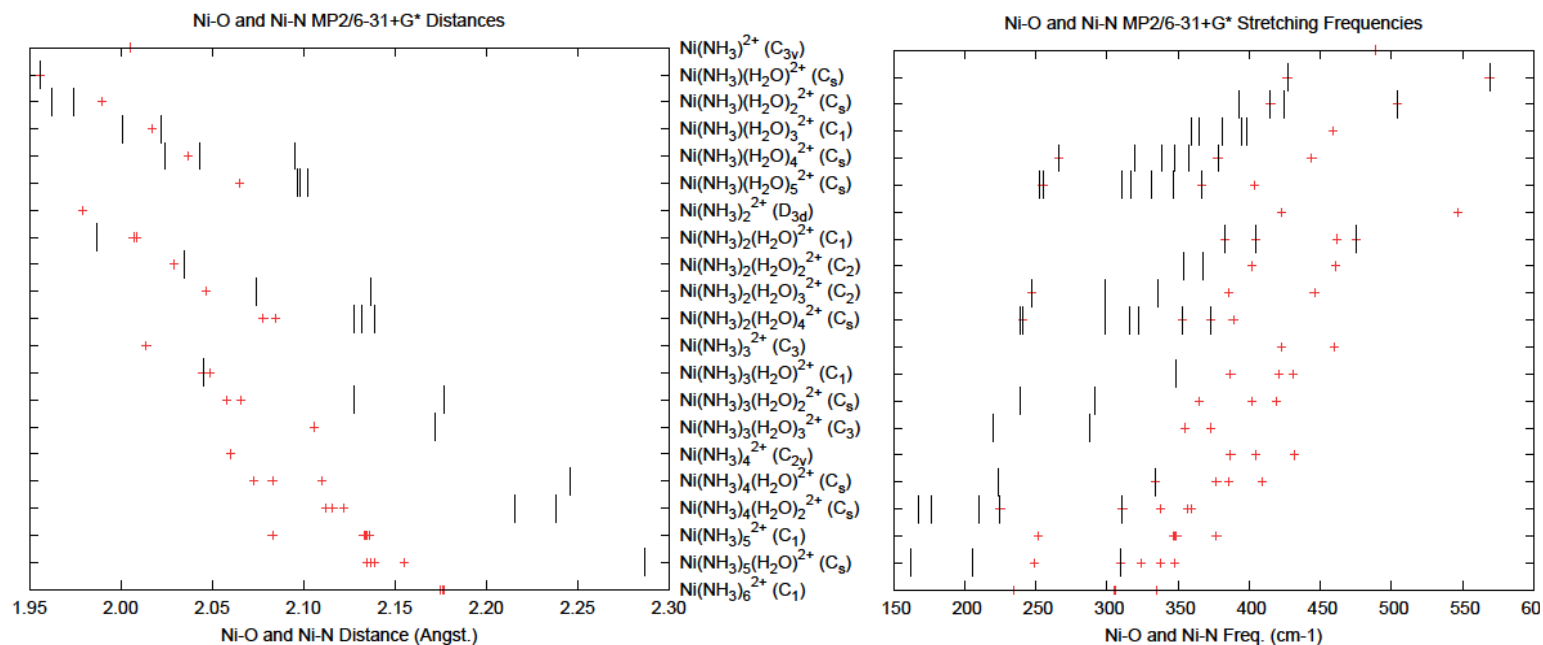


Figure 3-19: Ni-O and Ni-N (red “+”) bond lengths and vibrational stretching frequencies for [Ni(NH₃)_m(H₂O)_n]²⁺, where m=1-6, n=0-(6-n), calculated at the MP2/6-31+G* level.

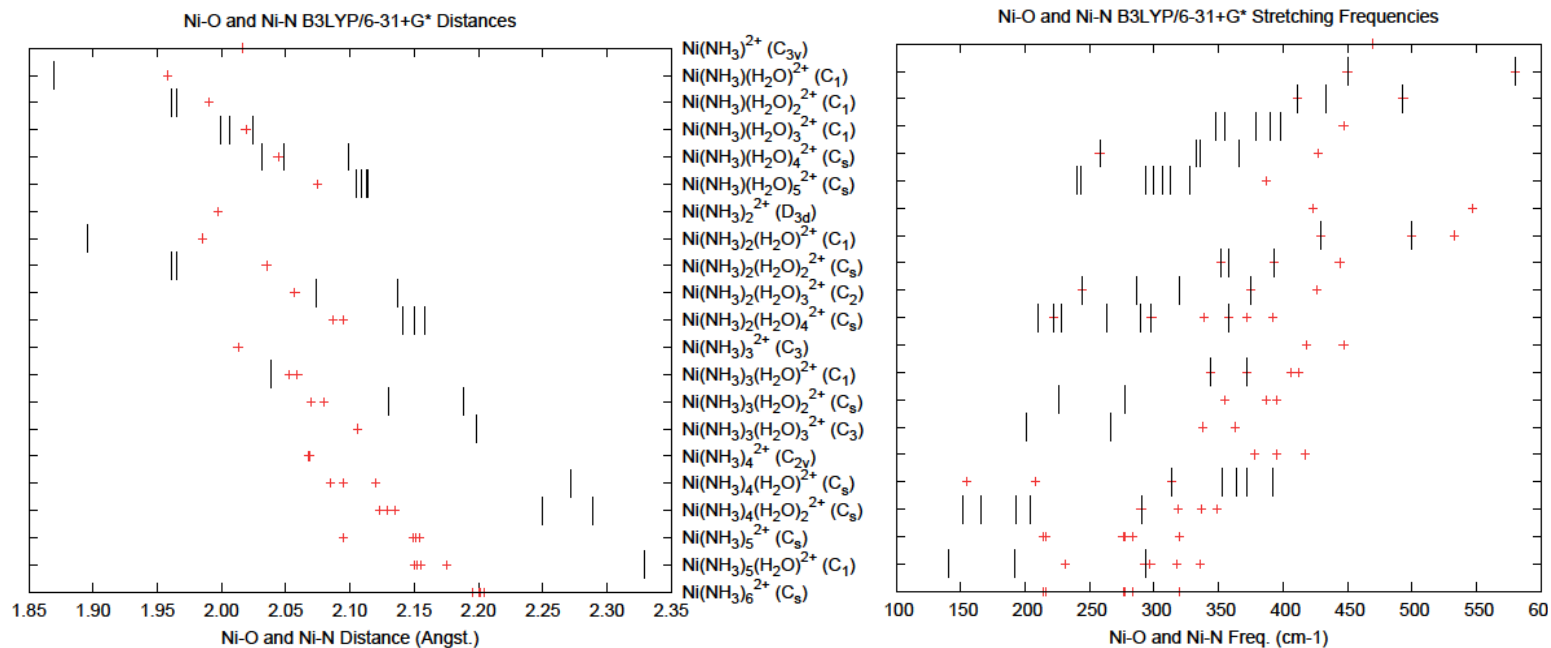


Figure 3-20: Ni-O and Ni-N (red “+”) bond lengths and vibrational stretching frequencies for [Ni(NH₃)_m(H₂O)_n]²⁺, where m=1-6, n=0-(6-n), calculated at the B3LYP/6-31+G* level.

3.6 Chlorohydroxonickel(II) Complexes, $[\text{NiCl}_m(\text{OH})_n(\text{H}_2\text{O})_l]^{2-m-n}$, where $m=1-3$, $n=1-(4-m)$, $l=0-(6-m-n)$

This set of complexes was studied up to and including the overall hexa-coordinate species with various combinations of chloride, hydroxide and water. All complexes have at least one chloride and one hydroxide ligand. Although it was attempted, no stable structures were found for species with a combination of chloride and hydroxide ligands greater than four. Many of these complexes tended to form ion pairs. No computational or experimental data was found in the literature therefore the discussion will be limited to comparison of the optimized structures as well as bond distance and vibrational stretching frequency trends.

3.6.1 Results

Total energies have been tabulated for all successfully optimized geometries and can be seen in Table 3A.5 in the supplementary materials section for this chapter. The optimized geometries of stable structures can be seen in Figure 3-21 for chlorohydroxo and chlorodihydroxo complexes, Figure 3-22 for chlorotrihydroxo, dichlorohydroxo, dichlorodihydroxo, dichlorotrihydroxo and trichlorohydroxo complexes.

The anhydrous chlorohydroxo complexes posed no problems at the highest possible symmetry C_s . Two C_s structures were tried for the monohydrate, but they both show imaginary frequencies at all levels, and C_1 geometry is preferred. The dihydrate has stable C_s and C_1 structures at both levels, and C_1 is also energetically preferred at both levels. For the trihydrate, two C_s structures were also tried first, but the planar one showed dissociation of chloride atom, whereas the other showed imaginary frequencies at

all levels. A C_1 structure with one water molecule in the second solvation shell and hydrogen bonded to chloride and the other water molecule is preferred at both levels. The tetrahydrate has trans C_s (with lower energy) and cis C_1 symmetry with all the ligands directly bonded to the central nickel.

C_{2v} structure was tried first for the anhydrous chlorodihydroxo complex, and it is unstable at all levels. The C_2 structure is stable at MP2 level but becomes C_1 (although looks similar to C_2) at B3LYP level. For the monohydrate, C_{2v} and C_2 structures were attempted first, but neither of them were stable. The stable structures found are C_s and C_1 , and the C_s structure is energetically preferred at both levels. For both C_s and C_1 structures, all ligands are directly bonded to nickel at MP2 level, but one of the water molecules migrated to the second hydration sphere forming hydrogen bond with the other two water molecules at B3LYP level. For the dihydrate, C_{2v} and C_2 structures were also tried first, and they both show imaginary frequencies at both levels, and C_1 structure is preferred at both levels. For the trihydrate, C_{2v} , C_2 , C_s and C_1 structures were sequentially attempted and only the C_1 structure with one water molecule in the second hydration sphere and hydrogen bonded to water and hydroxide.

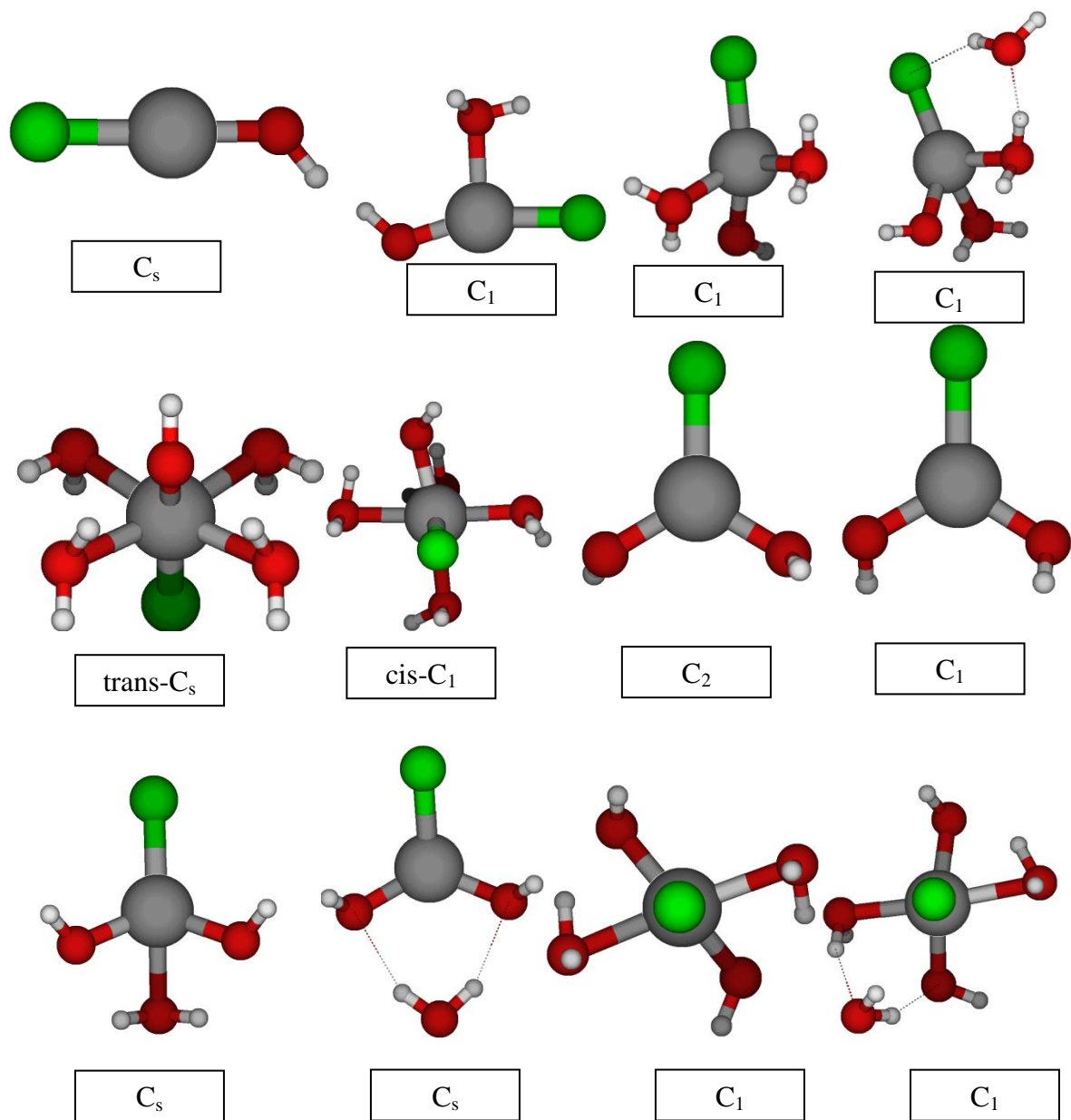


Figure 3-21: Optimized MP2 and B3LYP geometries for $[\text{NiCl}(\text{OH})_m(\text{H}_2\text{O})_l]^{2-n}$, where $m=1-3$, $l=0-(5-m)$. (grey=nickel, red=oxygen, white=hydrogen, green=chloride)

The anhydrous chlorotrihydroxo complex has C_3 symmetry, although C_{3v} was also tested and showed imaginary frequencies at all levels. Various C_s structures were

attempted for the monohydrate, and all of them showed either dissociation or imaginary frequencies. A C_1 structure with one water molecule in the second hydration shell and hydrogen bonded to two hydroxides is stable at both levels. When one more water is added, a C_1 structure is formed with only all the hydroxides directly bonded to central nickel, two water molecules migrated to the second solvation sphere and hydrogen bonded to the same hydroxide, whereas the chloride in the third hydration shell and hydrogen bonded to the two water molecules.

Two C_s geometries were tried for the anhydrous dichlorohydroxo complex. The planar one is only stable at B3LYP level, whereas the other is only stable at MP2 levels. A stable C_1 structure is located and is energetically preferred at both levels. Four C_s structures were tried for the monohydrate, but they all show imaginary frequencies at both levels. The only stable structure been found is C_1 . The dihydrate (C_1) and trihydrate (C_1) presented a similar result, except the trihydrate has the chloride in the second hydration sphere and hydrogen bonded to the three water molecules.

Two C_{2v} , two C_2 , four C_s and various C_1 structures were attempted for the dichlorodihydroxo complex. Both of the C_{2v} structures and the C_2 structure with the Cl-Ni-Cl rotation axis showed dissociation of chloride ions. The C_2 structure in which the rotation axis only passes the nickel atom is stable at MP2 level. The only stable C_s structure (MP2) is the one with the two hydroxides symmetric with the Cl-Ni-Cl plane and is energetically preferred at MP2 level. All the C_1 structures reverted back to C_2 or C_s after optimization. For the B3LYP level, all the structures mentioned previously showed dissociation of chlorides or imaginary frequencies, so no stable structure was found at

this level. The stable structure for the monohydrate has C_s symmetry with two chlorides in the second hydration shell and hydrogen bonded to the water and hydroxide. For the dihydrate, the highest possible symmetry C_{2h} and C_{2v} were tried first. The C_{2h} structure showed dissociation of chlorides, whereas the C_{2v} structure with two chlorides hydrogen bonded to water molecules is stable at both levels. 27 different C_s structures were also attempted, and only the structures reverted back to C_{2v} are stable whereas others all showed dissociations of chlorides or imaginary frequencies.

The trichloromonohydroxo complex is only stable with C_1 symmetry at both levels, as all the C_s structures attempted are unstable. The monohydrate also has C_1 symmetry with the water molecule in the second solvation sphere and hydrogen bonded to hydroxide and chloride. For the dihydrate, various C_s structures were attempted, and only the C_s structure with two hydrogen bonded chlorides is stable at both levels.

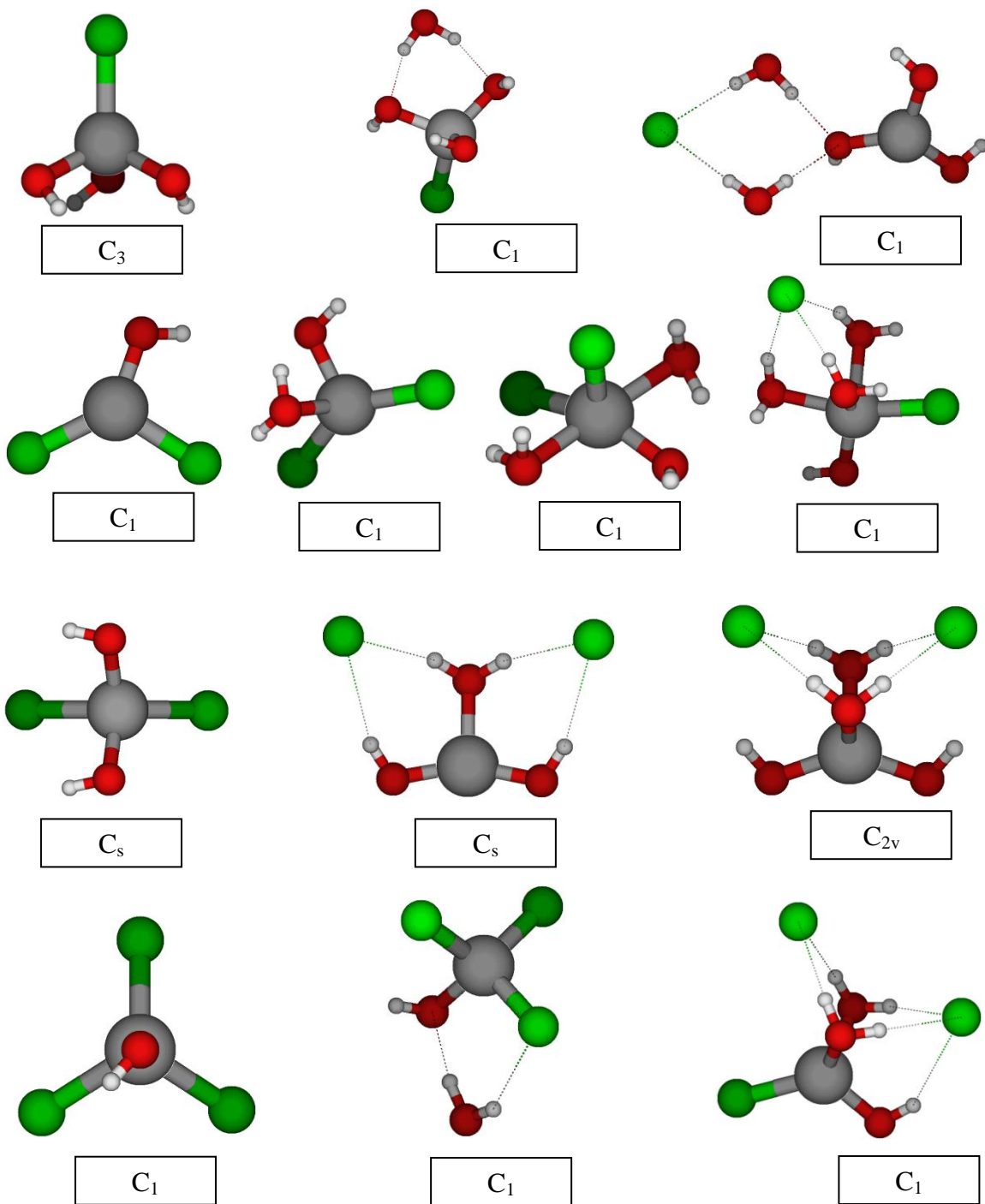


Figure 3-22: Optimized MP2 and B3LYP geometries for $[\text{NiCl}_m(\text{OH})_n(\text{H}_2\text{O})_l]^{2-m-n}$, where $m=1-3$, $n=0-(4-m)$, $l=0-(6-m-n)$.

3.6.2 Discussion/Literature Comparison

No data were found in the literature to compare the stable geometries with. However comment on the trends observed within the bond length and vibrational stretching plots constructed at each of the three levels of theory could be given. Within the bond length figures there is a general trend of increasing Ni-O and Ni-Cl bond distance as more water molecules are added to the system. However, when there are ion pairs, the trend is reversed. This could be caused by the dissociated chloride anion hydrogen bonding to the central complex, thereby stabilizing the structure, resulting in shorter bond distances. These trends are found with all three levels of theory. As mentioned in previous sections, when the bond lengths increase, the vibrational stretching frequencies associated with those bonds decrease. As the bond length trend reverses, the vibrational stretching frequency trend also changes. This trend with respect to the frequencies is also found with all levels of theory.

Since the results are going to be primarily used to compare with experimental Raman data generated by the colleagues at the University of Guelph, the Raman spectra based on the Raman intensities calculated at the HF/6-31+G* level of theory are constructed. These plots will be beneficial in the assignment of the experimental Raman bands. These plots are located in Figure 3A-5 in the supplementary material section.

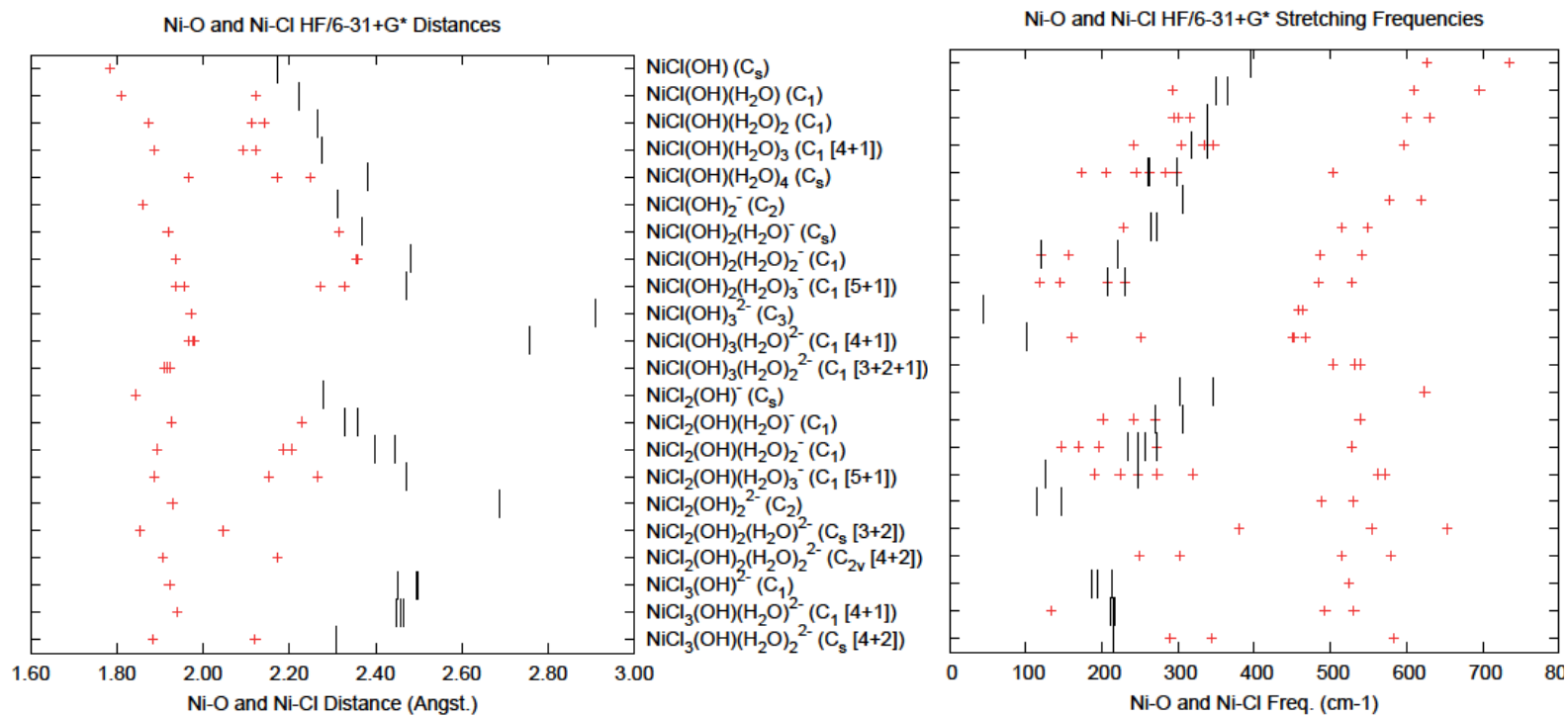


Figure 3-23: Ni-Cl and Ni-O (red “+”) bond lengths and vibrational stretching frequencies for $[\text{NiCl}_m(\text{OH})_n(\text{H}_2\text{O})_l]^{2-m-n}$, where $m=1-3$, $n=1-(4-n)$, and $l=0-(6-m-n)$, calculated at HF/6-31+G* level.

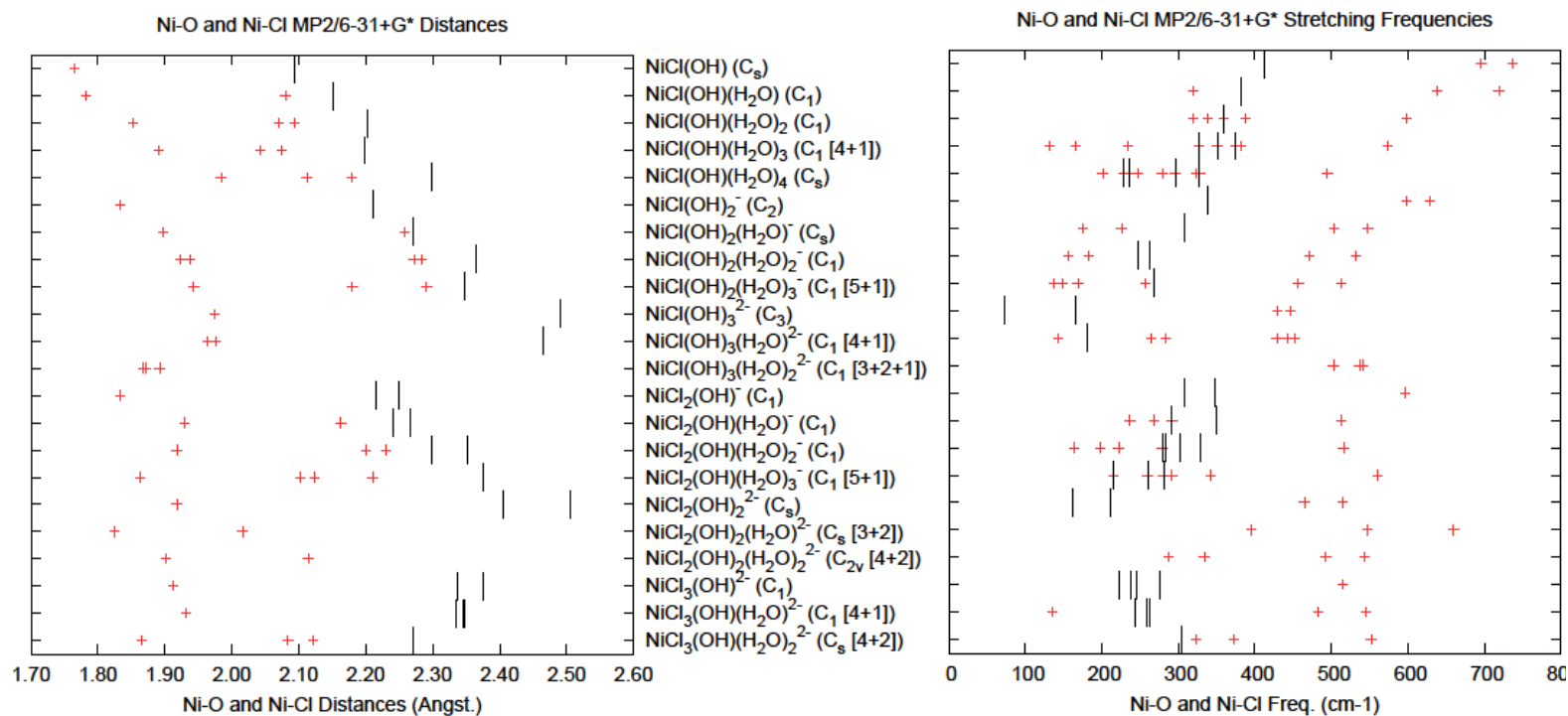


Figure 3-24: Ni-Cl and Ni-O (red “+”) bond lengths and vibrational stretching frequencies for $[\text{NiCl}_m(\text{OH})_n(\text{H}_2\text{O})_l]^{2-m-n}$, where $m=1-3$, $n=1-(4-n)$, and $l=0-(6-m-n)$, calculated at MP2/6-31+G* level.

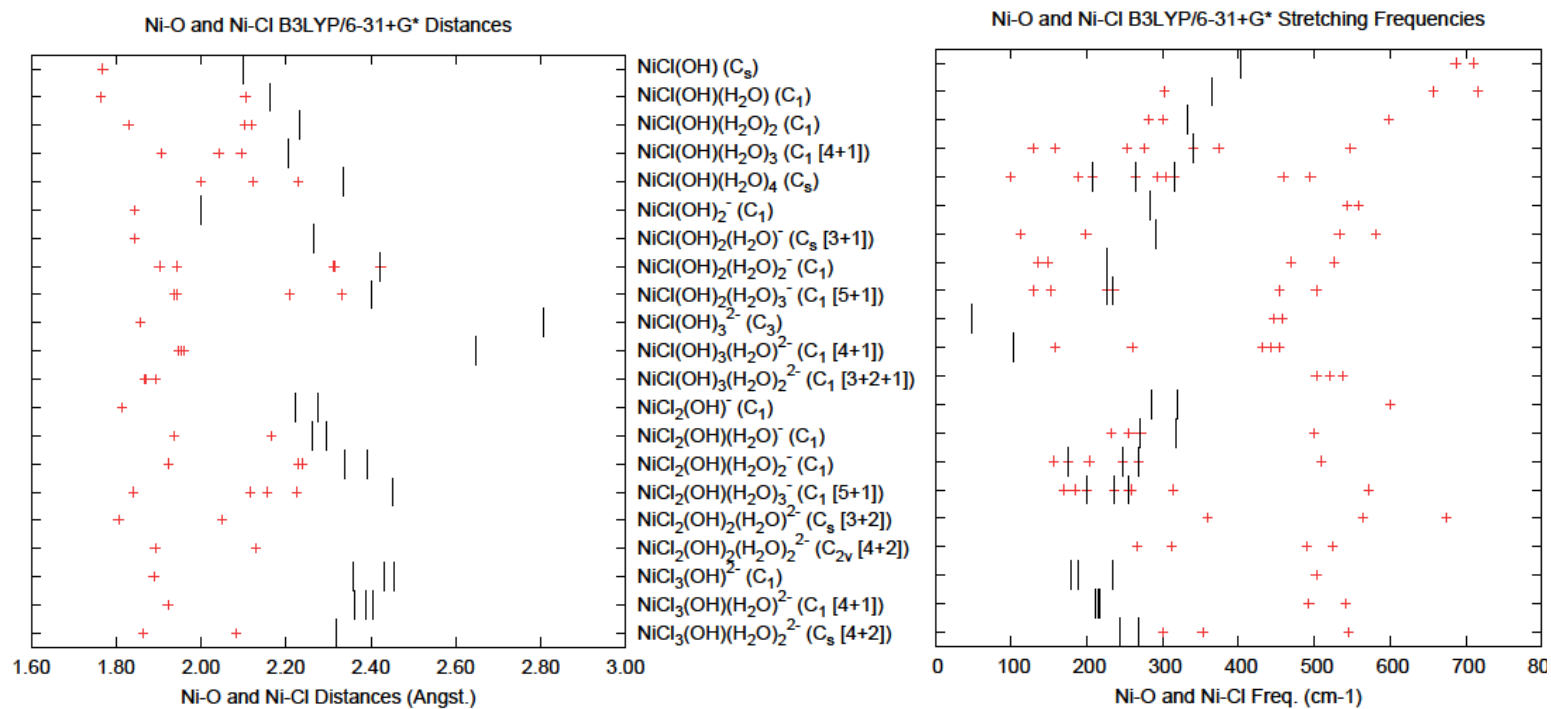


Figure 3-25: Ni-Cl and Ni-O (red “+”) bond lengths and vibrational stretching frequencies for $[\text{NiCl}_m(\text{OH})_n(\text{H}_2\text{O})_l]^{2-m-n}$, where $m=1-3$, $n=1-(4-n)$, and $l=0-(6-m-n)$, calculated at B3LYP/6-31+G* level.

3.7 Chloroamminenickel(II) Complexes, $[\text{NiCl}_m(\text{NH}_3)_n(\text{H}_2\text{O})_l]^{2-n}$, where $m=1-4$, $n=1-(6-m)$, $l=0-(6-m-n)$

This set of complexes was studied up to and including the hexa-coordinate complexes with various combinations of chloride, ammonia and water ligands. Every complex has at least one chloride and one ammonia ligand. Stable structures were found for all of the other combinations, although a few of them were not stable as completely bound structures as they preferred to have hydrogen bonded water or ammonia ligands and in a couple cases an ion pair was preferred. Only a couple of experimental studies have been completed regarding bond length or vibrational stretching frequency data for this set of complexes. Therefore, the discussion of the chloroamine species will be restricted to the findings regarding geometries, bond length and vibrational stretching frequency trends.

3.7.1 Results

Total energies have been collected and tabulated for all optimized geometries attempted, and can be found in Table 3A.6 of the supplementary materials section. The optimized MP2 and B3LYP geometries for the stable structures can be seen in Figure 3-26 for all monochloroamine and dichloroamine complexes, Figure 3-27 for all trichloroamine and tetrachloroamine complexes.

The monochloromonoamine complex is stable at the highest possible symmetry C_{3v} at both levels. For the monohydrate, four C_s and C_1 structures were attempted. The C_s structure in which the hydrogen atoms of water are in the symmetric plane with the hydrogen from ammine pointing to water is preferred at MP2 level, and C_1 structure is

preferred at B3LYP. For the dihydrate, various C_s structures were tried, but the only stable structure found is C_1 at both levels. For the trihydrate, high symmetry structures like C_{3v} and C_3 were tried first, but they all showed imaginary frequencies at both levels. A C_s structure is preferred at MP2 level, and it reduced to C_1 (with the ammonia slightly twisted) at B3LYP level. The tetrahydrate prefers C_1 (trans and cis) symmetry as all the C_s structures tested showed imaginary frequencies. The trans C_1 structure has lower energy.

For the chlorodiammine complex, C_{2v} and C_2 were tried first. The C_{2v} structure showed imaginary frequencies at both levels, whereas C_2 is only stable at B3LYP level. A C_s structure is stable at MP2 level, but C_1 is energetically preferred at both levels. The monohydrate is only stable with C_1 symmetry as all the structures with higher symmetry attempted are unstable. For the dihydrate, two C_{2v} structures were attempted, but neither of them is stable. A C_2 structure is proved to be a minimum. Various C_s structures were tried for the trihydrate, and only a fac C_s structure is stable at both levels. The most stable structure found for the trihydrate is mer C_1 .

For the chlorotriammine complex, C_{3v} and C_3 structures are unstable at both levels. Desymmetrization along the imaginary modes resulted in a stable C_s structure and is energetically preferred at MP2, whereas C_1 geometry with slightly lower energy is preferred at B3LYP level. The monohydrate has C_1 symmetry as all the C_s structures tried have imaginary frequencies at both levels. For the dihydrate, a mer C_s structure is only stable at B3LYP level, and mer C_1 is stable at both levels. A fac C_1 structure is energetically preferred.

The anhydrous chlorotetraammine complex has C_4 symmetry. For the monohydrate, trans C_2 is only stable at MP2 level, and trans C_1 is stable at both levels. A cis C_1 structure has the lowest energy. For the anhydrous chloropentaammine complex, various C_s structures were tested, and only one of them is stable at B3LYP level. A C_1 structure is preferred at MP2 level.

For the anhydrous dichloroammine complex, two C_s structures were attempted. The one with Cl-Ni-Cl symmetry plane is only stable at MP2, whereas the other is only stable at B3LYP level. For the monohydrate, various C_s structures were tried, and only the one in which the chlorides are symmetric about the O-Ni-N plane is stable at both levels. The dihydrate also has C_s symmetry in which nickel, oxygen atoms and nitrogen are in the symmetric plane. The trihydrate is only stable with fac C_1 and mer C_1 (with lower energy) symmetry.

For the dichlorodiammine complex, C_{2v} structure is only stable at MP2 level, and C_1 is preferred at B3LYP. C_{2v} , C_2 and various C_s structures has been tested for the monohydrate, but they all showed imaginary frequencies at both levels, and ultimately it has C_1 symmetry. For the dihydrate, two all-trans C_{2h} structures were tried first, and the one in which the oxygen of water molecules are bisected by the horizontal plane is stable at MP2 level. An all-trans C_i structure is stable at both levels. Cl-trans C_1 structure is energetically preferred at both levels, and NH_3 -trans C_2 , all-cis C_1 and H_2O -trans C_{2v} structures are also stable and competitive in energy.

For the dichlorotriammine complex, high symmetry structures like C_{3h} , C_{3v} and C_3 were attempted first, but none of them is stable. A C_s structure is stable at MP2 level,

and it reduced to C_1 at B3LYP. The mer monohydrate has C_1 symmetry as all the C_s structures tried are unstable. A fac C_s structure has lower energy at B3LYP level, but it possesses an imaginary frequency at MP2 level, where a fac C_1 structure is preferred. For the anhydrous dichlorotetraammine complex, trans- C_{4h} and trans- C_{2v} are energetically preferred at B3LYP and MP2 respectively. Other stable structures as trans- C_2 (both levels), cis- C_{2v} (B3LYP), and cis- C_2 (both levels) are also found and competitive in energy.

Two C_{3v} structures were tried for trichloroammine complex, and only the one in which hydrogens are in the same direction with the chlorides is stable at B3LYP level. A stable C_s structure is located and is energetically preferred at both levels. The monohydrate has C_1 symmetry as all the C_s structures attempted are unstable. For the dihydrate, various C_s structures were attempted, and only the one with a chloride in the second hydration sphere and hydrogen bonded to the water molecules is stable at both levels.

For the anhydrous trichlorodiammine complex, D_{3h} , C_{3h} , C_3 , C_{2v} , C_2 and C_s structures were attempted. The D_{3h} , C_{3h} and C_3 structures have imaginary frequencies at both levels. The C_{2v} structure in which the hydrogens are in the same directions with chlorides is only stable at B3LYP level, whereas the other is only stable at MP2 at is preferred at this level. C_2 structure reverted back to one of the C_{2v} structures after optimization, and C_s structure is energetically preferred at B3LYP. The monohydrate has C_1 symmetry with one of the chloride in the second solvation shell and hydrogen bonded to ammonia and water. For the anhydrous trichlorotriammine complex, fac- C_{3v} structures

is only stable at B3LYP level, whereas the fac- C_3 structure is stable at both levels, and both of them have all the ligands directly bonded to central nickel. Attempts to create a mer isomer resulted in one of the chloride migrated to the second hydration sphere and hydrogen bonded to three ammonia ligands, forming a stable C_1 structures and is energetically preferred at both levels.

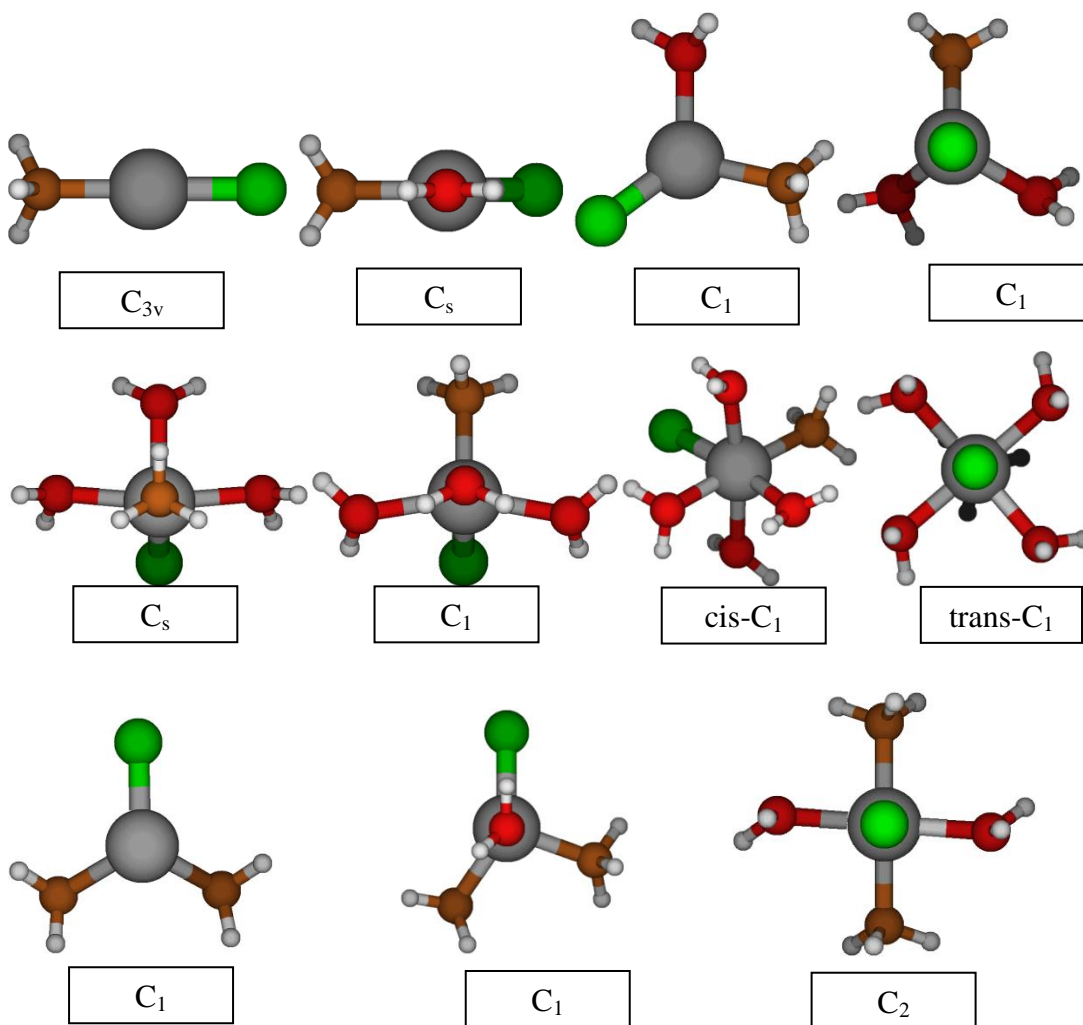


Figure 3-26: Optimized MP2 and B3LYP geometries for $[\text{NiCl}_m(\text{NH}_3)_n(\text{H}_2\text{O})_l]^{2-n}$, where $m=1-2$, $n=0-(6-m)$, $l=0-(6-m-n)$. All symmetries marked with "*" indicate B3LYP otherwise all MP2 and B3LYP structure are similar. (grey=nickel, red=oxygen, white=hydrogen, green=chloride)

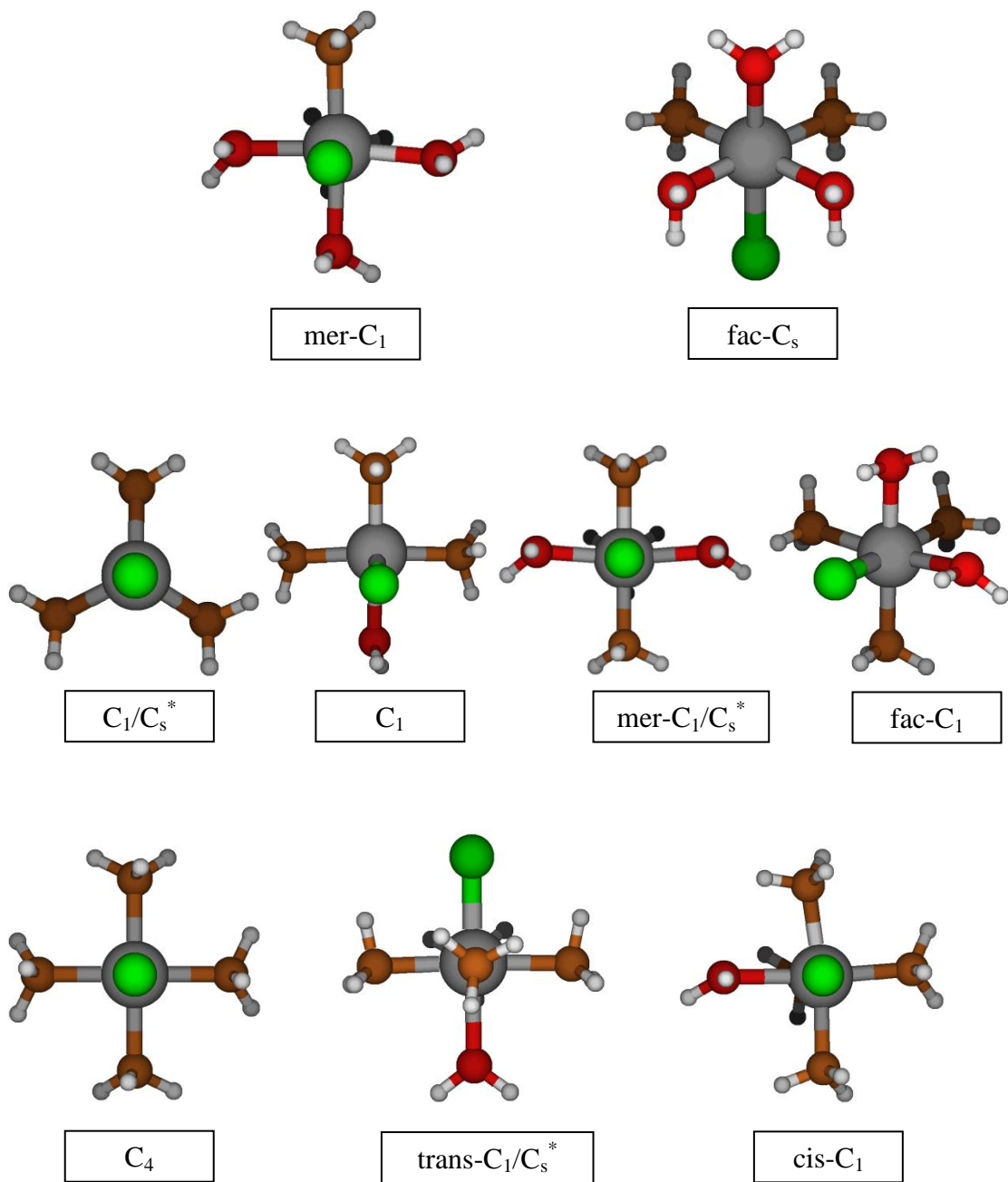


Figure 3-26: (continued)

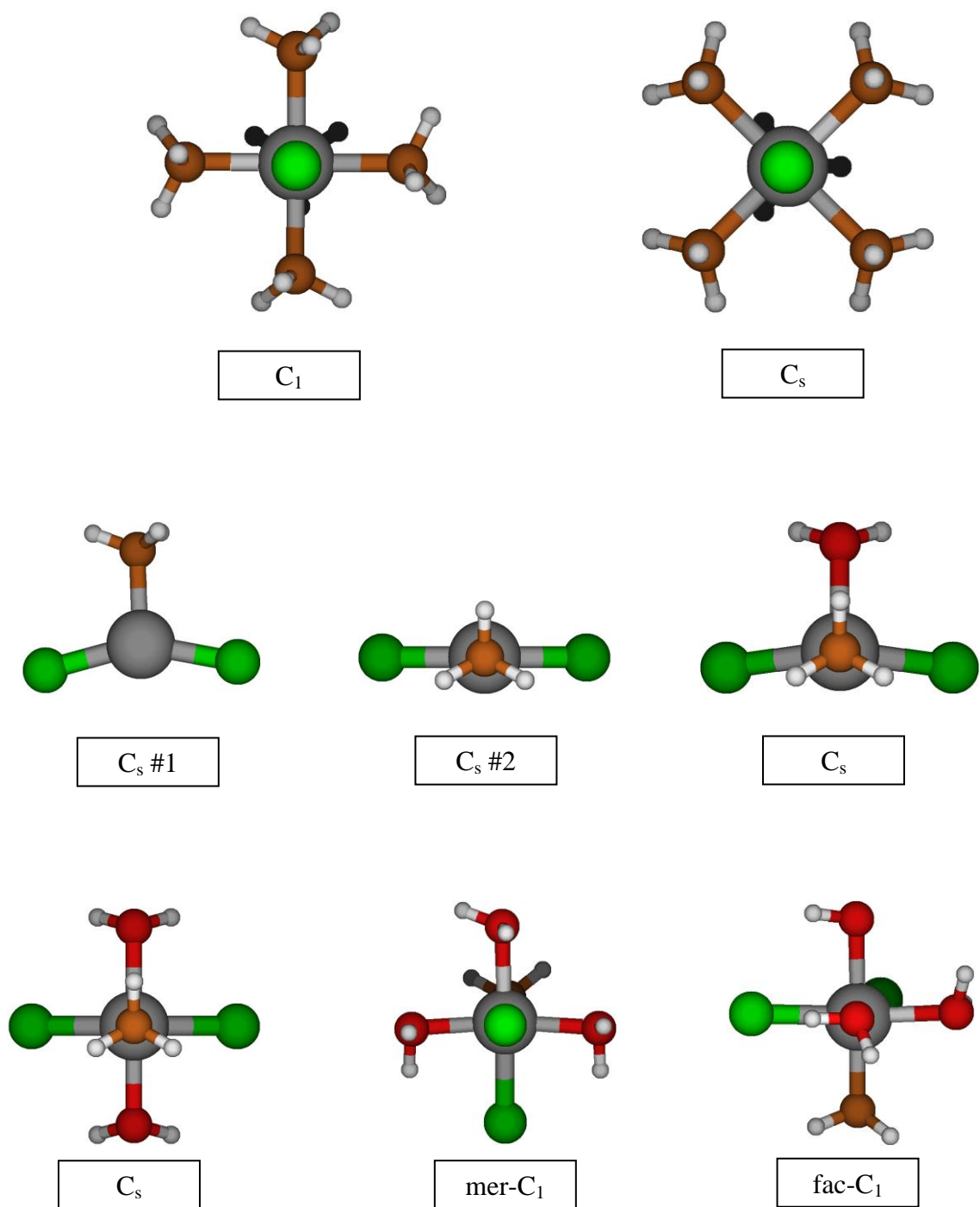


Figure 3-26: (continued)

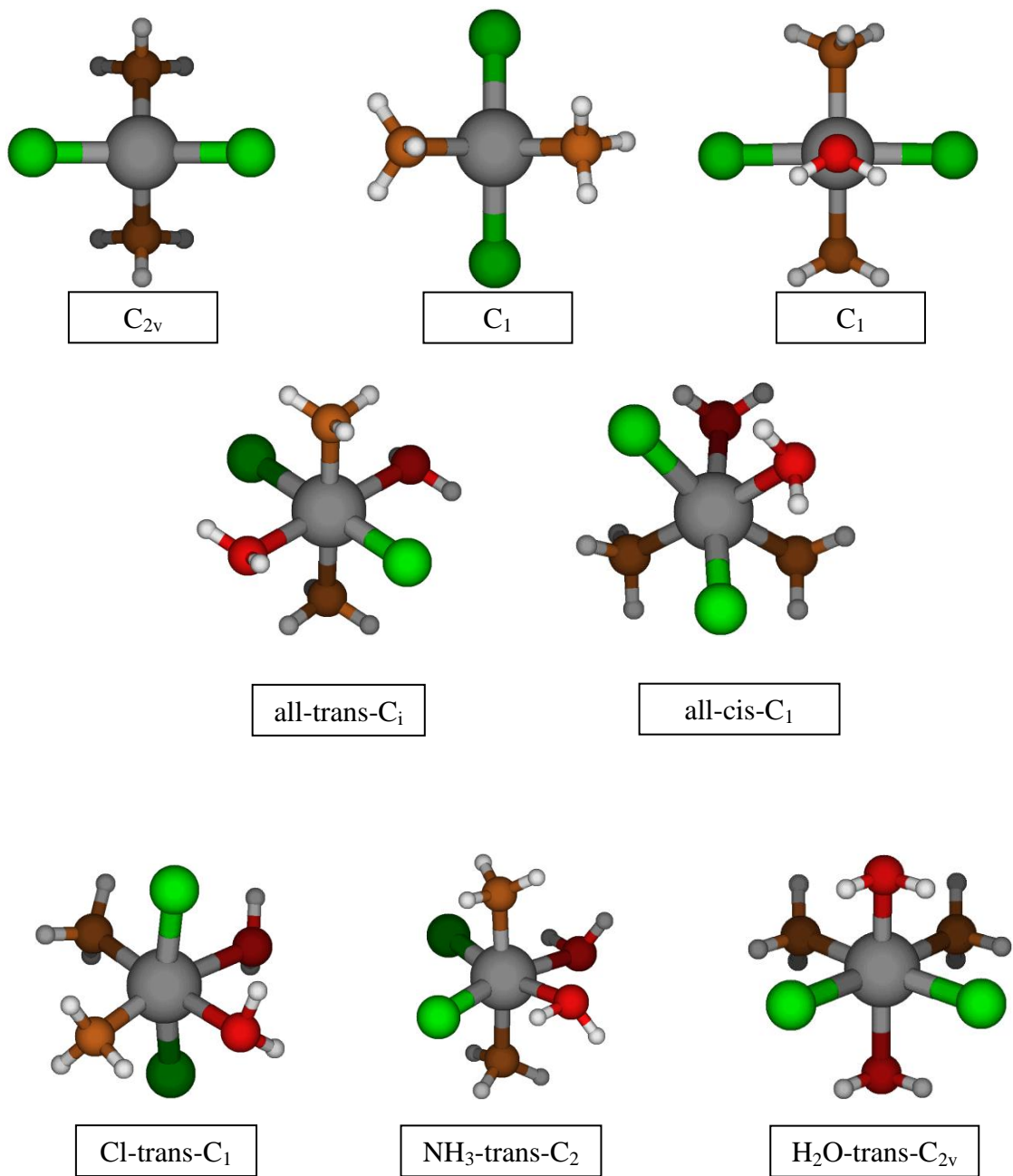


Figure 3-26: (continued)

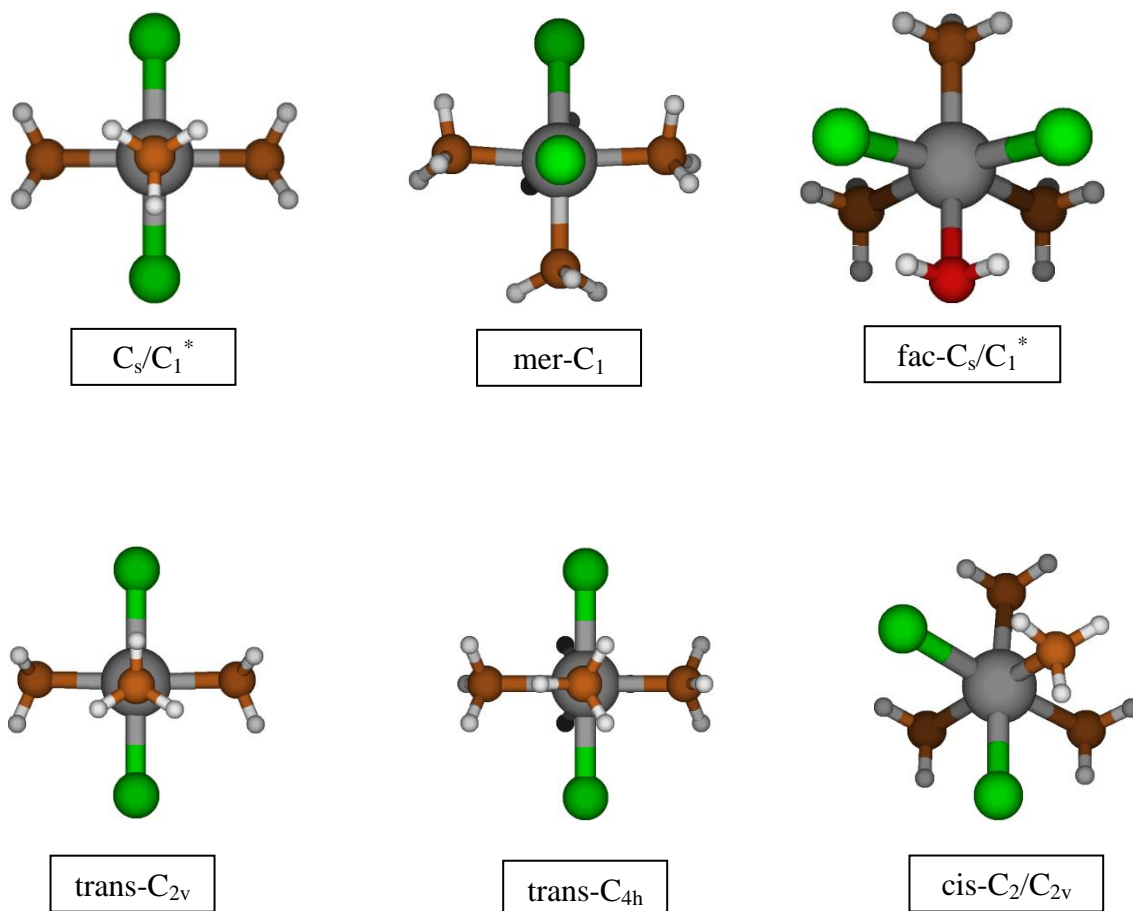


Figure 3-26: (continued)

For the anhydrous tetrachloroammine complex, two C_{3v} structures were tried first. The one in which the hydrogen atoms pointing to the opposite direction with the chlorides is only stable at MP2, whereas the other is only stable at B3LYP level. A C_3 structure is also only stable at B3LYP level and competitive in energy. A C_s structure is preferred at MP2 level. The monohydrate has C_1 symmetry with water and one of the chlorides in the second solvation shell. The anhydrous tetrachlorodiammine complex is stable with C_{2v} geometry in which one of the chlorides is hydrogen bonded to the ammonia ligands.

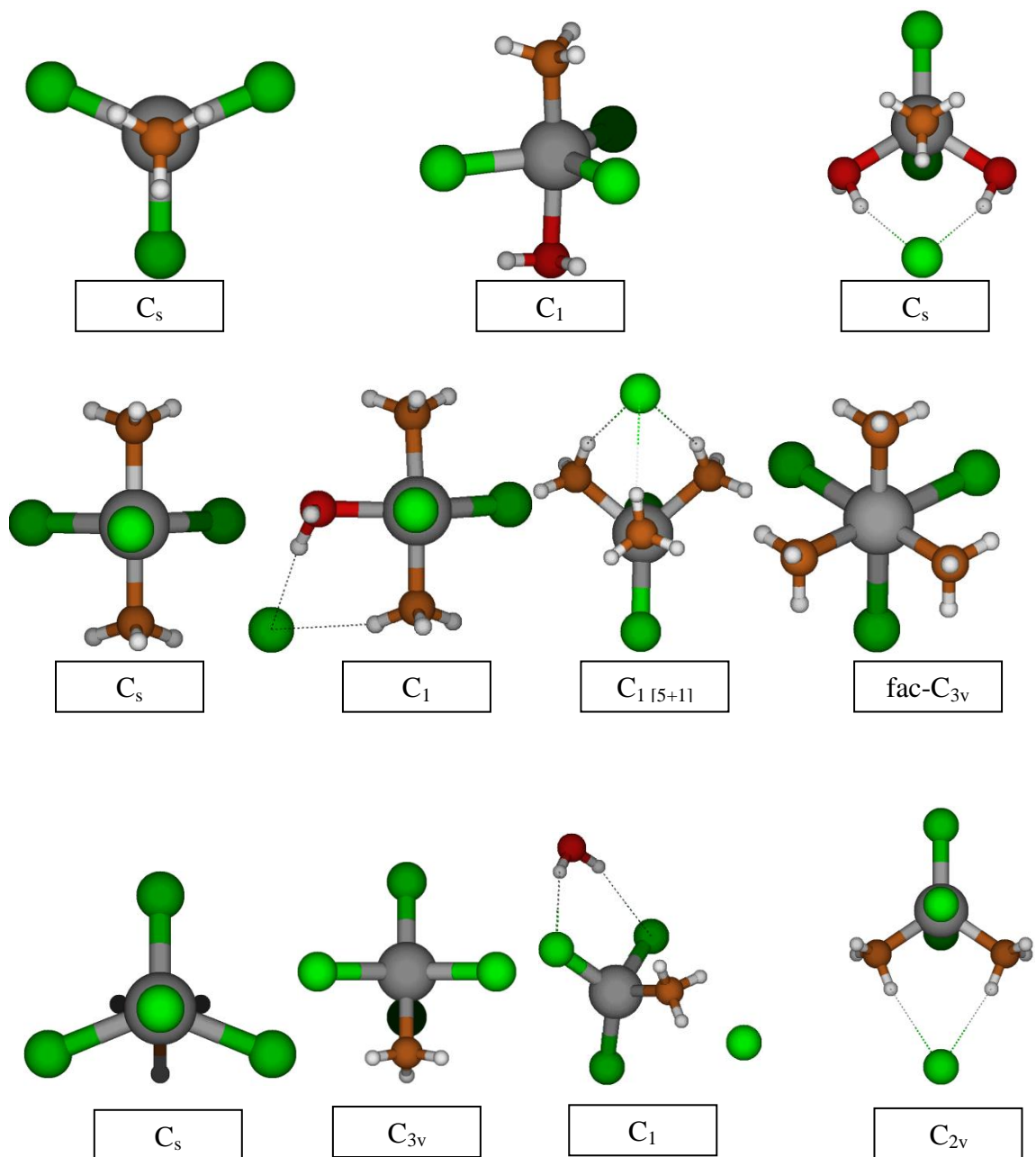


Figure 3-27: Optimized MP2 and B3LYP geometries for $[NiCl_m(NH_3)_n(H_2O)]^{2-n}$, where $m=3-4$, $n=0-(6-m)$, $l=0-(6-m-n)$

3.7.2 Discussion/Literature Comparison

To confirm the geometries that have been investigated, the best way is to compare with computational or experimental studies found in the literature. Stromberg et al. [117] performed B3LYP/BSI (double ζ valence quality) calculation on anhydrous dichloroamminenickel(II) and reported the Ni-Cl and Ni-O bond lengths to be 2.19 Å and 1.90 Å respectively which is comparable with our results of 2.15 Å and 2.04 Å at B3LYP level. Leineweber et al. reported the crystal structure of dichloroamminenickel(II) [118] and dichlorodiammine [119] by XRD. The reported Ni-O and Ni-Cl distances for the dichloroammine complex are 1.96-1.97 Å and 2.375-2.468 Å, and for dichlorodiammine complex are 2.089-2.513 Å. Our results for the dichloroammine complex are 2.05 Å and 2.11 Å at MP2 level, and 2.06 Å and 2.24 Å at B3LYP which are shorter than their results due to our calculations were performed on single molecule in gas phase whereas their experiments are for solid layered crystals with more ligands around a single nickel. Unfortunately no other studies were found containing the geometries of these mixed complexes and therefore there is nothing to compare with any of the remaining geometries.

Plots containing Ni-O, Ni-N and Ni-Cl bond lengths and vibrational stretching frequencies (Figure 3-28, Figure 3-29 and Figure 3-30) have been created and are located below. Each of these has a trend of increasing bond length, for a given complex, when more water molecules are added to the system. The trends become less clear when there are more chloride ligands. With more chloride ligands there is a greater tendency for water and chloride ligand dissociation and subsequent hydrogen bonding to the central

molecule. The effect is usually a small increase in stabilization (decrease in total energy) of the central molecule, thereby resulting in slightly shorter bond lengths. The inverse relationship between bond distance and stretching frequency is observed. A lot of the stretches were mixes of two or more of the Ni-Cl, Ni-N and Ni-O stretches as suggested by the overlap of the characteristic symbols.

Once again, calculated Raman spectra were constructed based on the intensities calculated at the HF level. There is no Raman data found in literature, but these will be useful for future work to be completed by our colleagues.

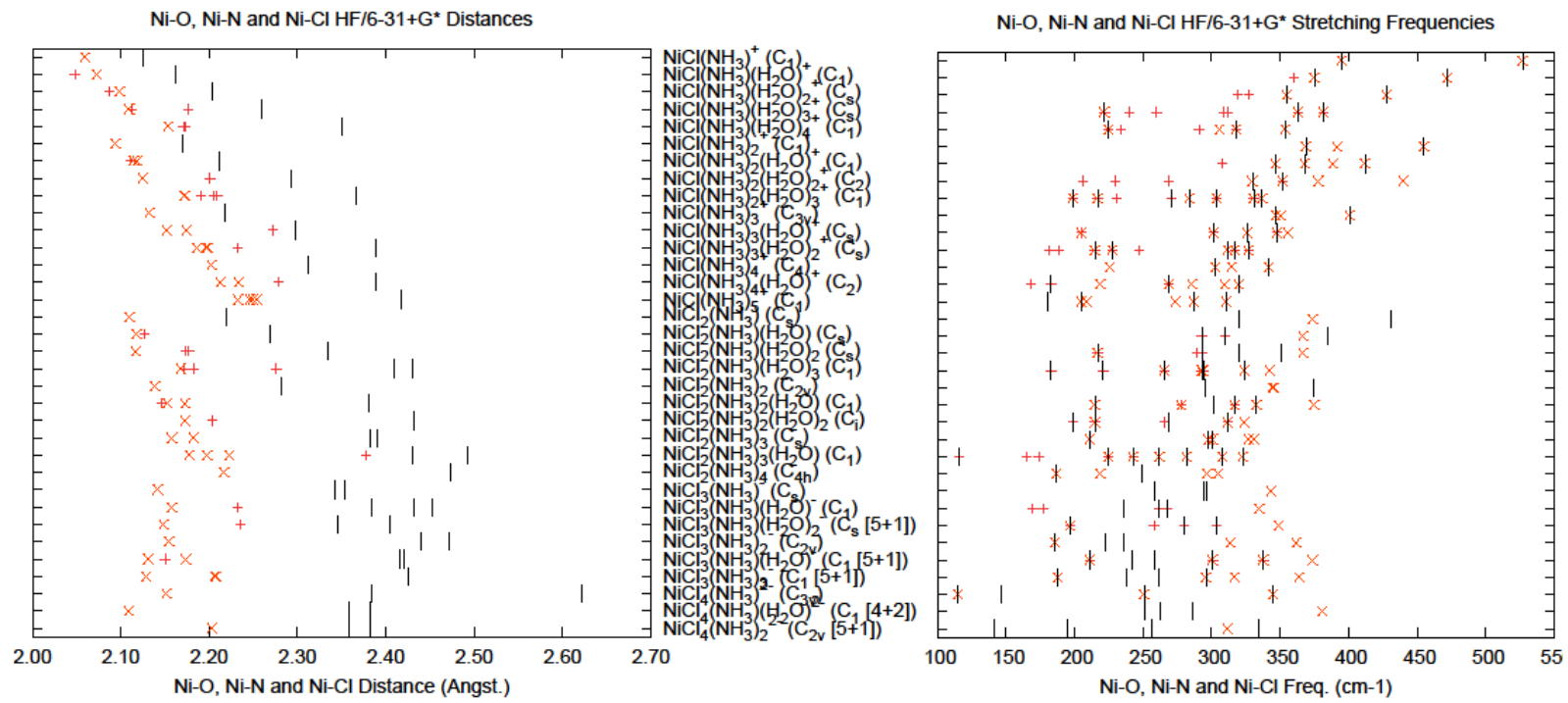


Figure 3-28: Ni-O (+), Ni-N (x) and Ni-Cl (|) bond lengths and vibrational stretching frequencies for $[\text{NiCl}_m(\text{NH}_3)_n(\text{H}_2\text{O})_l]^{2-n}$, where $m=1-4$, $n=1-(6-m)$, $l=0-(6-m-n)$, calculated at HF/6-31+G* level.

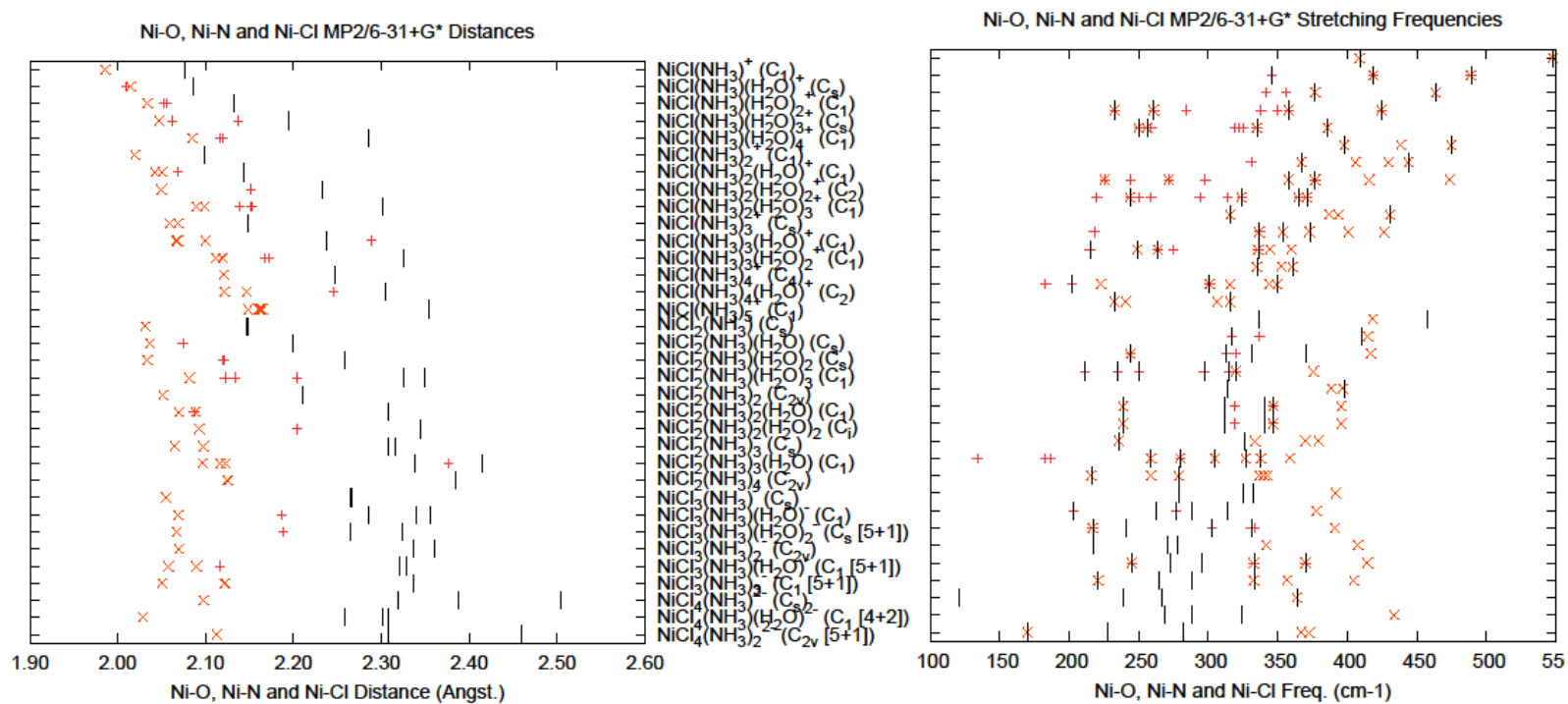


Figure 3-29: Ni-O (+), Ni-N (x) and Ni-Cl (|) bond lengths and vibrational stretching frequencies for $[\text{NiCl}_m(\text{NH}_3)_n(\text{H}_2\text{O})_l]^{2-n}$, where $m=1-4$, $n=1-(6-m)$, $l=0-(6-m-n)$, calculated at MP2/6-31+G* level.

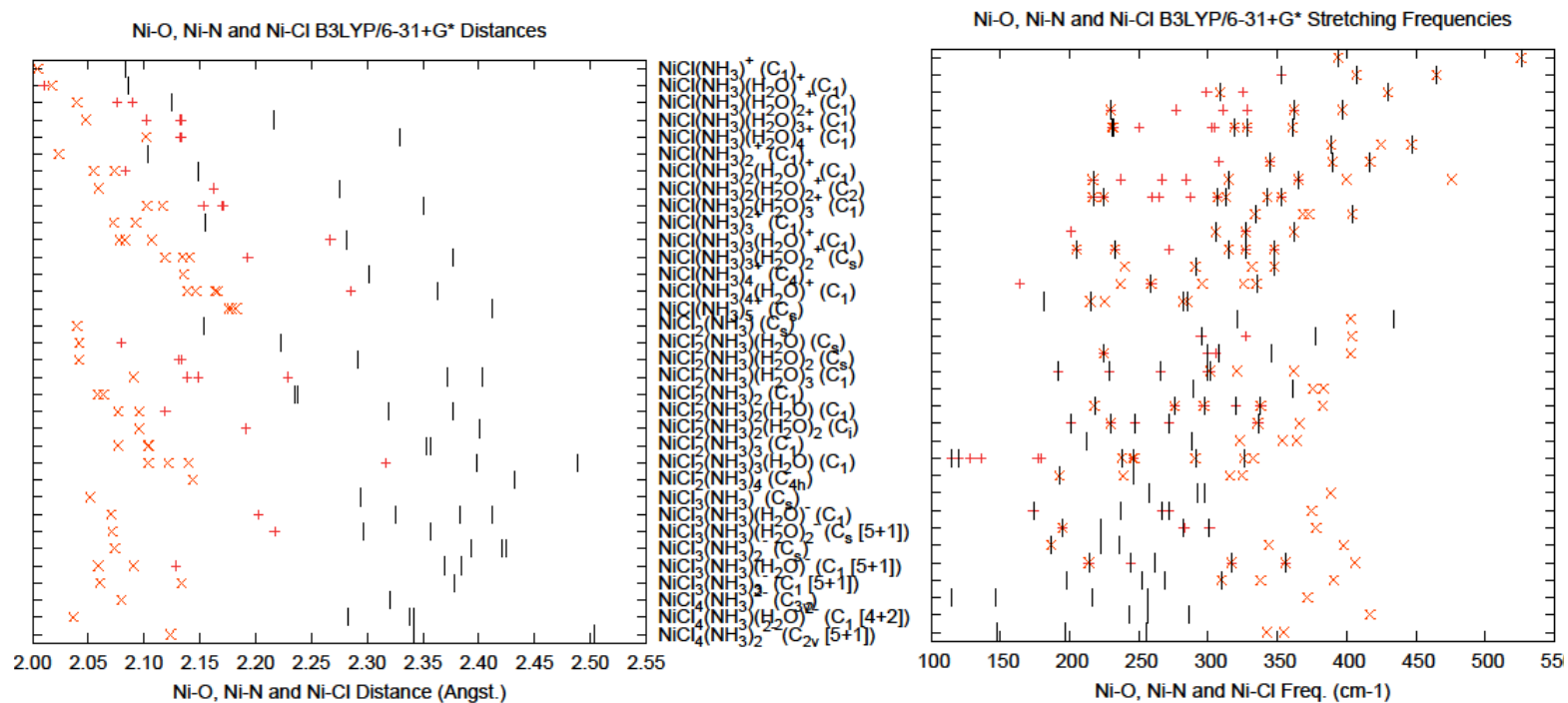


Figure 3-30: Ni-O (+), Ni-N (x) and Ni-Cl (|) bond lengths and vibrational stretching frequencies for $[\text{NiCl}_m(\text{NH}_3)_n(\text{H}_2\text{O})_l]^{2-n}$, where $m=1-4$, $n=1-(6-m)$, $l=0-(6-m-n)$, calculated at B3LYP/6-31+G* level.

3.8 Hydroxoamminenickel(II) Complexes, $[\text{Ni}(\text{OH})_m(\text{NH}_3)_n(\text{H}_2\text{O})_l]^{2-m}$, where $m=1-4$, $n=1-(6-m)$, $l=0-(6-m-n)$

The hydroxoamine complexes were studied up to and including all the combinations of hexa-coordinate complexes. Each molecule investigated has at least one hydroxide ligand and one ammonia ligand. Structures were found for all combinations of ligands with four or less hydroxide ligands. When there are more than four hydroxide ligands, there is significant ligand dissociation. Some of the complexes do not have a completely bound set of ligands as hydrogen bonding is sometimes more energetically preferred. Very few studies were found in the literature that contained hydroxoamine complexes. Therefore, the discussion will be restricted to what have been found regarding geometries, bond length trends and vibrational stretching frequency trends.

3.8.1 Results

The total molecular energies for all optimized structures were tabulated in Table 3A.7 of the supplementary materials. The stable MP2 and B3LYP structures are in Figure 3-31 for the monohydroxoamine and dihydroxoamine complexes, and in Figure 3-32 for the trihydroxoamine and tetrahydroxoamine complexes.

The most stable monohydroxoamine has C_s symmetry, although other stable C_s and C_1 structures exist with slightly higher energy. The monohydrate has C_1 symmetry as all the C_s structures tried are unstable. The dihydrate and trihydrate are similar as they all have C_1 symmetry at both levels. The tetrahydrate has stable trans C_1 (with lower energy) and cis C_1 structures.

Various C_s structures were tried for the anhydrous hydroxodiammine complex, but they all have imaginary frequencies at both levels. A C_1 structure is preferred. The monohydrate is only stable with C_1 symmetry. The dihydrate has a stable C_s structure at MP2 level, but a C_1 structure is energetically preferred at both levels. The trihydrate has stable fac- C_1 (with lower energy) and mer- C_1 structures.

The anhydrous hydroxotriammine complex has stable C_s structure at both levels, and C_1 is preferred at B3LYP level. For the monohydrate, the C_s structure has imaginary mode A'' at both levels. Using tight optimization convergence criterion still resulted in a low imaginary mode A'' (around -13 cm^{-1}) at both levels. A C_1 structure (looks similar to C_s) is preferred. For the dihydrate, a stable mer C_s and two mer C_1 structure has been located, but a fac C_s structure with lower energy is preferred.

The anhydrous hydroxotetraammine complex has C_s symmetry. For the monohydrate, all the C_s structures attempted have imaginary frequencies at both levels, and cis C_1 structure is preferred. A trans C_1 structure is also stable and competitive in energy. For the anhydrous hydroxopentaammine complex, the C_s structure is only stable at B3LYP level, and it reduced to C_1 at MP2.

The anhydrous dihydroxoammine complex is stable with the highest possible symmetry C_s . For the monohydrate, the C_s structure is only stable at B3LYP level, and C_1 structure is preferred at both levels. The dihydrate (C_1) and trihydrate (C_1) presented similar results, except the trihydrate has a water molecule in the second hydration sphere and hydrogen bonded to water and hydroxide.

The anhydrous dihydroxodiammine is stable with its highest possible symmetry C_{2h} , C_{2v} , C_2 , C_s and C_1 were sequentially tested for the monohydrate, but only the C_1 structure is stable at both levels with a water molecule in the second solvation shell and hydrogen bonded to one of the hydroxide. For the dihydrate, stable structures found were one C_s structure, two C_2 structures, and four C_1 structures. One of the C_2 structure in which two water molecules hydrogen bonded with only hydroxide ligands is preferred at both levels.

The anhydrous dihydroxotriammine complex is only stable with C_1 geometry. The monohydrate also has stable C_1 symmetry (preferred at MP2) with the water molecule in the second hydration sphere and hydrogen bonded to the ammonia and both of the two hydroxides. A fac C_s structure is energetically preferred at B3LYP level. The anhydrous dihydroxotetraammine complex has stable trans C_2 , trans C_1 (energetically preferred at B3LYP), and cis C_2 (with lowest energy at MP2).

For the anhydrous trihydroxoammine complex, two C_{3v} structures were tried first. They both possessed numerous imaginary frequencies at both levels, and so are C_3 and C_s structures. A C_1 structure is preferred at both levels. The monohydrate and dihydrate are both only stable with C_1 symmetry, and in which all the water molecules migrated to the second sphere and hydrogen bonded to hydroxides.

C_{3h} , C_{3v} , C_3 , C_s and C_1 structures were sequentially attempted for the anhydrous trihydroxodiammine complex, and only C_1 structure with one of the ammonia in the second solvation shell and hydrogen bonded to hydroxides. For the monohydrate, the added water molecules stayed with one of the ammonia in the second hydration sphere

and hydrogen bonded to hydroxides forming a C_1 structure. For the trihydroxotriammine complexes, stable structures found were C_3 [3+3] (energetically preferred at B3LYP) and C_1 [4+2] (with lowest energy at MP2).

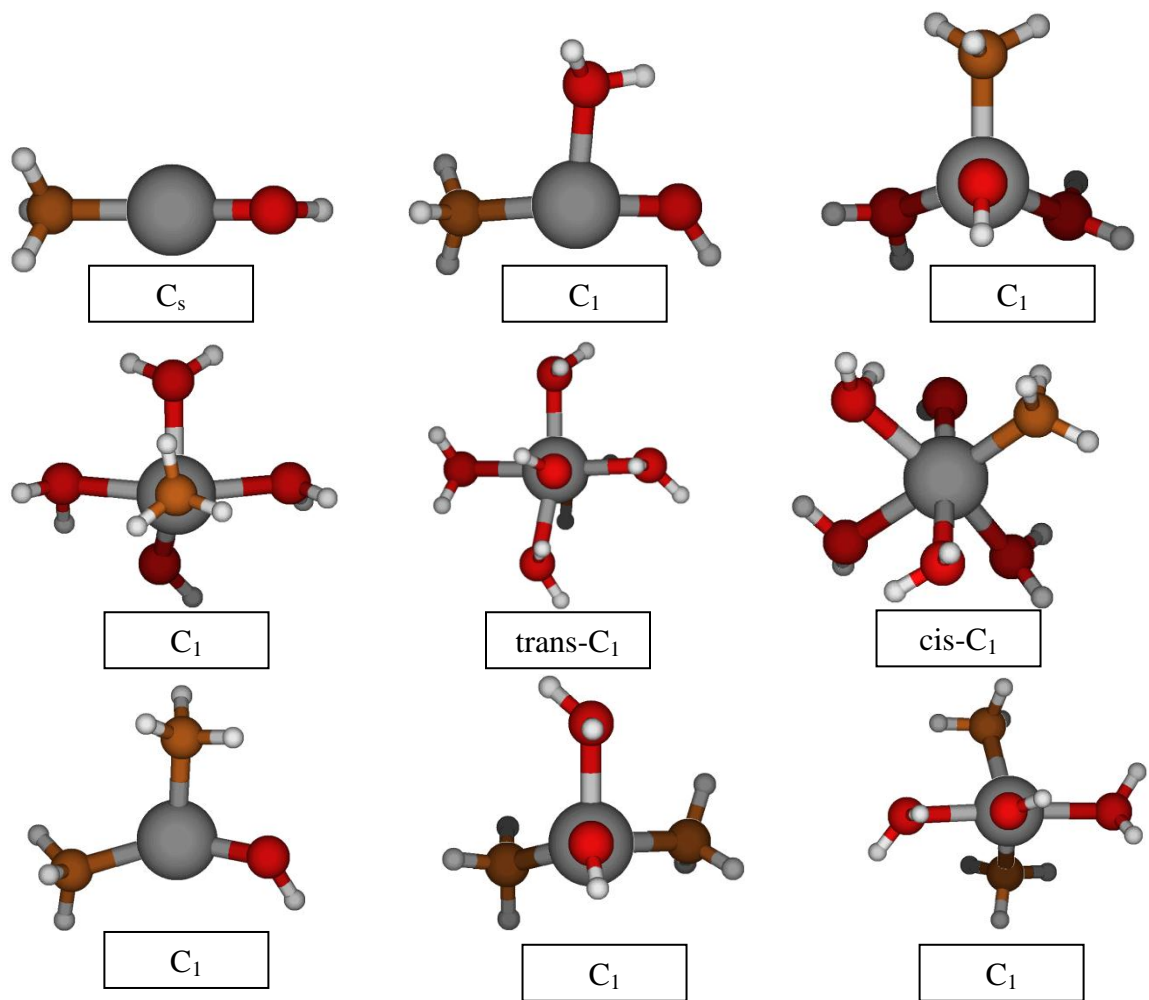


Figure 3-31: Optimized MP2 and B3LYP geometries for $[\text{Ni}(\text{OH})_m(\text{NH}_3)_n(\text{H}_2\text{O})_l]^{2-n}$, where $m=1-2$, $n=0-(6-m)$, $l=0-(6-m-n)$. (grey=nickel, white=hydrogen, brown=nitrogen)

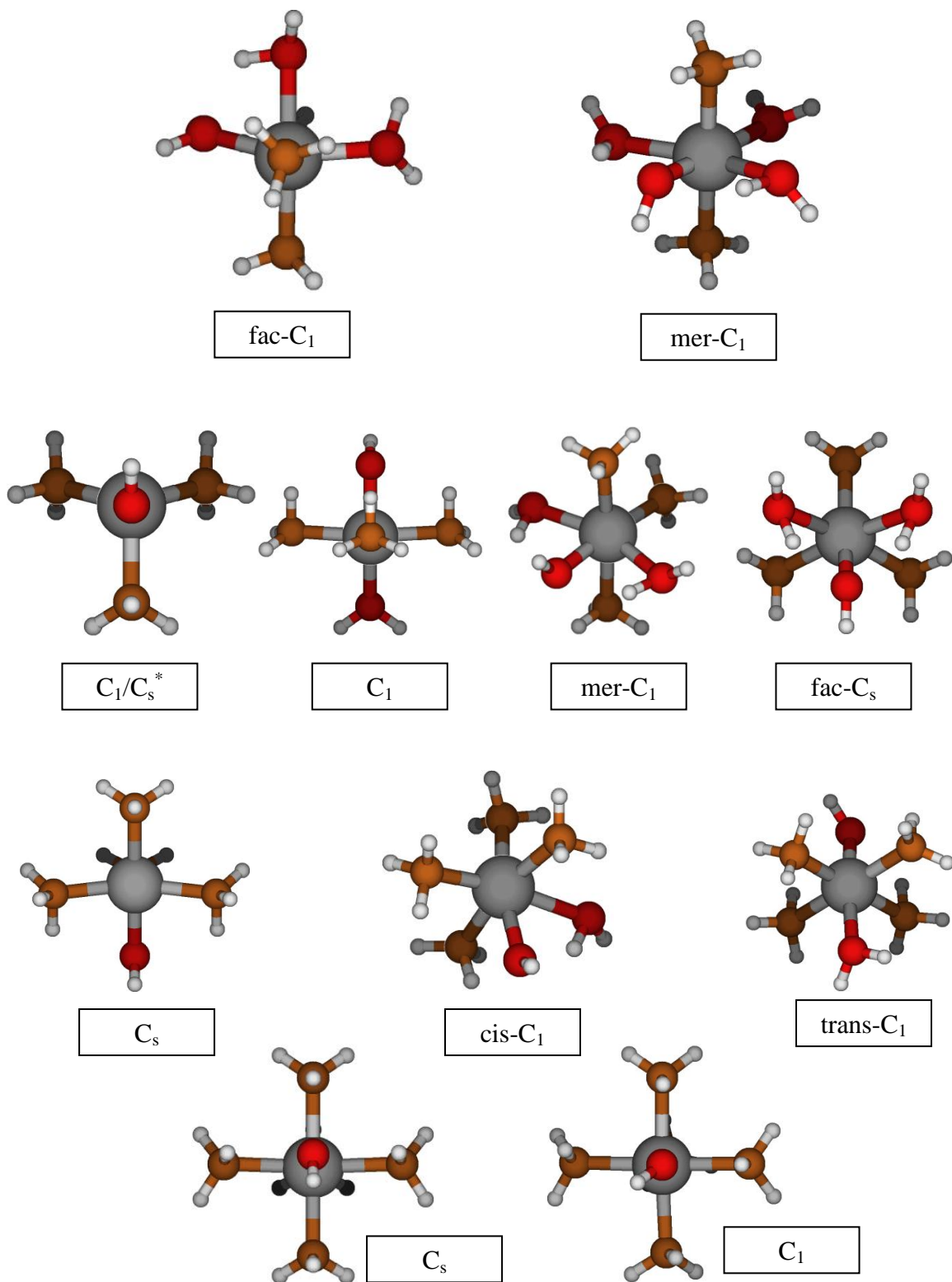


Figure 3-31: (continued)

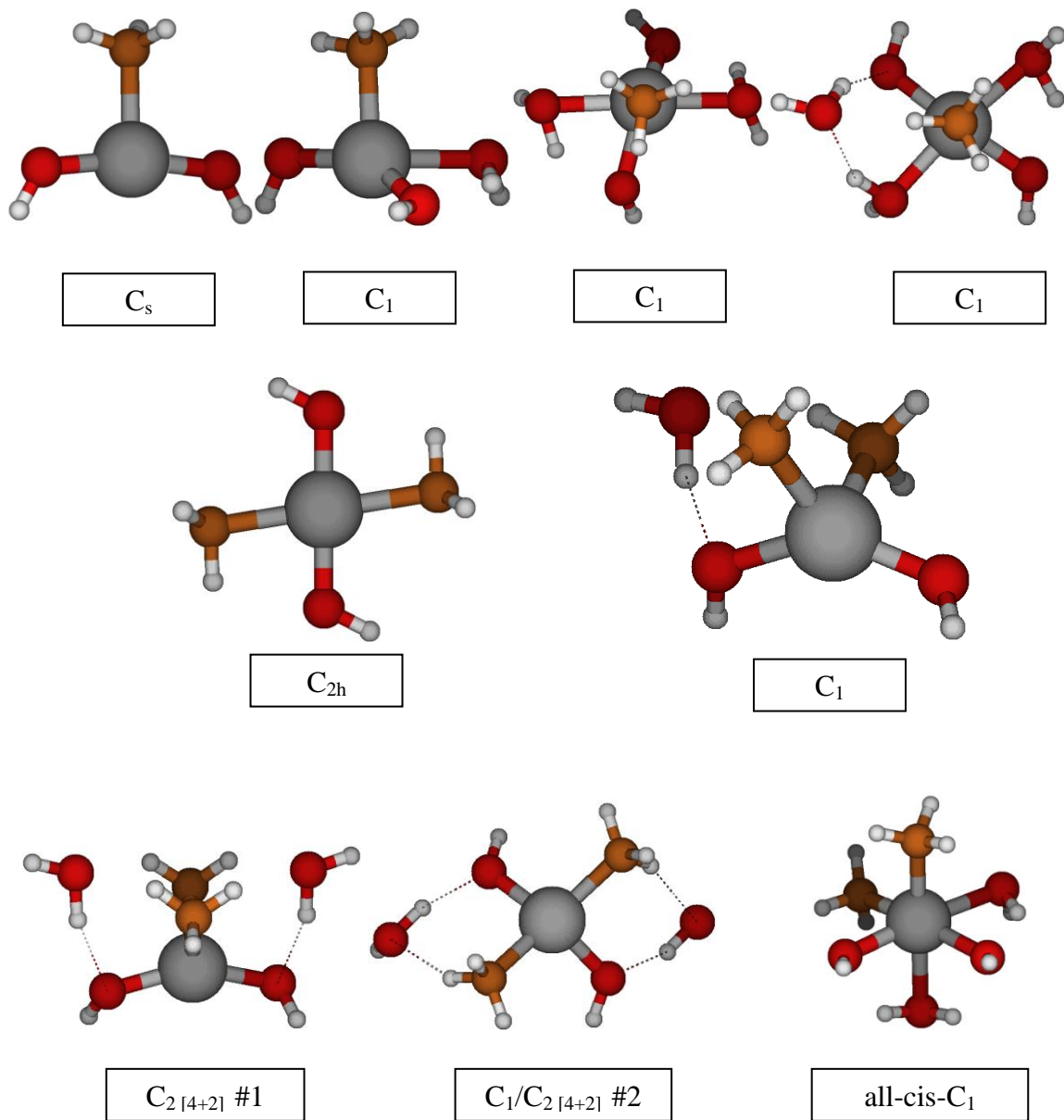
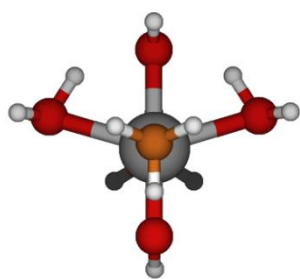
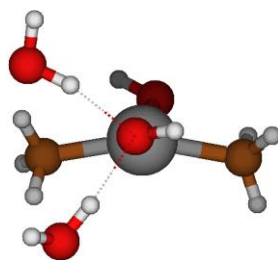


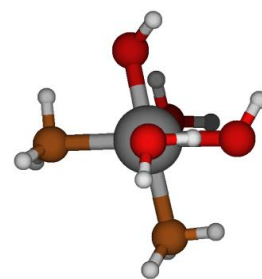
Figure 3-31: (continued)



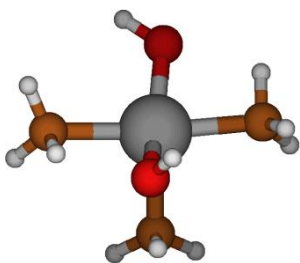
all-trans- C_s



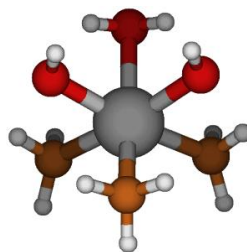
$C_1 [4+2]$



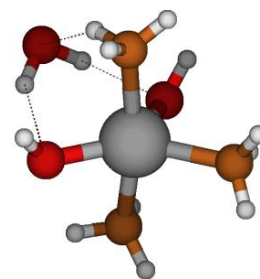
H_2O -trans- C_1



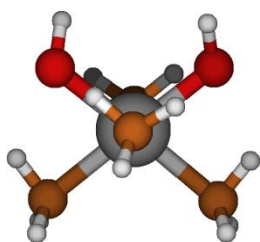
C_1



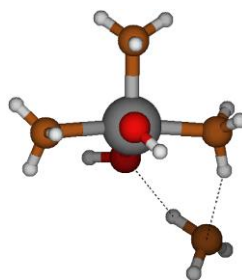
fac- C_s



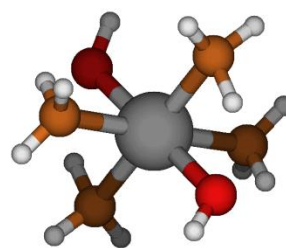
$C_1 [5+1]$



cis- C_2



trans- C_1



trans- C_2

Figure 3-31: (continued)

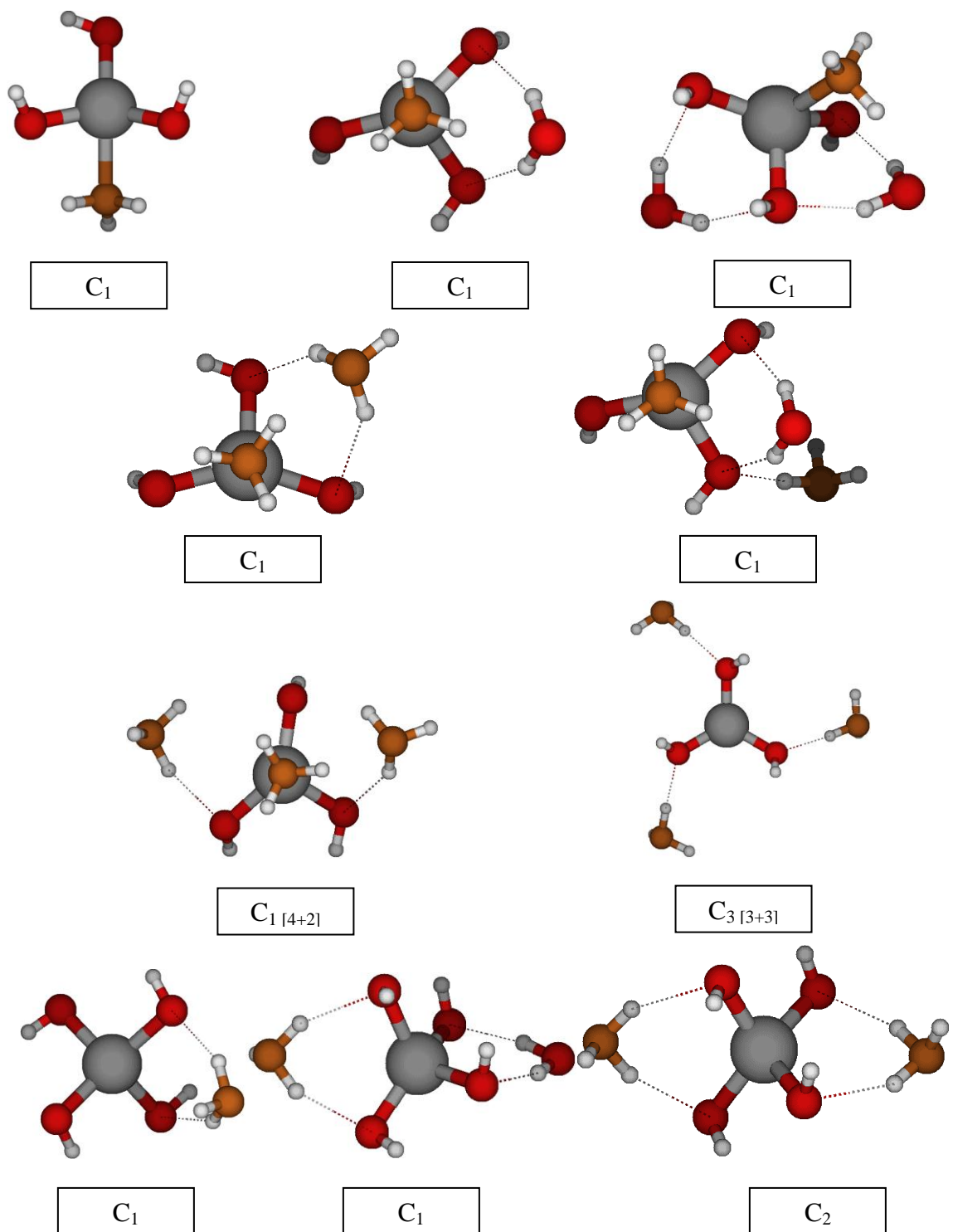


Figure 3-32: Optimized MP2 and B3LYP geometries for $[\text{Ni}(\text{OH})_m(\text{NH}_3)_n(\text{H}_2\text{O})_l]^{2-n}$, where $m=3-4$, $n=0-(6-m)$, $l=0-(6-m-n)$

The anhydrate tetrahydroxoammine complex is stable with C_1 symmetry with the ammonia in the second solvation shell and hydrogen bonded to hydroxides. For the monohydrate, only the four hydroxides are directly bonded to central nickel, whereas the water and ammonia are in the second hydration shell and hydrogen bonded to hydroxides. The anhydrate tetrahydroxodiammine complex has C_2 symmetry with both of the ammonia hydrogen bonded to the hydroxides.

3.8.1 Discussion/Literature Comparison

No structural information was found in the literature for the hydroxoammine complexes, therefore there is no data to compare with what have been found in this research. However, the trends within the bond length and vibrational frequency plots those need is discussed. Plots containing Ni-O and Ni-N bond lengths and vibrational stretching frequencies (Figure 3-33, Figure 3-34 and Figure 3-35) have been created and are located below. The general trend within all the bond distance plots is that the Ni-O and Ni-N bond distances increase as more water molecules are added to the given complex. There was no ion pair formation among this set of complexes (i.e. no dissociation of hydroxide ligands). An inverse relationship exists between the bond distances and the vibrational stretching frequencies associated with those bonds. This is evident when looking at both the bond distance and stretching frequency plots side by side. As the bond lengths are increasing the vibrational stretching frequencies are decreasing to lower wavenumbers.

Raman intensity plots were created from the data obtained at the HF/6-31+G* level of theory. Although no experimental data could be found related to Raman activity

for this set of complexes, it is still of importance to our colleagues to have this information for comparison with their experimental Raman work in the future. Plots were constructed for all the HF energy minimum structures. Having this information will help in either assigning or confirming the experimental Raman bands.

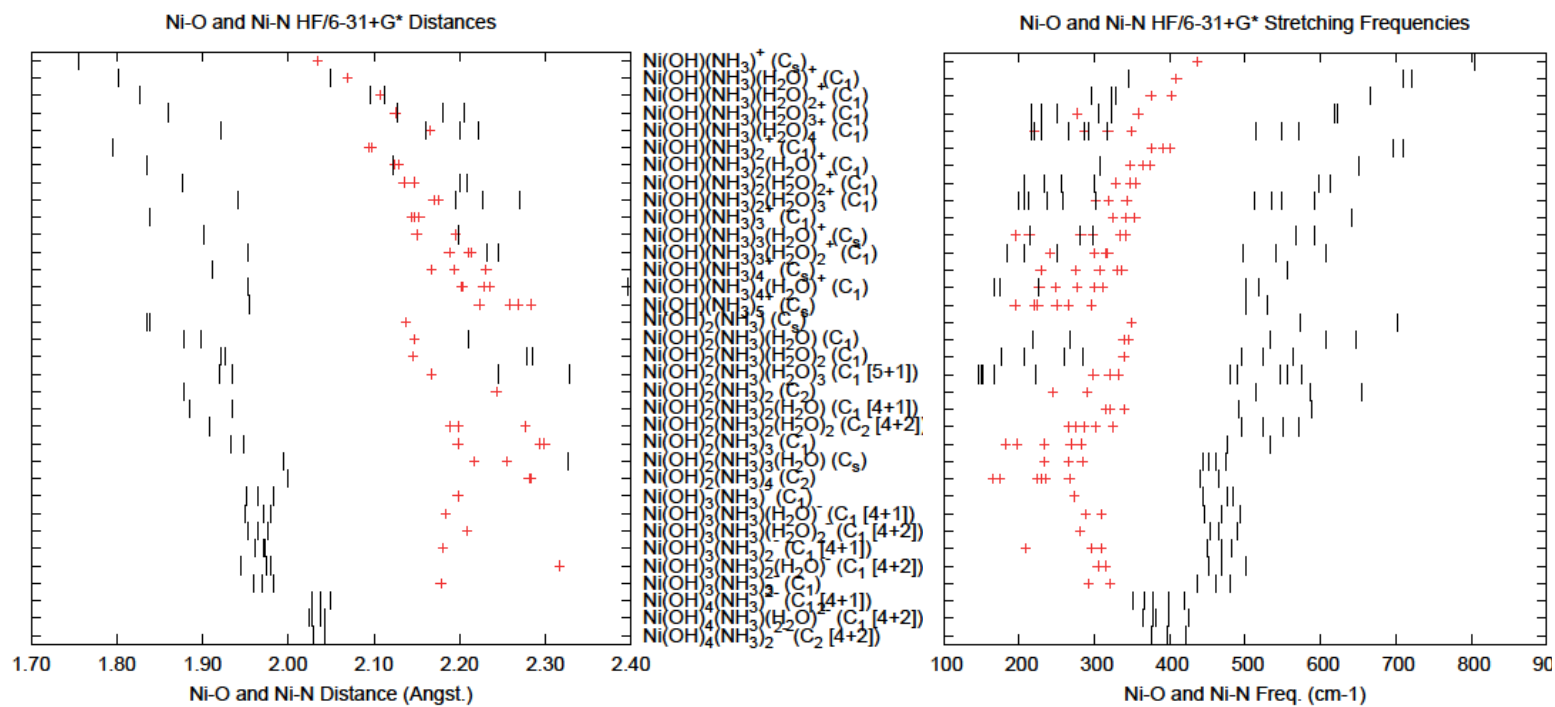


Figure 3-33: Ni-O (|) and Ni-N (+) bond lengths and vibrational stretching frequencies for $[\text{Ni(OH)}_m(\text{NH}_3)_n(\text{H}_2\text{O})_l]^{2-n}$, where $m=1-4$, $n=1-(6-m)$, $l=0-(6-m-n)$, calculated at HF/6-31+G* level.

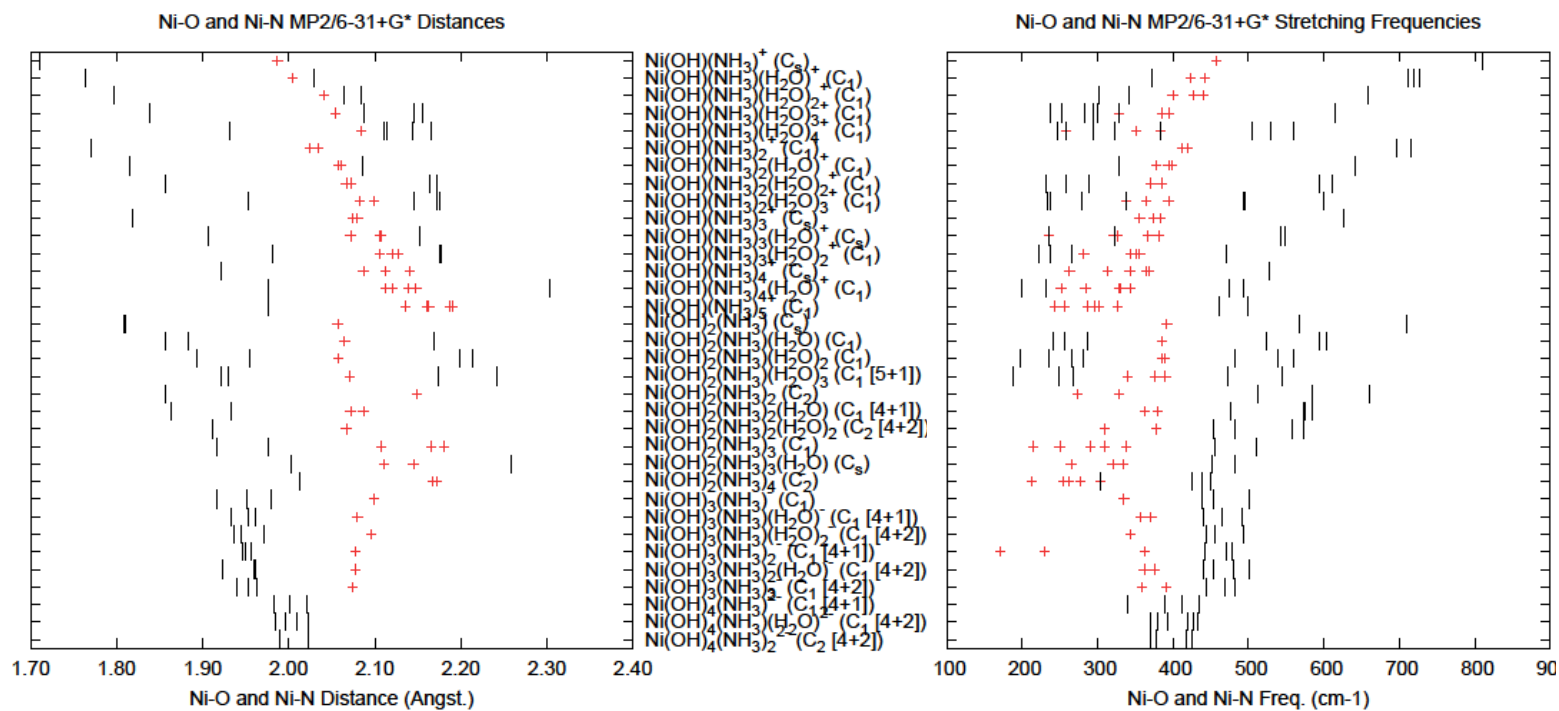


Figure 3-34: Ni-O (|) and Ni-N (+) bond lengths and vibrational stretching frequencies for $[\text{Ni(OH)}_m(\text{NH}_3)_n(\text{H}_2\text{O})_l]^{2-n}$, where $m=1-4$, $n=1-(6-m)$, $l=0-(6-m-n)$, calculated at MP2/6-31+G* level.

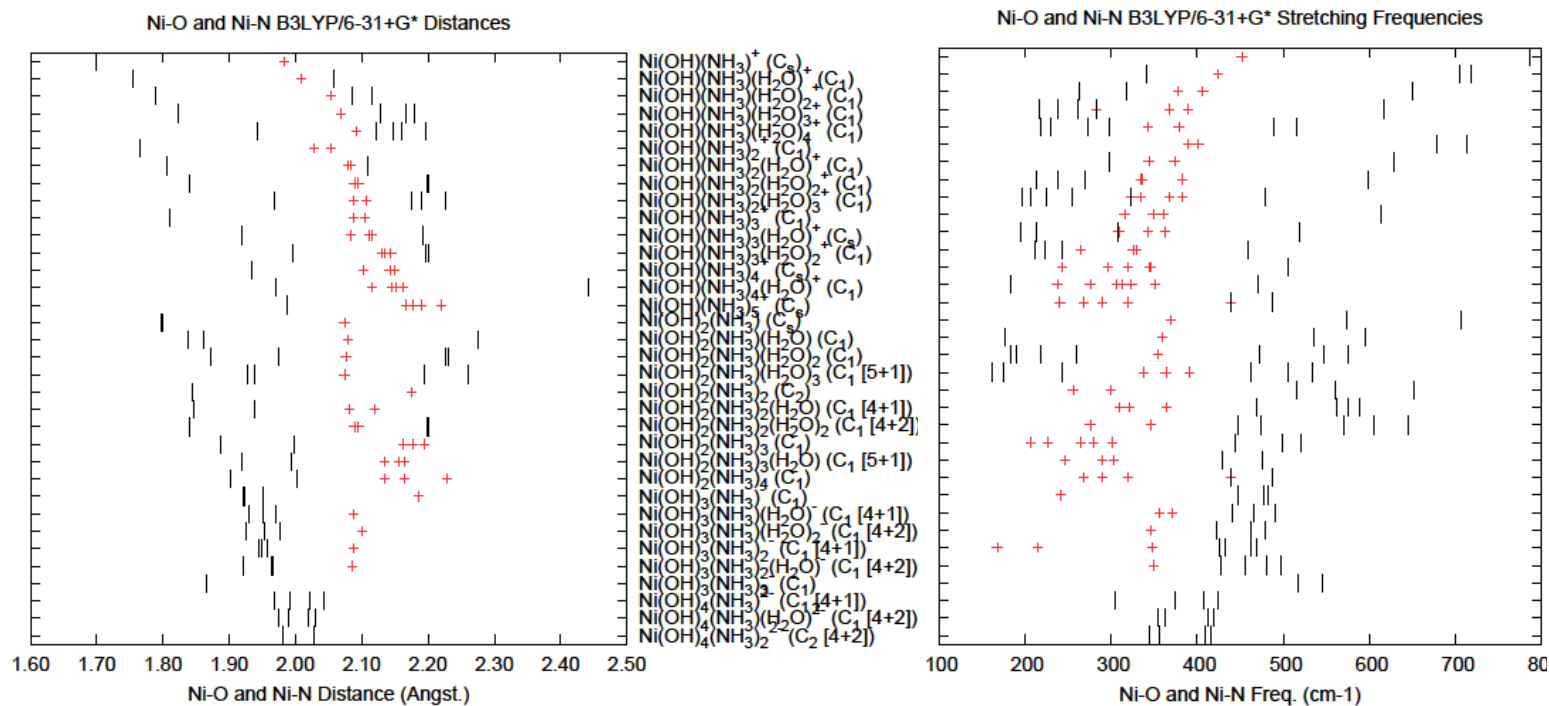


Figure 3-35: Ni-O (|) and Ni-N (+) bond lengths and vibrational stretching frequencies for $[\text{Ni}(\text{OH})_m(\text{NH}_3)_n(\text{H}_2\text{O})_l]^{2-n}$, where $m=1-4$, $n=1-(6-m)$, $l=0-(6-m-n)$, calculated at B3LYP/6-31+G* level.

3.9 Chlorohydroxoamminenickel(II) Complexes, $[\text{NiCl}_m(\text{OH})_n(\text{NH}_3)_l(\text{H}_2\text{O})_k]^{2-}$ ^{m-n}, where m=1-3, n=1-(4-m), l=0-(6-m-n), k=0-(6-m-n-l).

This set of complexes was studied up to and including the overall hexa-coordinate species with various combinations of chloride, hydroxide, ammonia and water. All complexes have at least one chloride, one hydroxide, and one ammonia ligand. Many of these complexes tended to form ion pairs. No stable structures were found for anhydrous trihydroxochlorodiammine complex as all the possible geometries attempted resulted in dissociation of chloride ligand. No experimental or computational studies were found in the literature therefore the discussion will be limited to our findings regarding geometries, bond length and vibrational stretching frequency trends.

3.9.1 Results

Total energies have been tabulated for all successfully optimized geometries and can be seen in Table 3A.8 in the supplementary materials section. The optimized geometries of stable structures can be seen in Figure 3-36 for chlorohydroxoammine complexes, and Figure 3-37 for dichlorohydroxoammine and trichlorohydroxoammine complexes.

For the anhydrous chlorohydroxoammine complex, four C_s structures were attempted and only two of them are stable at both levels, and one is energetically preferred at MP2 level, whereas the other is preferred at B3LYP level. The monohydrate and dihydrate are both stable with C_1 symmetry as all the C_s structures attempted are all unstable. For the trihydrate, both fac and mer (with lower energy) isomers are stable with C_1 symmetry.

The anhydrous chlorohydroxodiammine complex has C_1 symmetry. The monohydrate is stable with C_1 symmetry with all the ligands directly bonded to central nickel(II) at MP2 level, but the water molecule dissociated and hydrogen bonded to hydroxide ligand at B3LYP level. For the dihydrate, depending on the trans-cis isomers, five stable C_1 structures and a C_s structure were located, and two of which has water molecules involved in the formation of hydrogen bonds, and one of them is energetically preferred at both levels.

The anhydrous chlorohydroxotriammine complex is only stable with C_1 symmetry. For the monohydrate, a fac C_1 structure with all the ligands directly bonded to nickel is most stable at MP2 level, and a C_1 structure with the water molecule in the second hydration sphere is energetically preferred at B3LYP level. Various C_s structures were tried for chlorohydroxotetraammine complex, and only one of the trans C_s is stable at B3LYP level, and a trans C_1 structure is stable at both levels. A cis C_s structure is energetically preferred at both levels.

Stable structures as C_s and C_1 were located for anhydrous chlorodihydroxoammine complex, and C_s has lower energy at B3LYP level whereas C_1 is energetically preferred at MP2. The monohydrate has a stable C_s structure at MP2 level, but C_1 structure with water molecule in the second solvation shell and hydrogen bonded to hydroxide ligands has lower energy at both levels. The dihydrate was similar except the C_s structure is stable at both levels and the C_1 structure (looks similar to C_s) with the chloride ligand hydrogen bonded to hydroxide and ammonia ligands instead of water molecule.

The anhydrous chlorodihydroxodiammine complex has stable C_2 (MP2) and C_1 (both levels with lower energy) structures and both of them have the chloride ligand in the second hydration sphere and hydrogen bonded to the ammonia ligands. The monohydrate has C_1 symmetry in which the water molecule is not coordinated to the central Ni^{2+} but is involved in the formation of hydrogen bond with coordinated hydroxide ligand. The anhydrous chlorodihydroxotriammine complex also have C_1 symmetry with the chloride and one of the ammonia ligands involved in the formation of hydrogen bonds with hydroxide and ammonia ligands.

Various geometries as C_{3v} , C_3 , C_s and C_1 were tried for chlorotrihydroxoammine complex, but only one of the C_1 structure with ammonia ligand in the second hydration sphere and hydrogen bonded to the hydroxide ligands is stable at MP2 level. All the structures attempted showed dissociation of either ammonia or chloride ligand at B3LYP level, so no stable structures were found at this level. For the monohydrate, all the C_s and C_1 structures tried also showed dissociation of chloride or ammonia ligand at both levels, so no stable structure was found for this complex. Also, no stable structures were located for chlorotrihydroxodiammine complex.

The anhydrous dichlorohydroxoammine complex is only stable with C_1 symmetry. The monohydrate is stable with its highest symmetry C_s . Attempt to add a second water result in the formation of hydrogen bonds of water with chloride ligands and a C_1 structure is formed.

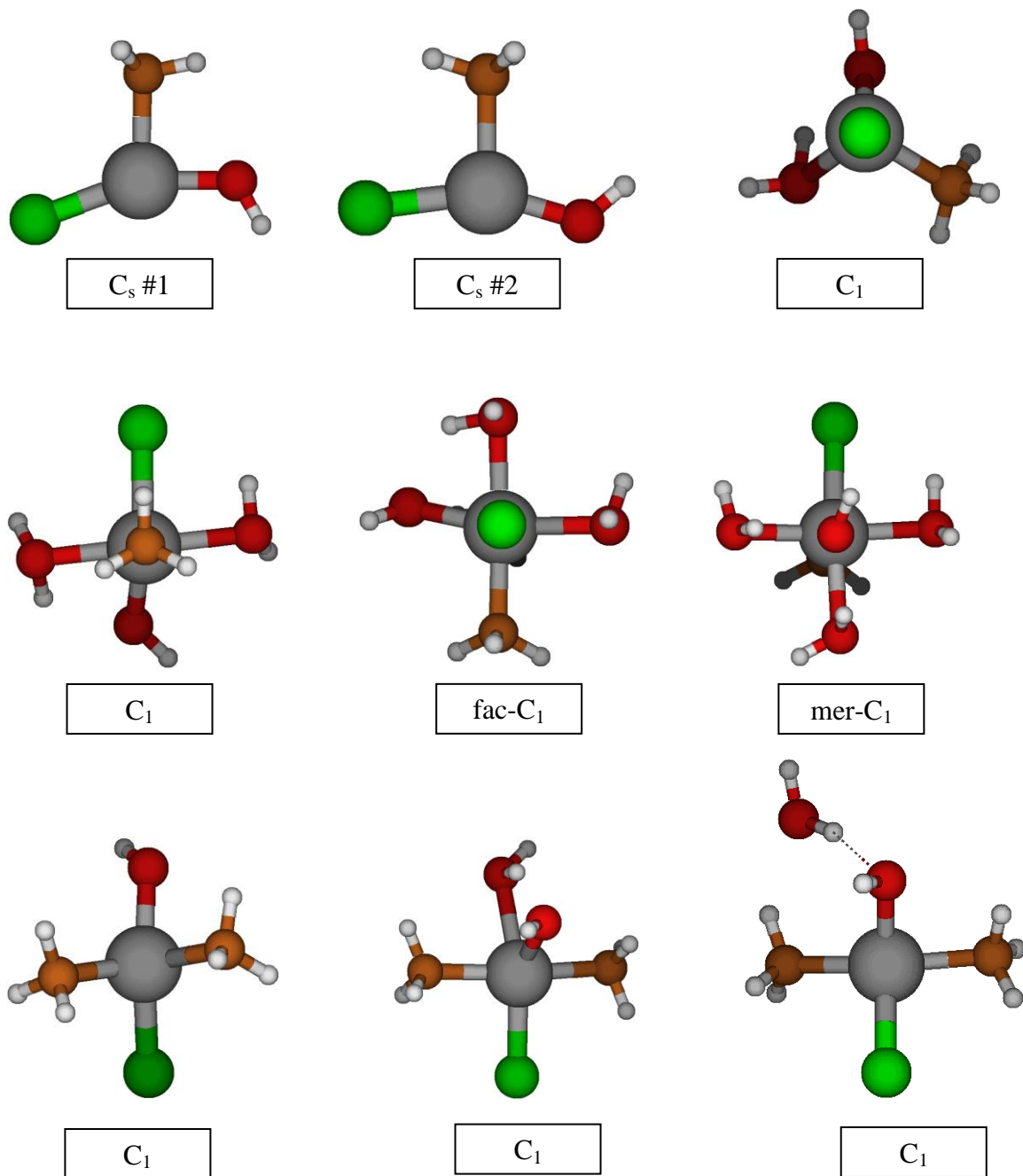


Figure 3-36: Optimized MP2 and B3LYP geometries for $[\text{NiCl}(\text{OH})_n(\text{NH}_3)_l(\text{H}_2\text{O})_k]^{1-n}$, where $n=1-3$, $l=1-(5-n)$, $k=0-(5-n-l)$. (grey=nickel, brown=nitrogen, green=chloride, white=hydrogen)

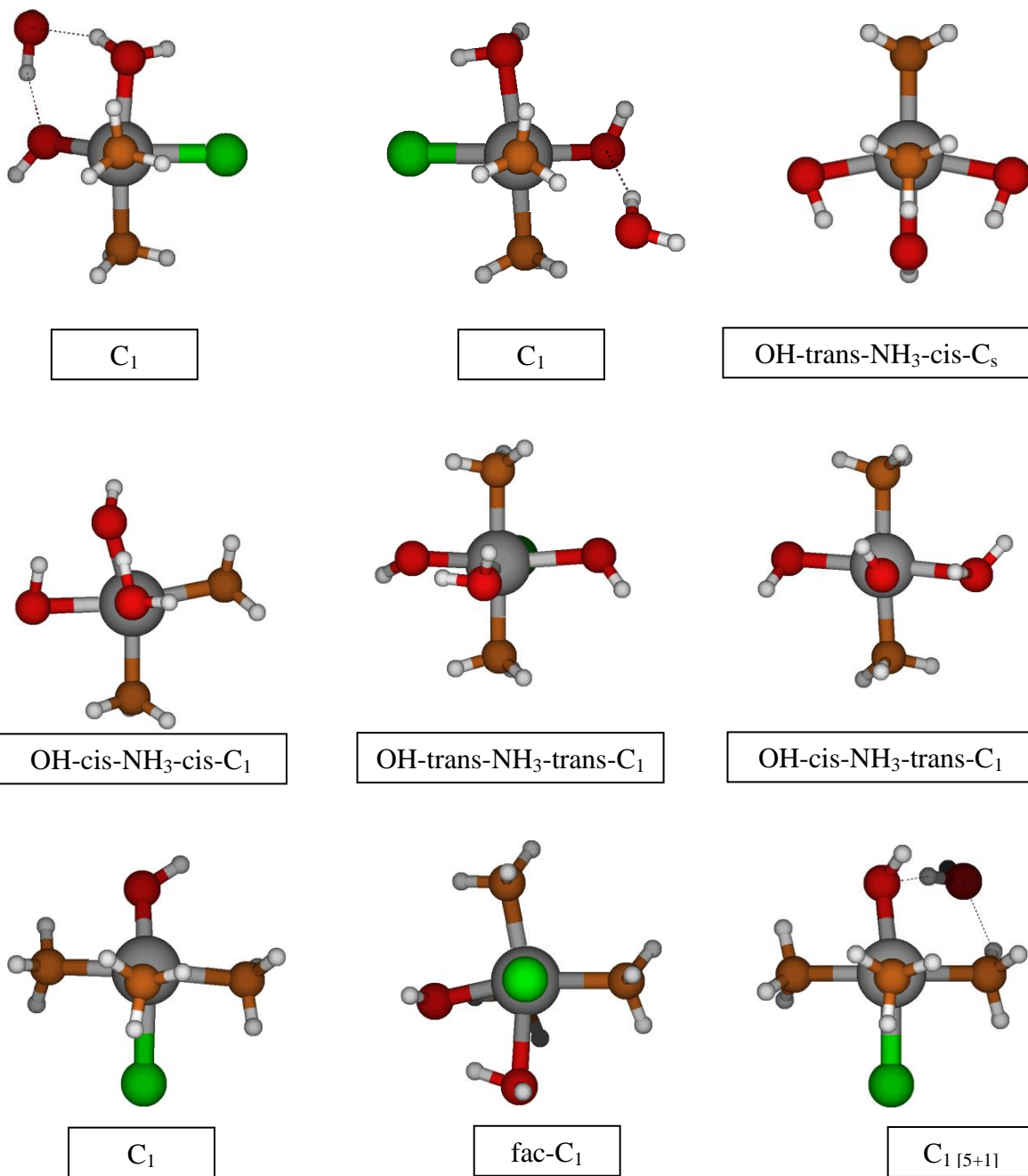


Figure 3-36: (continued)

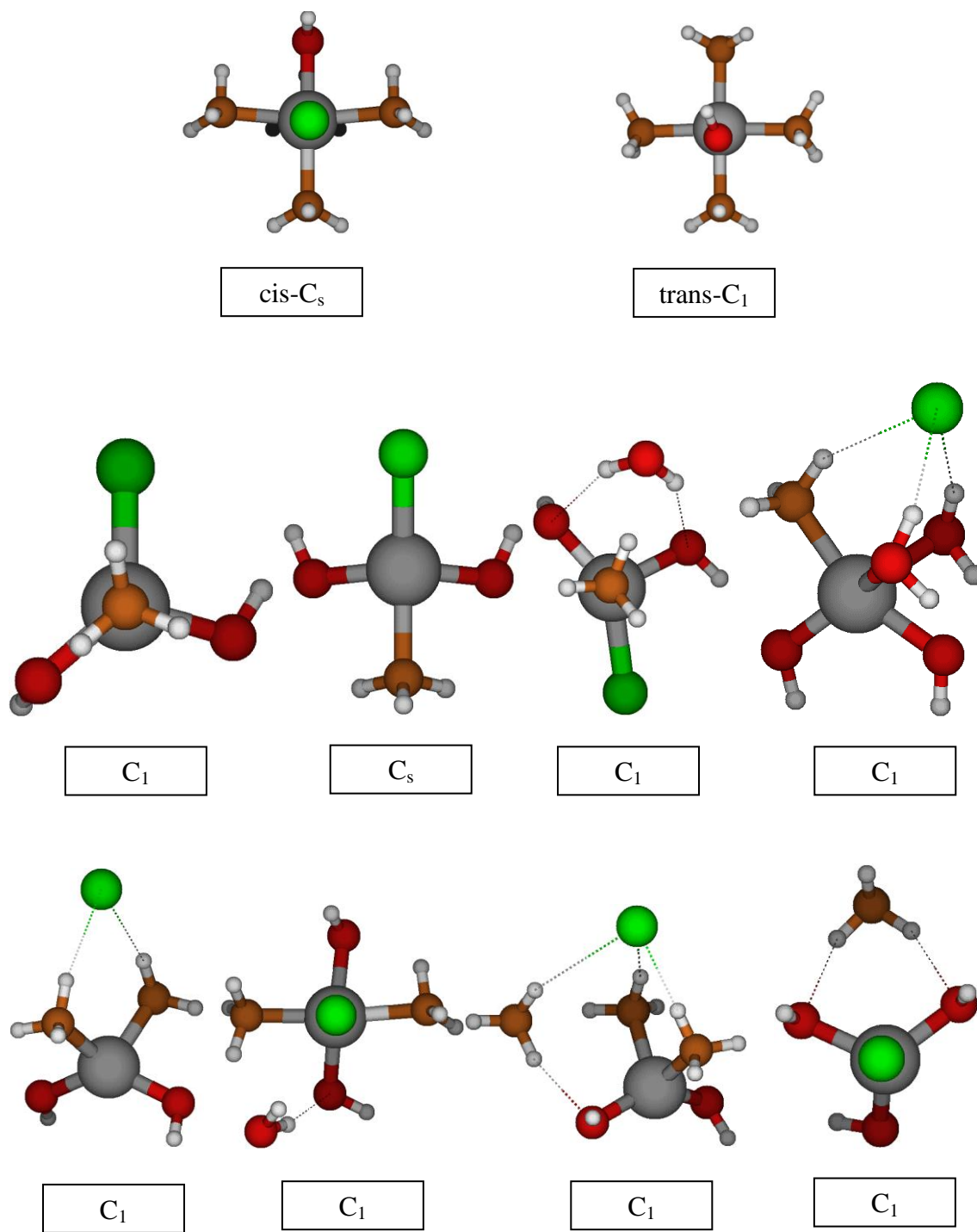


Figure 3-36: (continued)

The dichlorohydroxodiammine complex has C_s symmetry. The monohydrate is only stable with C_1 symmetry with one of the chloride ligand in the second solvation shell forming hydrogen bond with water and ammonia ligands. The anhydrous dichlorohydroxotriammine complex has stable C_s (MP2 with all ligands directly bonded to nickel) and C_1 (both levels with lower energy and with the chloride hydrogen bonded with ammonia ligands).

Various C_s structures were attempted for dichlorodihydroxoammine complex, but only the one in which both of chloride ligands hydrogen bonded to hydroxide and ammonia is stable. The monohydrate has C_1 symmetry and also has both of the chloride ligands involved in the formation of hydrogen bonds with ammonia and water. The dichlorodihydroxodiammine complexes is stable with C_2 symmetry in which the two chloride ligands are involved in the formation of hydrogen bonds with ammonia ligands.

The trichlorohydroxoammina complex is only stable with C_1 symmetry with the ammonia ligand hydrogen bonded to hydroxide. Attempt to add a single water result in two chloride ligands dissociated and hydrogen bonded to water and ammonia respectively. The anhydrous trichlorohydroxodiammine complex has C_s symmetry with two chloride ligands in the second hydration sphere and hydrogen bonded to hydroxide and ammonia ligands.

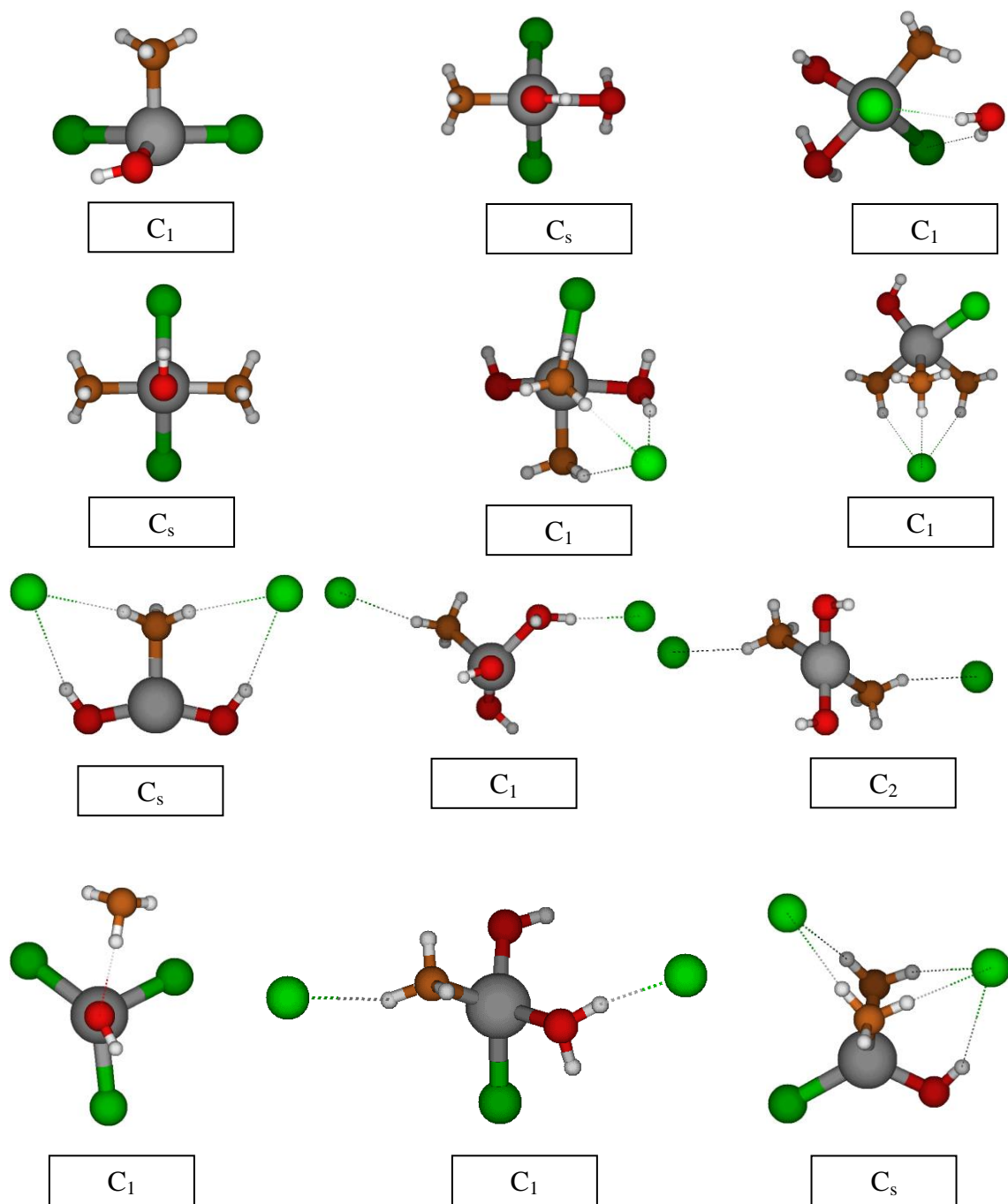


Figure 3-37: Optimized MP2 and B3LYP geometries for $[\text{NiCl}_m(\text{OH})_n(\text{NH}_3)_l(\text{H}_2\text{O})_k]^{2-m-n}$, where $m=2-3$, $n=1-(4-m)$, $l=0-(6-m-n)$, $k=0-(6-m-n-l)$.

3.9.2 Discussion/Literature Comparison

The structures that have been investigated in this research could be compared with those in the literature to see if the calculated geometries are viable, however, no studies on this set of complexes were found in the literature. Thus only the trends of the bond lengths and vibrational stretching frequencies for each group of complexes could be discussed. Generally there is a trend that with more water molecules been added, the Ni-O, Ni-N and Ni-Cl bond lengths increase and stretching frequencies decrease. However, water, chloride or ammonia dissociated and involved in the formation of hydrogen bonds result in the shorter bond distances between those ligands which still directly bonded to nickel(II) and the central nickel(II), and in these cases the trends become less clear.

In most cases, no experimental or prior computational data exist for nickel complexes with more than two ligand types. However, favourable comparisons can be made for nickel complexes with one or two ligand types. Therefore, it is assumed that the more complicated nickel complexes have the same relative errors as the simpler nickel complexes.

The plots of Raman spectra which can be found in supplementary materials section were also constructed based on the Raman intensities for future experimental comparison by our colleagues at the University of Guelph.

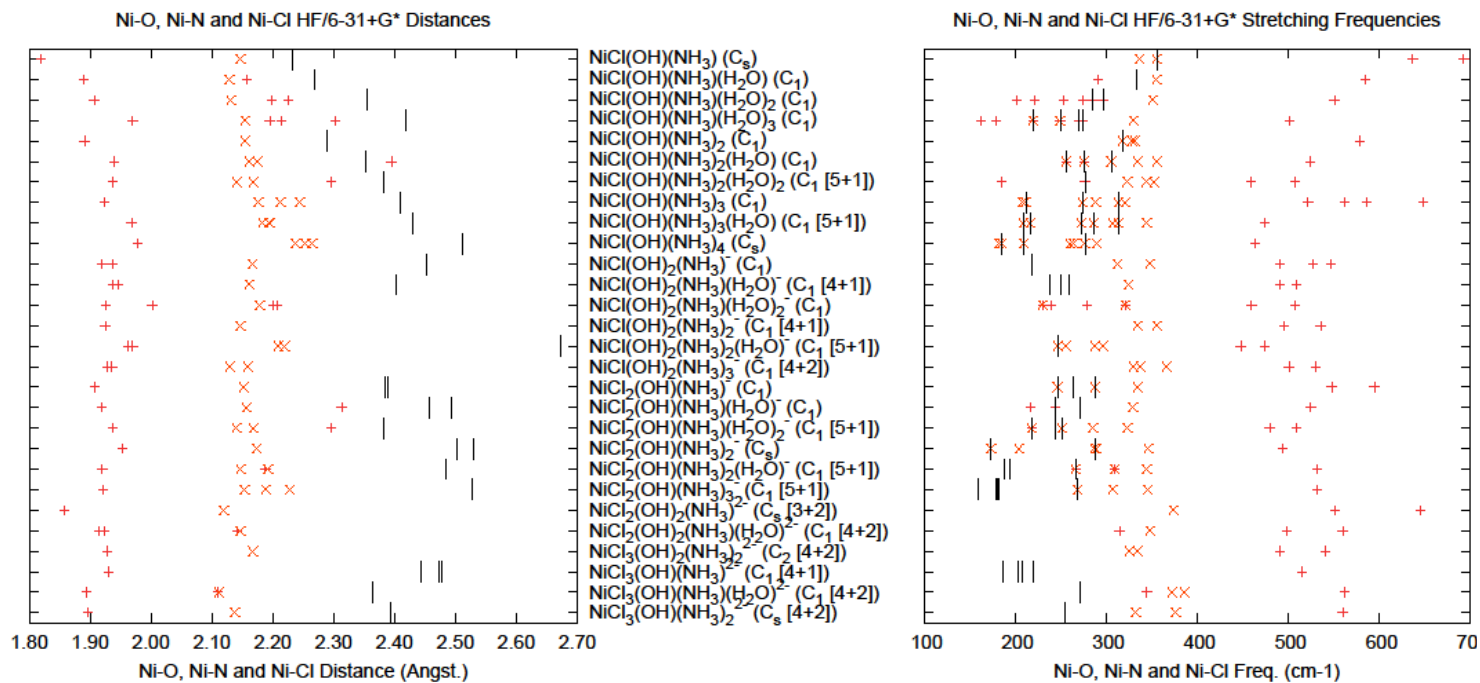


Figure 3-38: Ni-O (+), Ni-Cl (|) and Ni-N (x) bond lengths and vibrational stretching frequencies for $[\text{NiCl}_m(\text{OH})_n(\text{NH}_3)_l(\text{H}_2\text{O})_k]^{2-m-n}$, where $m=1-3$, $n=1-(4-m)$, $l=0-(6-m-n)$, $k=0-(6-m-n-l)$, calculated at HF/6-31+G* level.

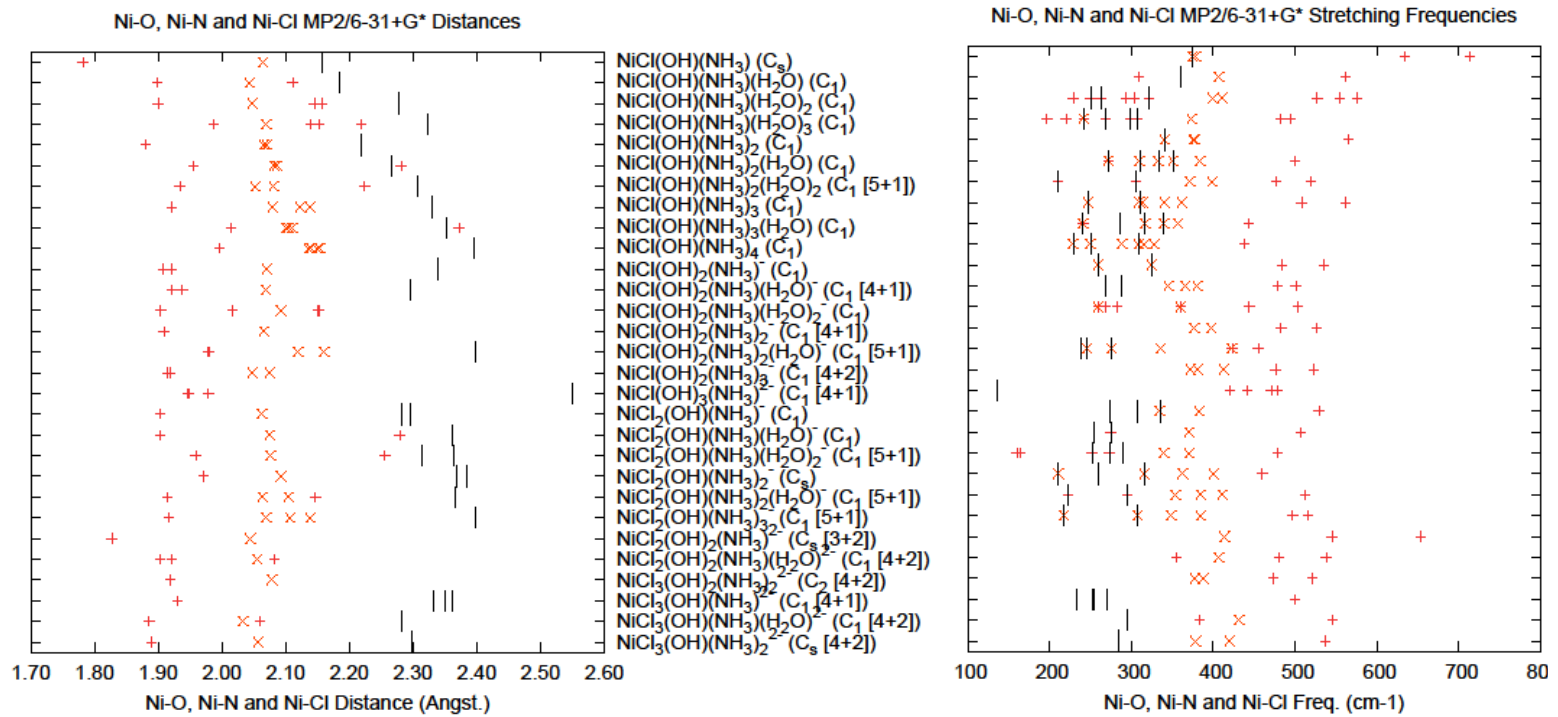


Figure 3-39: Ni-O (+), Ni-Cl (|) and Ni-N (x) bond lengths and vibrational stretching frequencies for $[\text{NiCl}_m(\text{OH})_n(\text{NH}_3)_l(\text{H}_2\text{O})_k]^{2-m-n}$, where $m=1-3$, $n=1-(4-m)$, $l=0-(6-m-n)$, $k=0-(6-m-n-1)$, calculated at MP2/6-31+G* level.

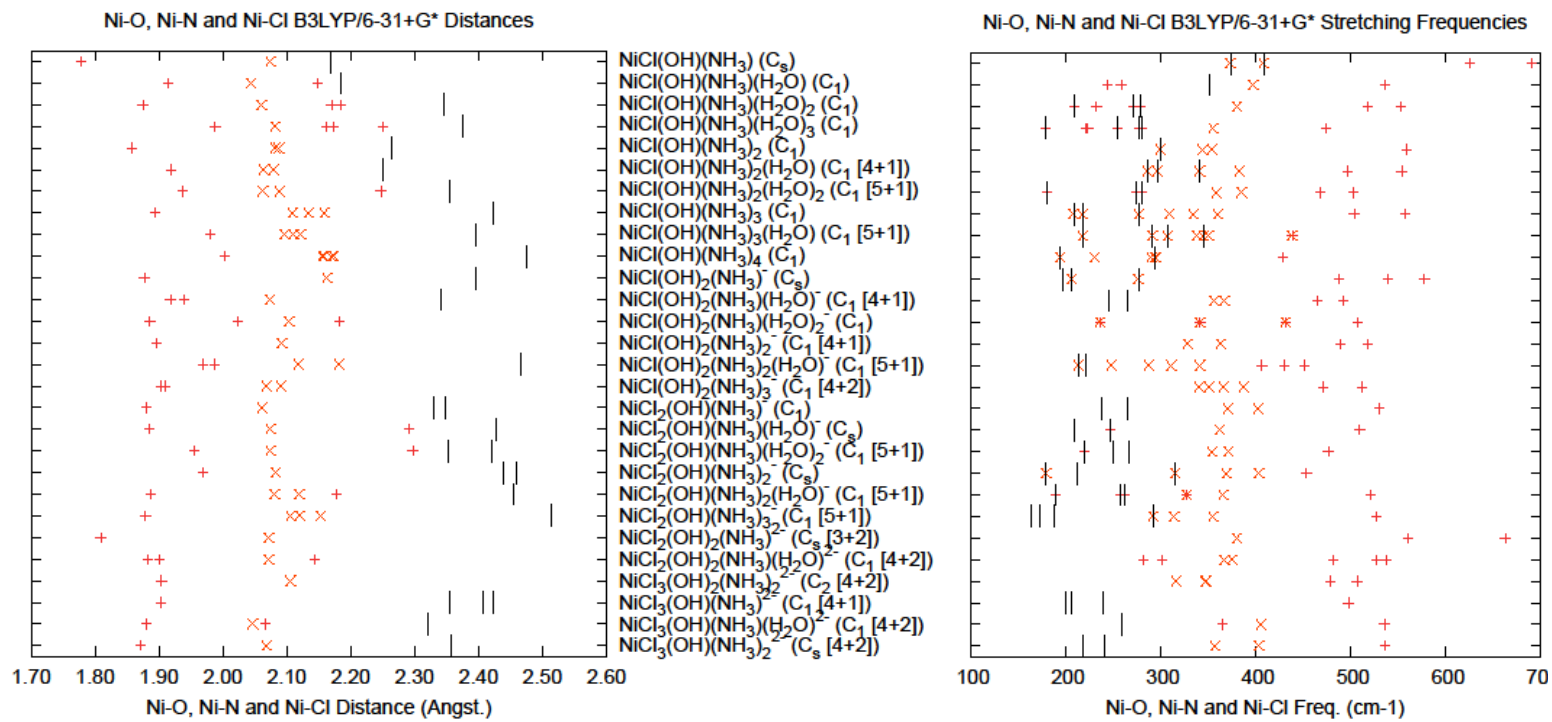


Figure 3-40: Ni-O (+), Ni-Cl (|) and Ni-N (x) bond lengths and vibrational stretching frequencies for $[\text{NiCl}_m(\text{OH})_n(\text{NH}_3)_l(\text{H}_2\text{O})_k]^{2-m-n}$, where $m=1-3$, $n=1-(4-m)$, $l=0-(6-m-n)$, $k=0-(6-m-n-1)$, calculated at B3LYP/6-31+G* level.

Chapter 4: Conclusion and Future Work

4.1 Conclusions

The present study was performed on possible nickel(II) complexes with all the combinations of chloride, hydroxide, water and ammonia ligands which may exist in CANDU Gen IV Supercritical Water-Cooled Reactors as corrosion products by ab initio computational chemistry methods. The geometries, total energies (with and without solvation effects), and vibrational stretching frequencies were obtained for all the stable complexes based on our calculations. Among most of the molecules with neutral or negative charge, chloride, ammonia or water ligands tend to be involved in the formation of hydrogen bonds instead of directly bonded to central nickel(II) ion based on our calculations. Although the Raman experimental results from the colleagues at the University of Guelph are still needed to compare with in order to predict the most likely corrosion products (as this study is performed on all the possible nickel complexes at zero Kelvin in the gas phase), the lists could also been narrowed down to a certain extent based on the calculation results and comparison with experimental data. Therefore, each set of complexes will be gone through and a list of what might be the best candidates will be provided.

4.1.1 Aquanickel(II)

Stable structures were found for all of the species up to and including the hexa-coordinate complex. The calculated structures are in good agreements with structural data and other calculation results. As discussed in Chapter three, the most possible complex to

exist in SCWR would be the hexaaquanickel(II) which has been reported in experimental literature.

4.1.2 Chloronickel(II)

Nickel(II) complexes with water and chloride ligands (from river water for the coolant system) were found up to and including the hexacoordinate species, and those complexes with more than four chloride ligands showed dissociation of chloride ions. In order to form deposition, it is needed to keep electronically neutral, so that the neutral complexes NiCl_2 and with water ligands up to and including hexacoordinate species are preferred. The hydrated tetrachloronickel(II) complexes tend to form ion pairs indicating relatively instability. Other complexes with positive or negative charges in this set are also possible to exist in SCWR, and they need other cations or anions to form deposits.

4.1.3 Hydroxonickel(II)

This set of complexes are similar as the chloronickel(II) species in this case. Therefore, the most possible complexes to exist in SCWR would be the neutral Ni(OH)_2 and with one, two or three molecules. The tetrahydratedihydroxonickel(II), $\text{Ni(OH)}_2(\text{H}_2\text{O})_4$, has one of the water molecules involved in the formation of hydrogen bond which indicate instability according to the calculations. The hydrated trihydroxo- and tetrahydroxonickel(II) complexes also have water molecules in the second hydration sphere. Thus, for the nickel(II) complexes which may exist in SCWR environment, the suggested complexes could be the monohydroxonickel(II) and its hydrated complexes. However, based on the calculations one of the water molecules migrated to the second

hydration sphere and hydrogen bonded to hydroxide within the trihydrate chlorohydroxonickel(II) indicating the instability.

4.1.4 Amminenickel(II)

This set of complexes are similar with hydrated nickel(II) complexes as in which all the ligands are directly bonded to central nickel(II) and with the same charge (2+). Furthermore, other computational studies reported that in this set of complexes, it becomes more stable when the water molecules are replaced by ammonia ligands. [108] The most possible complex to exist in SCWR would be the hexaamminenickel(II) which has been experimentally studied comprehensively. The hexaamminenickel(II) could also combine with other anions such as Cl^- to form neutral complex which has been reported in literature. [112]

4.1.5 Chlorohydroxonickel(II)

This set of complexes contain both chloride and hydroxide ligands and have studied up to and including the hexacoordinate species. The charges of this set of complexes are range from 0 to (-2). Therefore, the most probable complexes would be neutral $\text{NiCl}(\text{OH})$ and with water molecules up to hexacoordinate. Those complexes with negative charges of this set of complexes tend to form ion pairs which also suggested that they are unstable.

4.1.6 Chloroamminenickel(II)

This set of complexes contains neutral ammonia ligands and chloride ligands with a single negative charge, and stable structures were found up to and including the

hexacoordinate species. The neutral complexes in this set would be NiCl_2 with different combinations of water and ammonia ligands up to hexacoordinate species. Based on the calculations and comparison with experimental studies, the most possible complexes to exist in SCWR would be diaquadichlorodiamminenickel(II), dichlorotetraamminenickel(II), and dichlorodiamminenickel(II). The dichloromonoamminenickel(II) and its hydrated complexes are also possible to be the candidates in SCWR. When more chloride ligands are added to the central nickel(II), they tend to form ion pairs which suggest that they may be less stable.

4.1.7 Hydroxoamminenickel(II)

This set of complexes are similar with chloroamminenickel(II) to certain degrees. The neutral complexes would be Ni(OH)_2 with different combinations of water and ammonia ligands. As the nickel(II) complexes tend to form tetrahedral and octahedral species, the possible complexes to exist in SCWR would be $\text{Ni(OH)}_2(\text{NH}_3)_2$, $\text{Ni(OH)}_2(\text{NH}_3)_2(\text{H}_2\text{O})$ (H_2O in the second hydration shell), $\text{Ni(OH)}_2(\text{NH}_3)_2(\text{H}_2\text{O})_2$ (both of H_2O in the second hydration shell) and $\text{Ni(OH)}_2(\text{NH}_3)_4$. Nickel(II) complexes with more than two hydroxide ligands tend to have water or ammonia ligands involved in the formation of hydrogen bonds. The monohydroxidenickel complex with ammonia and water could also exist if combine with other anions.

4.1.8 Chlorohydroxoamminenickel(II)

The complexes in this set contain at least one chloride, one hydroxide and one ammine ligands with 0, -1, or -2 charges, like the aquachlorohydroxocomplexes. The neutral complexes would be NiCl(OH) combine with different number of ammonia and

water ligands. As more hydroxide or chloride ligands been added, they tend to form ion pairs which suggest instability.

4.2 Future Work

Ab initio calculations were carried out on nickel(II) complexes with chloride, hydroxide, ammonia and water in this work. As the SCWR construction materials also contain other transition metal alloys, ions such as iron and chromium may be leached into environment and form complexes with those anions and molecules as well. Therefore ab initio investigations on iron(II) and chromium(II) complexes could be included in future work.

Reference:

- [1] Torgerson, D., Shalaby, B., Pang, S. "CANDU technology for Generation III+ and IV reactors", *Nucl. Eng. Des.*, Vol. 236, Issue 14-16, **2006**, pp.1565-1572.
- [2] Sun, C., Hui, R., Qu, W., Yick, S. "Progress in corrosion resistant materials for supercritical water reactors", *Corros. Sci.* Vol. 51, **2009**, 2508-2523.
- [3] Bushby, S. J., Dimmick, G. R., Duffey, R. B., Burrill, K. A., Chan, P. S. W. "Conceptual designs for advanced , high-temperature CANDU reactors." *8th International Conference on Nuclear Engineering.* **2000**. Baltimore, MD, USA.
- [4] Gupta, G., Amponrat, P., Ren, X., Sridharan, K., Allen, T. R., Was, G. S. "Role of grain boundary engineering in the SCC behavior of ferritic-martensitic alloy HT-9". *J. Nucl. Mater.* Vol. 361, **2007**, 160-173.
- [5] Chow, C. K., Khartabil, H. F. "Conceptual fuel channel designs for CANDU-SCWR", *J. Eng. Technol.*, Vol. 40, **2007**, 139-146.
- [6] Amponrat, P., Was, G. S. "Oxidization of ferritic-martensitic alloys T91, HCM12A and HT9 in supercritical water." *J. Nucl. Mater.* Vol. 371, **2007**, 1-17.
- [7] Bouzoubaa, A., Diawara, B., Maurice, V., Minot, C., Marcus, P. "Ab initio modeling of localized corrosion: Study of the role of surface steps in the interaction of chlorides with passivated nickel surface." *Corros. Sci.* Vol. 51, **2009**, 2174-2182.
- [8] Svishchev, I. M., Guzonas, D. A. "Supercritical water and particle nucleation: Implication for water chemistry control in a GEN IV supercritical water cooled nuclear reactor." *J. Supflu.* Vol. 60, **2011**, 121-126.
- [9] Weeks, M. E., Leicester, H. "Discovery of the elements, 6th, ed." *J. Chem. Educ.* Vol. 33, **1956**, 161-167.
- [10] Feng, A., Moore, J. W., Harwood, W., Gayhart, R. "Exploring the properties of the chemical elements." *J. Chem. Educ.* Vol. 65, **1988**, p695.
- [11] Latimer, W. M. "The oxidization states of the elements and their potentials in aqueous solution, 2nd ed." New York, **1952**, p208.
- [12] Davis, J. R. "ASM specialty handbook: Nickel, cobalt, and their alloys." Materials Park, Ohio, **2000**.
- [13] Young, B. A., Gao, X., Srivatsan, T. S. "A study of life prediction difference for a nickel-base alloy 690 using a threshold and a non-threshold model." *J. Nucl. Mater.* Vol. 394, **2009**, 63-66.
- [14] Meng, L. J., Sun, J., Xing, H., Pang, G. W., " Serrated flow behavior in AL6XN austenitic stainless steel." *J. Nucl. Mater.* Vol. 394, **2009**, 288-293.

- [15] Jin, S. X., Guo, L. P., Yang, Z., Fu, D. J., Liu, C. S., Xiao, W., Tang, R., Liu, F. H., Qiao, Y. X. "Microstructural evolution in nickel alloy C-276 after Ar⁺ ion irradiation." *Instrum. Methods. Phys. Res. Sect.* Vol. 269, **2011**, 209-215.
- [16] Magnussen, O. M., Scherer, J., Ocko, B. M., Behm, R. J. "In situ X-ray scattering study of the passive film on Ni(111) in sulfuric acid solution." *J. Phys. Chem.* Vol. 104, **2000**, 1222-1226.
- [17] Lu, B. L., Chen, G. Q., Zhou, W. L., Su, H., Liu, R. "Ab initio study of influence of 3d alloying elements on corrosion properties of non-passivated nickel-base alloys." *J. Nucl. Mater.* Vol. 418, **2011**, 286-291.
- [18] Levine, I. N. *Quantum Chemistry*, 6th Edition; Prentice Hall: New Jersey, **2009**.
- [19] Lowe, J. P., Peterson, K. A. *Quantum Chemistry*, 3rd Edition; Elsevier Academic Press: Burlington, **2006**.
- [20] Compton, A. H. "The Compton effect". *Phys. Rev.* Vol. 21, **1923**, 483.
- [21] Heisenburg, W. Z. *Phys.* 172, **1927**.
- [22] McQuarrie, D. A. "Quantum Chemistry". Second Edition, University Science Book: California, **2008**.
- [23] Schrödinger, E. *Phys. Rev.* **1926**, 28, 1049.
- [24] Dykstra, C. E. "Introduction to Quantum Chemistry". Prentice Hall: New Jersey, **1991**.
- [25] Born, M. Oppenheimer, J, R. *Ann. Phys.* 84:457, **1927**.
- [26] Cramer, C. J. "Essentials of Computational Chemistry: Theories and Models". John Wiley & Sons: England, **2002**.
- [27] Lewars, E. G. "Computational Chemistry: Introduction to the Theory and Applications of Molecular and Quantum Mechanics". Second Edition, Springer: New York, **2011**.
- [28] Hartree, D. R. *Proc. Camb. Phil. Soc.* 24:89, **1928**.
- [29] Jensen, F. "Introduction to Computational Chemistry." Second Edition, Wiley: Hoboken, **2007**.
- [30] Slater, J. C. *Phys. Rev.* **1930**, 36, 57.
- [31] Boys, S. F. *Proc. R. Soc.* **1950**. 200, 542.
- [32] Møller, C., Plesset, M, S. *Phys. Rev.* **1934**, 46, 618.
- [33] Binkley, J. S., Pople, J. A. *Int. J. Quant. Chem.* **1975**, 9, 229.

- [34] Hohenberg, P., Kohn, W. *Phys. Rev.* **1964**, 136, B864.
- [35] Bader, R. F. W. “*Atoms in Molecules.*” Oxford: New York, **1990**.
- [36] Kohn, W., Sham, L. J. *Phys. Rev.* **1965**, 140, A1133.
- [37] Becke, A. D. *Phys. Rev.* **1988**, 38, 3098.
- [38] Foresman, J. B., Frisch, A. E. “*In Exploring Chemistry with Electronic Structure Methods, Second Edition*”; Gaussian, Inc: U.S.A, **1996**.
- [39] Klamt, A., Schüürmann, G. *J. Chem. Soc. Perkin Trans.* **1993**, 2, 799.
- [40] Gaussian 03, Revision C.02, Frisch, M. J.; Trucks, G. W.; Schlegel, H. B.; Scuseria, G. E.; Robb, M. A.; Cheeseman, J. R.; Montgomery, Jr., J. A.; Vreven, T.; Kudin, K. N.; Burant, J. C.; Millam, J. M.; Iyengar, S. S.; Tomasi, J.; Barone, V.; Mennucci, B.; Cossi, M.; Scalmani, G.; Rega, N.; Petersson, G. A.; Nakatsuji, H.; Hada, M.; Ehara, M.; Toyota, K.; Fukuda, R.; Hasegawa, J.; Ishida, M.; Nakajima, T.; Honda, Y.; Kitao, O.; Nakai, H.; Klene, M.; Li, X.; Knox, J. E.; Hratchian, H. P.; Cross, J. B.; Bakken, V.; Adamo, C.; Jaramillo, J.; Gomperts, R.; Stratmann, R. E.; Yazyev, O.; Austin, A. J.; Cammi, R.; Pomelli, C.; Ochterski, J. W.; Ayala, P. Y.; Morokuma, K.; Voth, G. A.; Salvador, P.; Dannenberg, J. J.; Zakrzewski, V. G.; Dapprich, S.; Daniels, A. D.; Strain, M. C.; Farkas, O.; Malick, D. K.; Rabuck, A. D.; Raghavachari, K.; Foresman, J. B.; Ortiz, J. V.; Cui, Q.; Baboul, A. G.; Clifford, S.; Cioslowski, J.; Stefanov, B. B.; Liu, G.; Liashenko, A.; Piskorz, P.; Komaromi, I.; Martin, R. L.; Fox, D. J.; Keith, T.; Al-Laham, M. A.; Peng, C. Y.; Nanayakkara, A.; Challacombe, M.; Gill, P. M. W.; Johnson, B.; Chen, W.; Wong, M. W.; Gonzalez, C.; and Pople, J. A.; Gaussian, Inc., Wallingford CT, **2004**.
- [41] Hehre, W. J., Lathan, W. A., Ditchfield, R., Newton, M. D., Pople, J. A. Gaussian 70. Quantum Chemistry Program Change, Program No. 237, **1970**.
- [42] (March 29, 2011). ACEnet: Accelerating Discovery. Retrieved September 7, 2011 from <http://www.ace-net.ca/wiki/ACEnet>
- [43] Schaftenaar, G. and Noordik, J.H., *J. Comput.-Aided Mol. Design*, 2000, 14, 123.
- [44] Bustamante, M., Valencia, I., Castro, M. “Theoretical Study of $[\text{Ni}(\text{H}_2\text{O})_n]^{2+}(\text{H}_2\text{O})_m$ ($n \leq 6, m \leq 18$)” *J. Phys. Chem.* Vol. 115, **2011**, 4115-4134.
- [45] Iuchi, S., Morita, A., Kato, S. “Potential energy surface and dynamics of Ni^{2+} ion aqueous solution: molecular dynamics simulation of the electronic absorption spectrum.” *J. Chem. Phys.* Vol. 121, **2004**, 8446-8457.
- [46] Ohtaki, H. “Structure and dynamics of hydrated ions”. *Chem. Rev.* Vol. 93, **1993**, 1157-1204.

- [47] Inada, Y., Mohammed, A. M., Loeffler, H. H., Rode, B. M. "Hydration structure and water exchange reaction of nickel(II) ion: classical and QM/MM simulations." *J. Phys. Chem. A*. Vol. 106, **2002**, 6783-6791.
- [48] Cotton, F. A., Daniels, L. M., Murillo, C. A., Quesada, J. F. "Hexaaqua dipositive ions of the first transition series: new and accurate structures; expected and unexpected trends." *Inorg. Chem.* Vol. 32, **1993**, 4681-4687.
- [49] Natália, M., Cordeiro, D. S., Ignaczak, A., Gomes, A. N. F. "Simulation of water solutions of Ni²⁺ at infinite dilution." *Chem. Phys.* Vol. 176, **1993**, 97-108.
- [50] D'Angelo, P. D., Roscioni, O. M., Chillemi, G., Longa, S. D., Benfatto, M. "Detection of second hydration shells in ionic solutions by XANES: computed spectra for Ni²⁺ in water based on molecular dynamics." *J. Am. Chem. Soc.* Vol. 128, **2006**, 1853-1858.
- [51] Aguilar, C. M., Almeida, W. B. D., Rocha, W. R. "Solvation and electronic spectrum of Ni²⁺ ion in aqueous and ammonia solutions: a sequential Monte Carlo/TD-DFT study." *Chem. Phys.* Vol. 353, **2008**, 66-72.
- [52] Inada, Y., Funahashi, S. "Solvation structure determination of nickel(II) ion in six nitriles using extended x-ray absorption fine structure spectroscopy." *Anal. Sci.* Vol. 13, **1997**, 373-377.
- [53] Mareš, J., Liimatainen, H., Laasonen, K., Vaara, J. "Solvation structure and dynamics of Ni²⁺(aq) from first principles." *J. Chem. Theory. Comput.* Vol. 7, **2011**, 2937-2946
- [54] Neilson, G. W., Ansell, S., Wilson, G. Z. "The structure and dynamic properties of some transition-metal aqua cations – results from neutron scattering." *Z. Naturforsch.* Vol. 50, **1995**, 247-256.
- [55] Varadwaj, P. R., Cukrowski, I., Marques, H. M. "Low-spin complexes of Ni²⁺ with six NH₃ and H₂O ligands: a DFT-RX3LYP study." *J. Mol. Struct.* Vol. 902, **2009**, 21-32.
- [56] Rulišek, L., Havlas, Z. "Ab initio calculations of monosubstituted (CH₃OH, CH₃SH, NH₃) hydrated ions of Zn²⁺ and Ni²⁺." *J. Phys. Chem. A*. Vol. 103, **1999**, 1634-1639.
- [57] Akesson, R., Pettersson, L. G., Sandstrom, M., Wahlgred, U. "Theoretical study of water exchange reactions of the divalent and trivalent metal ions of the first transition period." *J. Am. Chem. Soc.* Vol. 116, **1994**, 8705-8713.
- [58] Yamaguchi, T., Ohzono, H., Yamagami, M., Yamanaka, K., Yoshida, K., Wakita, H. "Ion hydration in aqueous solutions of lithium chloride, nickel chloride, and caesium chloride in ambient to supercritical water." *J. Mol. Liq.* Vol. 153, **2010**, 2-8.

- [59] Hoffmann, M. M., Darab, J. G. Palmer, B. J., Fulton, J. L. "A transition in the Ni²⁺ complex structure from six- to four-coordinate upon formation of ion pair species in supercritical water: an X-ray absorption fine structure, near-infrared, and molecular dynamics study." *J. Phys. Chem. A*. Vol. 103, **1999**, 8471-8482.
- [60] Magnusson, E., Moriarty, N. W. "Binding patterns in single-ligand complexes of NH₃, H₂O, OH⁻, and F⁻ with first series transition metals." *Inorg. Chem.* Vol. 35, **1996**, 5711-5719.
- [61] Fujii, T., Moynier, F., Dauphas, N., Abe, M. "Theoretical and experimental investigation of nickel isotopic fractionation in species relevant to modern and ancient oceans." *Geochim. Cosmochim. Acta*. Vol. 75, **2011**, 469-482.
- [62] Waizumi, K., Masuda, H., Ohtaki, H. "X-ray structure studies of FeBr₂·4H₂O, CoBr₂·4H₂O, NiCl₂·4H₂O and CuBr₂·4H₂O. cis/trans selectivity in transition metal(II) dihalide tetrahydrate." *Inorg. Chim. Acta*. Vol. 192, **1992**, 173-181.
- [63] Magini, M. "Hydration and complexes formation study on concentrated solutions [M=Co(II), Ni(II), Cu(II)] by X-ray diffraction technique." *J. Chem. Phys.* Vol. 74, **1981**, 2523-2529.
- [64] Magini, M., Paschina, G., Piccaluga, G. "Ni-Cl bonding in concentrated Ni(II) aqueous solutions at high Cl⁻/Ni²⁺ ratios. An X-ray diffraction investigation." *J. Chem. Phys.* Vol. 76, **1982**, 1116-1121.
- [65] Caminiti, R., Licheri, G., Piccaluga, G., Pinna, G. "X-ray diffraction and structure of NiCl₂ aqueous solutions." *Faraday. Discuss.* Vol. 64, **1977**, 62-68.
- [66] Sandström, D. R. "Ni²⁺ coordination in aqueous NiCl₂ solutions: study of the extended X-ray absorption fine structure." *J. Chem. Phys.* Vol. 71, **1979**, 2381-2386.
- [67] Pilme, J., Silvi, B. "Comparative study of the bonding in the first series of transition metal 1:1 complexes M-L (M=Sc, ... ,Cu; L=CO, N₂, C₂H₂, CN⁻, NH₃, H₂O, and F⁻)." *J. Phys. Chem. A*. Vol. 109, 2005, 10028-10037.
- [68] Edwards, H. G. M., Knowles, A. "Vibrational spectroscopic study of nickel (II) formate, Ni(HCO₂)₂, and its aqueous solution." *J. Mol. Struct.* Vol. 268, Issue. 1-3, 1992, pp. 13-22.
- [69] Bickley, R. I., Edwards, H. G. M., Knowles, A., Gustar, R. E., Mihara, D., Rose, S. J. "Vibrational spectroscopic study of nickel (II) malonate, Ni(COO·CH₂·COO)·2H₂O and its aqueous solution". *J. Mol. Struct.* Vol. 296, Issue. 1-2, 1993, pp. 21-28.
- [70] Pye, C. C., Corbeil, C. R., Rudolph, W. W. "An ab initio investigation of zinc chloro complexes." *Phys. Chem. Chem. Phys.* Vol. 8, **2006**, 5428-5436.

- [71] Pye, C. C., Corbeil, C. R. "An ab initio study of scandium chloro complexes." *Can. J. Chem.* Vol. 80, **2002**, 1331-1342.
- [72] Lemaire, G., Hebant, P., Picard, G. S. "DFT analysis of interfacial processes occurring in the first steps of electrodeposition of nickel from chloride melt." *J. Mol. Struct.* Vol. 419, **1997**, 1-10.
- [73] Hargittai, M., Subbotina, N. Y., Kolonits, M., Gershikov, A. G. "Molecular structure of first row transition metal dihalides from combined electron diffraction and vibrational spectroscopic analysis." *J. Chem. Phys.* Vol. 94, **1991**, 7278-7286.
- [74] Waizumi, K., Kouda, T., Tanio, A., Fukushima, N., Ohtaki, H. "Structural studies on saturated aqueous solutions of manganese(II), cobalt(II), and nickel(II) chlorides by X-ray diffraction." *J. Sol. Chem.* Vol. 28, 1999, 83-100.
- [75] Ashworth, S. H., Grieman, F. J., Brown, J. M. "Structure of nickel dichloride." *J. Am. Chem. Soc.* Vol. 115, 1993, 2978-2979.
- [76] Marcus, Y. "Ionic radii in aqueous solutions." *Chem. Rev.* Vol. 88, 1988, 1475-1498.
- [77] Ptasiwicz-Bak, H., Olovsson, I., McIntyre, G. J. "Charge density in NiCl₂·4H₂O at 295 and 30 K." *Acta. Crystallogr.*, 1999, Vol. 55, 830-840.
- [78] Freire, A. I., Alves, W. A. "Using vibrational and electronic spectroscopies to investigate different complexes in the formamide/nickel chloride system." *Spectrochim. Acta. Part. A.* Vol. 89, 2012, 259-263.
- [79] Lever, A. B. P. "Inorganic Electronic Spectroscopy", 2nd ed.; Elsevier: Amsterdam, 1984.
- [80] O'Brien, J. T., Williams, E. R. "Coordination numbers of hydrated divalent transition metal ions investigated with IPRD spectroscopy". *Phys. Chem.* Vol. 115, 2011, 14612-14619.
- [81] D'Angelo, P., Barone, V., Chillemi, G., Sanna, N., Meyer-Klaucke, W., Pavel, N. V. "Hydrogen and higher shell contributions in Zn²⁺, Ni²⁺, and Co²⁺ aqueous solutions: An X-ray absorption fine structure and molecular dynamics study." *J. Am. Chem. Soc.* Vol. 124, 2002, 1958-1967.
- [82] Egorov, A. V., Komolkin, A. V., Lyubartsev, A. P., Laaksonen, A. "First and second hydration shell of Ni²⁺ studied by molecular dynamics simulations." *Theor. Chem. Acc.* Vol. 115, 2006, 170-176.
- [83] Landry-Hum, J., Bussiere, G., Daniel, C., Reber, C. "Triplet electronic states in d² and d⁸ complexes probed by absorption spectroscopy: A CASSCF/CASPT2 analysis of [V(H₂O)₆]³⁺ and [Ni(H₂O)₆]²⁺". *Inorg. Chem.* Vol. 40, 2001, 2595-2601.
- [84] Charles, W., Bauschlicher, Jr. "Transition metal-ligand bonding. II." *J. Chem. Phys.* Vol. 84, 1986, 260-267.

- [85] Rakitin, Y. V., Kalinnikov, V. T., Khodasevich, S. G., Novotortsev, V. M, "Mechanism of formation of short metal-ligand bonds in linear molecules CuCl₂ and NiCl₂ molecules." *Russ. J. Coord. Chem.* Vol. 33, 2007, 643-645.
- [86] Kammoun, S., Dammak, M., Maalej, R., Kamoun, M. "Crystal-field analysis for d8 ions at D_{4h} symmetry sites: Electronic states in trans-NiCl₂(H₂O)₄ complex." *J. Lumin.* Vol. 124, 2007, 316-320.
- [87] Brik, M. G. "Comparative first-principles study of the Ni²⁺ absorption spectra and covalence effects on isostructural crystals NiCl₂, NiBr₂ and NiI₂." *J. Physb.* Vol. 387, 2007, 69-76.
- [88] Brik, M. G., Avram, N. M., Avram, C. N. "Comparative crystal field study of Ni²⁺ energy levels in NiCl₂, NiBr₂, and NiI₂ crystals." *J. Physb.* Vol. 371. 2006, 43-49.
- [89] Beattie, I. R., Jones, P. J., Young, N. A. "The interaction of some metal dichlorides (Ca, Cr, Mn, Fe, Co, Ni, Zn) with dinitrogen." *Chem. Phys. Lett.* Vol. 177, 1991, 579-584.
- [90] Bukhmarina, V. N., Predtechensky, Y. B. "Electronic and vibrational-spectra of NiCl₂ isolated in Ne and air matrices." *Opt. Spectrosc.* Vol. 66, **1989**, 1026-1031.
- [91] Mishra, S. K., Kanungo, S. B. "Thermal dehydration and decomposition of nickel chloride hydrate." *J. Therm. Anal.* Vol. 38, **1992**, 2417-2436.
- [92] Trachtman, M., Markham, G. D., Glusker, J. P., George, P., Bock, C, W. "Interactions of metal ions with water: Ab initio molecular orbital studies of structure, vibrational frequencies, charge distributions, bonding enthalpies, and deprotonation enthalpies. 2. Monohydroxides." *Inorg. Chem.* Vol. 40, **2001**, 4230-4241.
- [93] Ricca, A., Bauschlicher, C. W. "Successive OH binding energies of M(OH)_n⁺ for n=1-3 and M=Sc, Ti, V, Co, Ni and Cu." *J. Phys. Chem. A.* Vol. 101, **1997**, 8949-8955.
- [94] Wang, X., Andrews, L. "Infrared spectra of M(OH)_{1,2,3} (M=Mn, Fe, Co, Ni) molecules in solid argon and the character of first row transition metal hydroxide bonding." *J. Phys. Chem.* Vol. 110, **2006**, 10035-10045.
- [95] Godelitsas, A., Charistos, D., Tsipis, A., Tsipis, C., Filippidis, A., Triantafyllidis, C., Manos, G., Siapkias, D. "Characterisation of zeolitic materials with a HEU-type structure modified by transition metal elements: definition of acid sites in nickel-loaded crystals in the light of experimental and quantum-chemical results." *Chem. Eur. J.* Vol. 7, **2001**, 3705-3721.
- [96] Pandya, K. I., Grady, W. E. O., Corrigan, D. A., McBreen, J., Hoffman, R. W. "Extended X-ray absorption fine structure investigations of nickel hydroxides." *J. Phys. Chem.* Vol. 94, **1990**, 21-26.
- [97] Vespa, M., Dahn, R., Grolimund, D., Wieland, E., Scheidegger, A. M. "Spectroscopic investigation of Ni speciation in hardened cement paste." *Environ. Sci. Technol.* Vol. 40, **2006**, 2275-2282.

- [98] McEwen, R. S. "Crystallographic studies on nickel hydroxide and the higher nickel oxides." *J. Phys. Chem.* Vol. 75, **1971**, 1782-1789.
- [99] Li, Y., Yao, J., Zhu, Y., Zou, Z., Wang, H. "Synthesis and electrochemical performance of mixed phase α/β nickel hydroxide." *J. Pow. Sour.* Vol. 203, **2012**, 177-183.
- [100] Jeevanandam, P.; Koltypin, Y.; Gedanken. "Synthesis of nanosized α -nickel hydroxide by a sonochemical method." *Nano Lett.* Vol. 1, **2001**, 263-266.
- [101] Oliva, P.; Leonardi, J.; Laurent, J.F. "Review of the structure and the electrochemistry of nickel hydroxides and oxy-hydroxides". *J. Pow. Sour.* Vol. 8, **1982**, 229-255.
- [102] Bantignies, J. L., Deabate, S., Righi, A., Rols, S., Hermet, P., Sauvajol, J. L., Henn, F. "New insight into the vibrational behavior of nickel hydroxide and oxyhydroxide using inelastic neutron scattering, far/mid-infrared and Raman spectroscopies." *J. Phys. Chem. C.* Vol. 112, **2008**, 2193-2201.
- [103] Deabate, S., Fourgeot, F., Henn, F. "X-ray diffraction and micro-Raman spectroscopy analysis of new nickel hydroxide obtained by electro dialysis. *J. Pow. Sour.* Vol. 87, **2000**, 125-136.
- [104] Palmer, D. A., Benezeth, P., Xiao, C., Wesolowski, D. J., Anovitz, L. M. "Solubility measurements of crystalline NiO in aqueous solution as a function of temperature and pH." *J. Sol. Chem.* Vol. 40, **2011**, 680-702.
- [105] Ziemniak, S. E., Goyette, M. A. "Nickel(II) oxide solubility and phase stability in high temperature aqueous solutions." *J. Sol. Chem.* Vol. 33, **2004**, 1135-1159.
- [106] Baes, C. F., Mesmer, M. H. "The hydrolysis of cations". Wiley, New York. **1994**.
- [107] Chen, B., Castleman, A. W., Ashman, C., Khanna, S. N. "NH₃ adsorption around Ni_n (n \leq 4) clusters." *Int. J. Mass. Spectrom.* Vol. 220, **2002**, 171-182.
- [108] Varadwaj, P. R., Cukrowski, I., Marques, H. M. "DFT-UX3LYP studies on the coordination chemistry of Ni²⁺. Part 1: Six coordinate [Ni(NH₃)_n(H₂O)_{6-n}]²⁺ complexes. *J. Phys. Chem. A.* Vol. 112, **2008**, 10657-10666.
- [109] Benedetto, A. F., Squattrito, P. J., Adani, T., Montoneri, E. "Structural chemistry of sulfonated flourobenzylphosphonate salts. I". *Inorg. Chim. Acta.* Vol. 260, **1997**, 207-216.
- [110] Schwenk, C. F., Hofer, T. S., Randolph, B. R., Rode, B. M. "The influence of heteroligands on the reactivity of Ni²⁺ in solution." *Phys. Chem. Chem. Phys.* Vol. 7, **2005**, 1669-1673.
- [111] Geet, A. L. V. "Ammonia exchange of nickel-ammine complex in aqueous ammonia measured by proton magnetic resonance." *Inorg. Chem.* Vol. 7, **1968**, 2026-2029.
- [112] Blyholder, G., Vergez, S. "Far-infrared spectra of some ammine and aqua complexes of chromium and nickel." *J. Phys. Chem.* Vol. 67, **1963**, 2149-2151.

- [113] Hunt, J. P., Dodgen, H. W., Klanberg, F. "The kinetics of ammonia exchange between nickel ammine complexes and ammonia in aqueous and anhydrous ammonia solutions measured by nuclear magnetic resonance of ^{14}N ." *Inorg. Chem.* Vol. 2, **1963**, 478-482.
- [114] Ergun, U., Atakol, O., Eris, F. Z., Yucel, A., Duzgun, E. "Estimation of coordination bond energies of NH_3 , H_2O and Et_2NH ligands in the Ni(II) and Cu(II) complexes." *J. Therm. Anal. Calorim.* Vol. 97, **2009**, 1007-1014.
- [115] Schmidt, K. H., Muller, A. "Skeletal vibrational spectra, force constants, and bond properties of transition metal ammine complexes." *Inorg. Chem.* Vol. 14, **1975**, 2183-2187.
- [116] Poulet, H., Delorme, P., Mathieu, J. P. "Spectres de vibration et fréquences fondamentales de composés de co-ordination hexamminés." *Spectrochim. Acta.* Vol. 20, **1964**, 305-315.
- [117] Stromberg, S., Svensson, M., Zetterberg, K. "Binding of ethylene to anionic, neutral, and cationic nickel(II), palladium(II), and platinum(II) cis/trans chloride ammonia complexes. A theoretical study." *Organomet. Chem.* Vol. 16, **1997**, 3165-3168.
- [118] Leineweber, A., Jacob, H., Ehrenberg, H. "Crystal structure of $\text{Ni}(\text{NH}_3)\text{Cl}_2$ and $\text{Ni}(\text{NH}_3)\text{Br}_2$." *Z. Anorg. Allg. Chem.* Vol. 626, **2000**, 2146-2152.
- [119] Leineweber, A., Jacob, H. "Preparation and crystal structures of $\text{Ni}(\text{NH}_3)_2\text{Cl}_2$ and of two modifications of $\text{Ni}(\text{NH}_3)_2\text{Br}_2$ and $\text{Ni}(\text{NH}_3)_2\text{I}_2$." *J. Solid. State. Chem.* Vol. 152, **2000**, 381-387.
- [120] Yang, Y., Weaver, M. N., Merz, K. M. "Assessment of the "6-31+G** + LANL2DZ" mixed basis set coupled with density functional theory methods and the effective core potential: prediction of heats of formation and ionization potentials for first-row-transition-metal complexes." *J. Phys. Chem. A.* Vol. 113, **2009**, 9843-9851.